Analysis of the bZIP transcription factor FDP and its interaction with floral regulators in *Arabidopsis thaliana*

Dissertation

der Mathematisch-Naturwissenschaftlichen Fakultät

der Eberhard Karls Universität Tübingen

zur Erlangung des Grades eines

Doktors der Naturwissenschaften

(Dr. rer. nat.)

vorgelegt von

Om Narayan

aus Dhanusha, Nepal

Tübingen

2018

Gedruckt mit Genehmigung der Mathematisch-Naturwissenschaftlichen Fakultät der Eberhard

Karls Universität Tübingen.

Tag der mündlichen Qualifikation: 09.11.2018

Dekan: Prof. Dr. Wolfgang Rosenstiel

1. Berichterstatter   Prof. Dr. Claudia Oecking

2. Berichterstatter   Prof. Dr. Klaus Harter

Table of Contents

List of Figures

List of Abbreviations

ABA   Abscisic acid

AP1   APPETALA 1

BR   Brassinosteroid

BZR1   BRASSINAZOLE RESISTANT 1

bZIP   basic zipper

CaMV   *Cauliflower mosaic virus*

CFP   Cyan fluorescent protein

CO   CONSTANS

Co-IP   Coimmunoprecipitation

CPK   Calcium dependent protein kinase

eGFP   Enhanced green fluorescent protein

FAC   Florigen activation complex

FRET-FLIM   Förster resonance energy transfer - fluorescence lifetime imaging microscopy

FT   FLOWERING LOCUS T

FUL   FRUITFULL

GA   Gibberellic acid

GST   Glutathione S- transferase

Hd3a   Heading date 3a

MBP   Maltose binding protein

MST   Microscale thermophoresis

pFDP   Phosphorylated FDP

rBiFC   Ratiometric biomolecular fluorescence complementation

RSG   Repression of shoot growth

TFL1   TERMINAL FLOWER 1

TF   Transcription factor

Y2H   Yeast 2-Hybrid

Summary

Flowering is essential for reproduction in plants. For photoperiodic flowering, the important floral transition regulators in *Arabidopsis thaliana* are FLOWERING LOCUS T (FT, a floral activator) and its close homolog with antagonistic function, TERMINAL FLOWER1 (TFL1, a floral repressor) as well as the bZIP transcription factors - FD and the close homolog FDP. In a previous yeast two-hybrid (Y2H) screen our lab identified FD and FDP as interactors of 14-3-3s, which are eukaryotic proteins and interact commonly with phosphorylated target proteins. Furthermore, the Y2H assays showed the phosphorylation of FDP is essential for association with 14-3-3. In rice, it has been shown that 14-3-3s mediate the interaction between FT and FD thus activating the floral transition. However, such a role of Arabidopsis 14-3-3 has not been studied. Moreover, the cell biological and biochemical information of FDP in regards to its interaction with these key floral regulators are largely limited.

To address these questions, I could show by means of the ratiometric bimolecular fluorescence complementation assay that the nuclear-localized FDP physically interacts *in planta* not only with 14-3-3, but also with floral antagonists FT and TFL1 in a phosphorylation-dependent manner. Moreover, colocalization studies exhibited that 14-3-3, FT and TFL1 localize both to the cytoplasm and the nucleus, but accumulate in the nucleus upon the phosphorylation of the transcription factor. Furthermore, these data indicated that 14-3-3 might modify the ability of FDP to interact with floral antagonists.

The molecular basis of antagonism between FT and TFL1 in plants is not well understood. In this study GST pull-down assays (performed with bacterially expressed proteins) demonstrated that TFL1, like FT, is able to interact with 14-3-3 in a phosphorylation-independent manner. Using the nuclear localization signal included version of 14-3-3 (14-3-3-NLS), I could show that 14-3-3 controls the subcellular localization of FT as well TFL1 and plays a role in piggybacking them from the cytoplasm to the nucleus. Furthermore, both *in vitro* and *in vivo* data including pull-down, coimmunoprecipitation, and Förster resonance energy transfer - fluorescence lifetime imaging microscopy (FRET-FLIM) experiments support that 14-3-3 and FT complex is stabilized in the presence of FDP, leading to the formation of the tripartite complex. In contrast, the complex formation between 14-3-3 and TFL1 is negatively affected in the presence of FDP. These findings have given a first clue about the mechanistic differences between FT and TFL1 and provide the explanation for the molecular basis of antagonism. Despite the antagonistic activity, TFL1 does not differ from FT with respect to its subcellular interaction and colocalization capability. Such a scenario suggests a hypothesis that the floral regulators might compete out for the association with the phosphorylated FDP. This hypothesis is supported by the lifetime analyses obtained from the FRET-FLIM experiments performed by transient expression in *Nicotiana benthamiana*. This further explains the significance of fine balance between FT and TFL1, which is crucial for achieving optimal reproductive success by adapting to various environmental changes.

Zusammenfassung

Die Blüte ist für die Fortpflanzung von Pflanzen unerlässlich. Wichtige pflanzliche Regulatoren für den Übergang in die durch die Photoperiode induzierte Blüte in *Arabidopsis thaliana* sind FLOWERING LOCUS T (FT, ein floraler Aktivator) und sein nahes Homolog mit der antagonistischen Funktion, TERMINAL FLOWER1 (TFL1, ein floraler Repressor) sowie die bZIP - Transkriptionsfaktoren FD und sein enges Homolog FDP. In einer früheren Hefe-Zwei-Hybrid-Sichtung identifizierte unser Labor FD und FDP als Interaktoren von 14-3-3s, die eukaryotische Proteine sind und mit phosphorylierten Zielproteinen interagieren. Darüber hinaus zeigten die Y2H-Assays, dass die Phosphorylierung von FDP essentiell für die Assoziation mit 14-3-3 ist. In Reis wurde gezeigt, dass 14-3-3 die Wechselwirkung zwischen FT und FD vermittelt und somit den Übergang zur Blüte aktiviert. Eine solche Rolle von 14-3-3 Proteinen in Arabidopsis wurde jedoch noch nicht untersucht. Darüber hinaus sind die zellbiologischen und biochemischen Informationen von FDP in Bezug auf seine Interaktion mit diesen wichtigen Blütenregulatoren weitestgehend begrenzt.

Um diese Fragen zu beantworten, konnte ich anhand des ratiometrischen bimolekularen Fluoreszenzkomplementationstests zeigen, dass die kernlokalisierte FDP nicht nur mit 14-3-3, sondern auch mit den auf die Blüte bezogenen Antagonisten FT und TFL1 in einer phosphorylierungsabhängigen Art und Weise physisch *in planta* interagiert. Darüber hinaus zeigten Kolokalisationsstudien, dass 14-3-3, FT und TFL1 sowohl im Zytoplasma als auch im Zellkern lokalisiert sind, sich jedoch bei der Phosphorylierung des Transkriptionsfaktors im Zellkern anreichern. Des Weiteren zeigten diese Daten, dass 14-3-3 die Fähigkeit von FDP, mit auf die Blüte bezogenen/floralen Antagonisten zu interagieren, modifizieren könnte.

Die molekulare Basis des Antagonismus zwischen FT und TFL1 in Pflanzen wird bis *dato* noch nicht gut verstanden. In dieser Studie zeigten GST-Pulldown-Assays (durchgeführt mit bakteriell exprimierten Proteinen), dass TFL1 sowie FT in der Lage sind, durch eine phosphorylierungs-unabhängige Interaktion mit 14-3-3 zu interagieren. Mit Hilfe einer Version von 14-3-3, die mit einem Kernlokalisierungssignal ausgestattet ist, dass 14-3-3 die subzelluläre Lokalisation von FT und TFL1 kontrolliert, indem es sie durch Huckepackübertragung aus dem Zytoplasma in den Zellkern transportiert. Darüber hinaus stützen sowohl *in-vitro*- als auch *in-vivo*-Daten, darunter Pull-Down-, Co-Immunopräzipitations- und Förster-Resonanz-Energietransfer-Fluoreszenzlebensdauer-Mikroskopie-Experimente (FRET-FLIM), dass der 14-3-3- und FT-Komplex in Gegenwart von FDP stabilisiert wird, was zur Bildung des dreiteiligen Komplexes führte. Im Gegensatz dazu wird die 14-3-3- und TFL1-Komplexbildung in Gegenwart von FDP negativ beeinflusst. Diese Befunde geben einen ersten Hinweis auf die mechanistischen Unterschiede zwischen FT und TFL1 und liefern die Erklärung für die molekularen Grundlagen des Antagonismus. Trotz der antagonistischen Aktivität unterscheidet sich TFL1 nicht von FT in Bezug auf seine subzelluläre

Interaktion und Kolokalisationsfähigkeit. Ein solches Szenario legt die Hypothese nahe, dass die Blütenregulatoren um die Assoziation mit der phosphoryliertem FDP konkurrieren könnten. Diese Hypothese wird durch die Analyse der GFP-Lebensdauer gestützt, welche aus FRET-FLIM-Experimenten, die durch transiente Expression in *Nicotiana benthamiana* durchgeführt wurden, erhalten wurden. Dies erklärt weiter die Bedeutung des Gleichgewichts zwischen FT und TFL1, die für die Erzielung optimaler reproduktiver Erfolge durch Anpassung an verschiedene Umweltveränderungen entscheidend ist.

1. Introduction

Plants as a sessile organisms encounter different environmental changes such as the availability of water and soil nutrient, light irradiation and quality. They have evolved many plastic strategies for optimal growth and survival according to these variable environmental conditions. In a favorable condition, they transfer their resources for a major development switch, which will ultimately lead to seed formation, and subsequently to next generation of progeny. Flowering formation is a crucial development switch for sexual propagation.

1.1 Flowering

Flowering is an important phase in the life cycle of flowering plants (or Angiosperms). Plants accomplish this phase by changing vegetative growth to reproductive one. This growth shift is termed as floral transition. The precise timing of floral transition is a critical step for successful reproduction. To accomplish this precision, the plants integrate various environmental cues such as day length, ambient temperature as well as endogenous cues such as hormonal and sugar status (Srikanth and Schmid, 2011). The number of seeds and fruits that the plants will produce is tightly dependent on the reproductive success. Seeds and fruits are the important source of nutrients not only for humans, but also livestock. Therefore, the understanding of flowering onset becomes very important to understand and optimize the floral components, thereby boosting the crop productivity. For such reasons, researchers and breeders have been drawn to study and optimize such factors and pathways influencing flowering.

There are five important flowering regulatory pathways namely – photoperiod, vernalization, gibberellic acid, ambient temperature and autonomous (reviewed in Srikanth and Schmid, 2011; Fig. **1.1**).
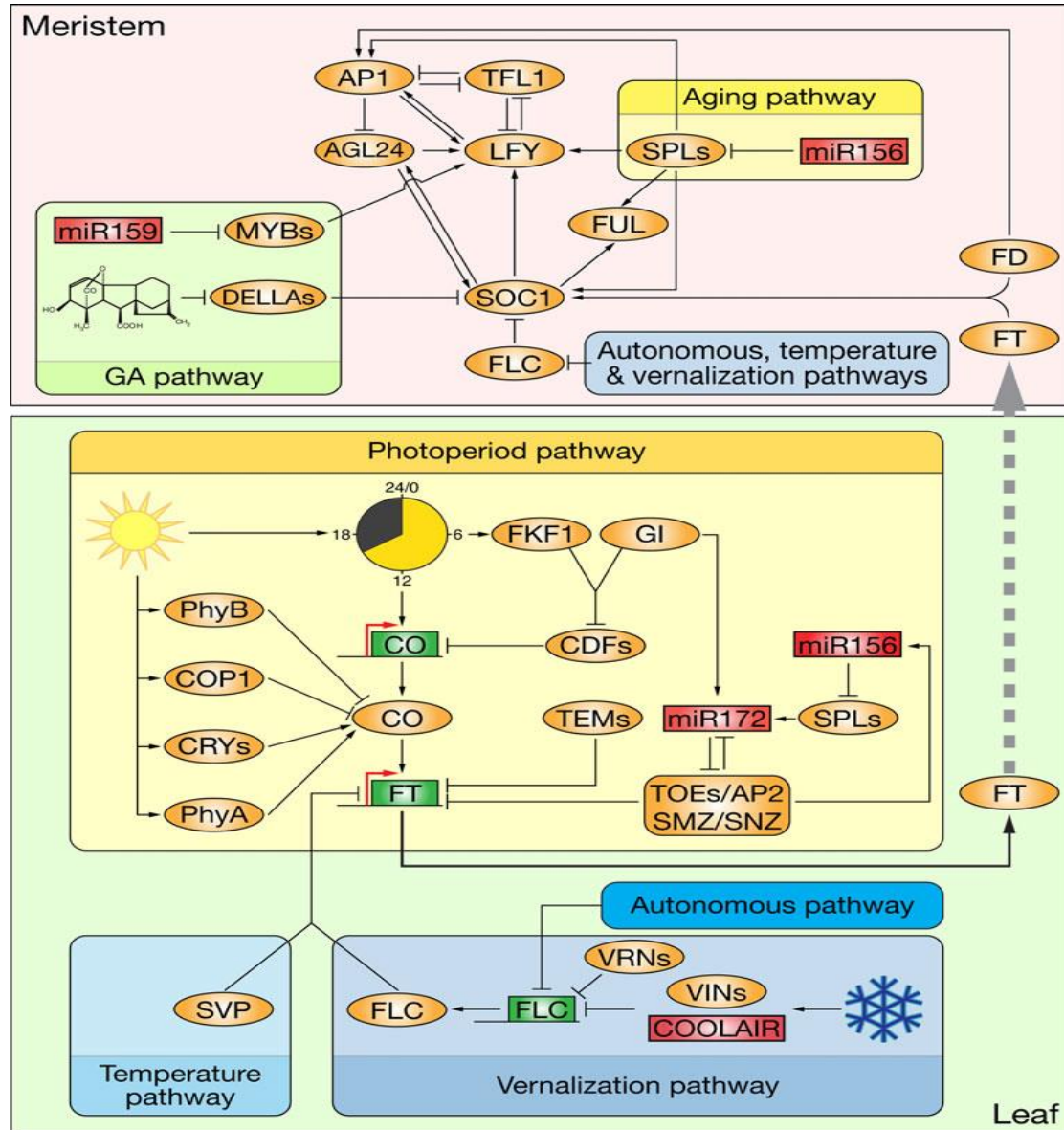
Figure 1. 1: Illustration of networks of major flowering pathways (modified from Srikanth and Schmid, 2011). Flowering time in Photoperiod pathway is regulated by inductive day-length condition. Here, the expression of CO is controlled directly or indirectly by Phytochrome A/B, Cryptochromes. CO protein is important component to perceive day-length in leaves and induce FT expression in leaves. FT is a mobile signal which moves from leaf to the meristem to induce floral initiation. Flowering time is regulated by temperature – prolonged period of cold in vernalization pathway, and another by ambient temperature that speeds up floral initiation. Endogenous signals that regulate flowering time arises from hormonal status of Gibberellic acid (GA pathway) as well as sugar levels in plants. Besides, microRNA is involved in the regulation of flowering time in aging pathway. Autonomous pathway regulates flowering time independent of day-length by repressing FLC. There is cross-talk among flowering pathways to ensure a successful reproduction in various environment.

1.2 Photoperiodic flowering regulation – a historical overview

How and where to flower are critical steps that plants take in their lifespan for optimal reproduction. Wightman Garner and Henry Allard were the first researchers who empirically explained that the duration of light in a 24-hour period acts as a key factor for flowering initiation. By simulating different seasonal light conditions through the control of light and dark duration, they determined the optimal duration of light or darkness that are crucial for flowering induction in more than 12 plant species. They termed this response triggered in plants by a change in day length as 'photoperiodism.' Furthermore, they grouped plants into three classes according to the day-length response. Those plants that flower when day length is longer as 'long-day', those when day length is shorter as 'short-day' and those that do not care day length as 'day-neutral'. This understanding raised many other questions such as how and where day-length in plant is sensed and which molecule is responsible for this regulation.

It turned out, the plants use the sophisticated mechanism to measure the length of day. It was Erwin Bünning in 1930 who suggested the existence of a biological clock. He proposed that this clock is entrained by day-night cycle and the 24h day is divided into two phases – light and dark. The regulation of shift from one phase to another is done by a circadian oscillator. Therefore, light as an external signal would indicate the plant whether the day length or photoperiod is long or short. The answer to another key question where the photoperiod is perceived came from grafting experiments performed first by Mikhail Chailakhyan. He suggested that a flower-triggering substance produced in leaf scions exposed to inductive photoperiod could induce flowering in non-induced graft stock. He formalized this idea as 'florigen hypothesis'. The search for this florigenic substance went on for decades until studies from *Arabidopsis* facilitated the discovery of FLOWERING LOCUS T (FT) protein. Subsequent grafting experiments proved that FT is a universal mobile signal in Arabidopsis and other plant species (Abe *et al.*, 2005; Corbesier *et al.*, 2007; Kobayashi and Weigel, 2007; Tamaki *et al.*, 2007; Wigge *et al.*, 2005).

1.3 Mechanism of Photoperiodic flowering regulation

Ground-breaking genetic analyses that were done with *Arabidopsis* wild accessions have revealed many essential flowering components that are known today. These accessions belong

to summer annual class, which flower earlier in a long day without vernalization (cold) treatment. George Rédei, in 1962, isolated *gigantea* (*gi*) and *constans* (*co*) from mutagenic screens. These loss-of-function mutant plants flowered later than the wild type. Later, Maarten Koorneef and colleagues identified many loci including *fd* and *ft*, which resulted in late flowering time in the Landsberg *erecta* (Ler) accession of *A. thaliana*. Based on the delayed flowering phenotypes of *co*, *gi* and *ft* mutants in inductive long day conditions, it was postulated that these genes are parts of the same regulatory pathway – the photoperiodic flowering pathway (Koorneef *et al.*, 1991). Later, it was demonstrated that under inductive long day condition, *CONSTANS* (*CO*) gene expression is regulated by the circadian clock (Suárez-Lopez *et al.*, 2001), and CO protein activates FT expression in phloem companion cells of leaves (Samach *et al.*, 2000). FT protein is a mobile signal, which moves from leaves to the shoot apical meristem to initiate flowering (Corbesier *et al.*, 2007). These findings lead to the understanding of day-length determination and floral transition under inductive photoperiod.

1.3.1   Activation of *FT* expression by CONSTANS

The *CONSTANS* (*CO*) gene encodes a zinc finger transcription factor. The expression of *CO* under the control of circadian clock is a critical mechanism for precise determination of day length. Thus, *CO* gene is tightly controlled by transcriptional and post-translational regulations. Such regulations ensure that CO activates the transcription of *FT* only under long days. Through the repression of CYCLING DOF FACTOR1 (CDF1) protein, *CO* expression is kept low in the morning (Fornara *et al.*, 2009). But in the afternoon, the combined activity of FLAVIN-BINDING, KELCH REPEAT, F-BOX1 (FKF1) and GIGANTEA (GI) proteins triggers the degradation of CDF1, which leads to an increase in *CO* transcript (Imaizumi *et al.*, 2005; Sawa *et al.*, 2007). In the late afternoon, this results in CO protein accumulation and its stability, which is crucial for day length-dependent *FT* activation. This accurate accumulation and stability of CO protein at this time point of day are controlled by various light signaling and proteasome-dependent protein degradation mechanisms. Photoreceptors, Phytochrome A (PhyA) and cryptochromes (CRYs), protect CO protein from degradation, while PhyB promotes degradation (Zuo *et al.*, 2011). CONSTITUTTIVE PHOTOMORPHOGENIC 1 (COP1; an E3 ubiquitin ligase) and SUPPRESSOR OF

PHYTOCHROME A (SPA1) facilitate CO degradation by the 26S proteasome. As COP1 and SPA1 complex is repressed by light, there is a degradation of CO protein only in the dark (Laubinger *et al.*, 2006; Liu *et al.*, 2008). Altogether, the complex regulation of CO enables the plant to discriminate short day from long day (LD), where CO protein accumulates only at the end of the day. These mechanisms pinpoint the internal and external coincidence mechanisms proposed by Pittendrigh (1976). Under LD, synchronized expression of GI and FKF1 boosting *CO* expression by timely degradation of CDFs fits in the internal model. The light-dependent regulation of FKF1 and COP1/SPA activity leads specifically to the accumulation of CO proteins towards the end of the long day (Song *et al.*, 2012b). This explains the external coincidence model, where light-dependent CO protein stability leads to the activation of *FT* expression.

The transcription of *FT* is a central integrator of various environmental signals. Hence its transcription is tightly controlled by a number of transcription factors. Especially, two groups of transcription factors play major roles in the activation of *FT* transcription. CO protein strongly activates the expression of *FT* transcript (Putterill *et al.*, 1995, Tiwari *et al.*, 2010). It binds to the *FT* promoter and has two modes of actions for *FT* gene activation. First is the direct binding of CO protein to the CONSTANS responsive element (CORE) via the CCT motif (Tiwari *et al.*, 2010). Second is the recruitment of CO by the CCAAT box-binding proteins such as Nuclear Factor-Y (NF-Y) and ASYMMETRIC LEAVES 1 (Wenkel *et al.*, 2006; Song *et al.*, 2012a). *FT* expression is largely dependent on CO protein. Another transcription factor family that is involved in *FT* induction includes CRYPTOCHROME-INTERACTING BASIC HELIX-LOOP-HELIX (CIB) protein (Liu *et al.*, 2008). This protein together with CRY2 forms a complex in a blue light-dependent manner, acting as *FT* activator (Liu *et al.*, 2008; Liu *et al.*, 2013c). This way the blue light signaling also plays a vital role in regulating *FT* expression.

1.3.2 Movement of FT protein from leaf to the shoot apex

The florigen production in the leaves differs from its function to promote floral induction at the shoot apex. As it became evident that FT is the mobile signal, there arises the debate whether this mobile signal is *FT* mRNA or FT protein (Corbesier *et al.*, 2007; Jaeger and Wigge, 2007; Yoo *et al.*, 2013b). Many studies, particularly with grafting experiments, proved to be useful tools in

establishing the movement of FT protein as a florigenic signal (Yoo *et al*., 2013a). FT movement is accompanied by a combination of diffusion through the companion cell and into the phloem, and more actively through the plasmodesmata of cells into the cells of the shoot apex.

Many components involved in the movement of FT protein have been identified, but their roles need to be further characterized (Liu *et al*., 2012, Yoo *et al*., 2013a). Recently, a heavy-metal-associated domain containing protein, SODIUM POTASSIUM ROOT DEFECTIVE 1 (NaKR1), has been reported to regulate the long-distance transport of FT (Zhu *et al*., 2016).

1.3.3   Interaction of FT with bZIP transcription factors FD/FDP in the shoot apex

In the shoot apical meristem (SAM), FT interacts with a basic leucine zipper (bZIP) transcription factors, FD and its homolog, FD PARALOG (FDP) to induce floral identity genes such as *APETALA 1* (*AP1*) and *FRUITFULL* (*FUL*) (Abe *et al*., 2005; Wigge *et al*., 2005). These bZIPs belong to Group A as bZIP 14 and bZIP 27, respectively. The other members of this group such as ABI5 are involved in abscisic acid (ABA) signaling. Both FD and FDP have a conserved STAPF-COOH motif (Fig. **1.3**), which is a phosphorylation site for calcium-dependent protein kinases (CPKs). After phosphorylation of threonine residue within this motif, 14-3-3s binding site is created (Abe *et al*., 2005; Kawamoto *et al*., 2015a).

fd-1 mutant plant has a clear delayed flowering phenotype, while *fdp* tilling lines did not flower (Hanano and Goto, 2011) or showed slightly late flowering (Jaeger *et al*., 2013). Threonine to serine substitution version of FD (FD^{T292S}) under a strong promoter *Cauliflower mosaic virus* (CaMV) 35S could complement *fd-1* plant, and even showed a slight early flowering phenotype, whereas alanine substitution could not rescue. This suggests the physiological significance of FD phosphorylation. Genetic studies demonstrated that besides *FD*, its paralog *FDP*, is also essential for both FT and TERMINAL FLOWER 1 (TFL1 – a floral repressor) signaling (Jaeger *et al*., 2013). FD orthologs in many plant species have been found to be important in flowering. For example, DLF1 in maize (Muszynski *et al*., 2006), OsFD1 in rice (Taoka *et al*., 2011), SSP in tomato (Park *et al*., 2014), RoFD in rose (Randoux *et al*., 2014). They all have conserved 14-3-3 binding motif, suggesting a similar mechanism for flowering regulation (Park *et al*., 2014).
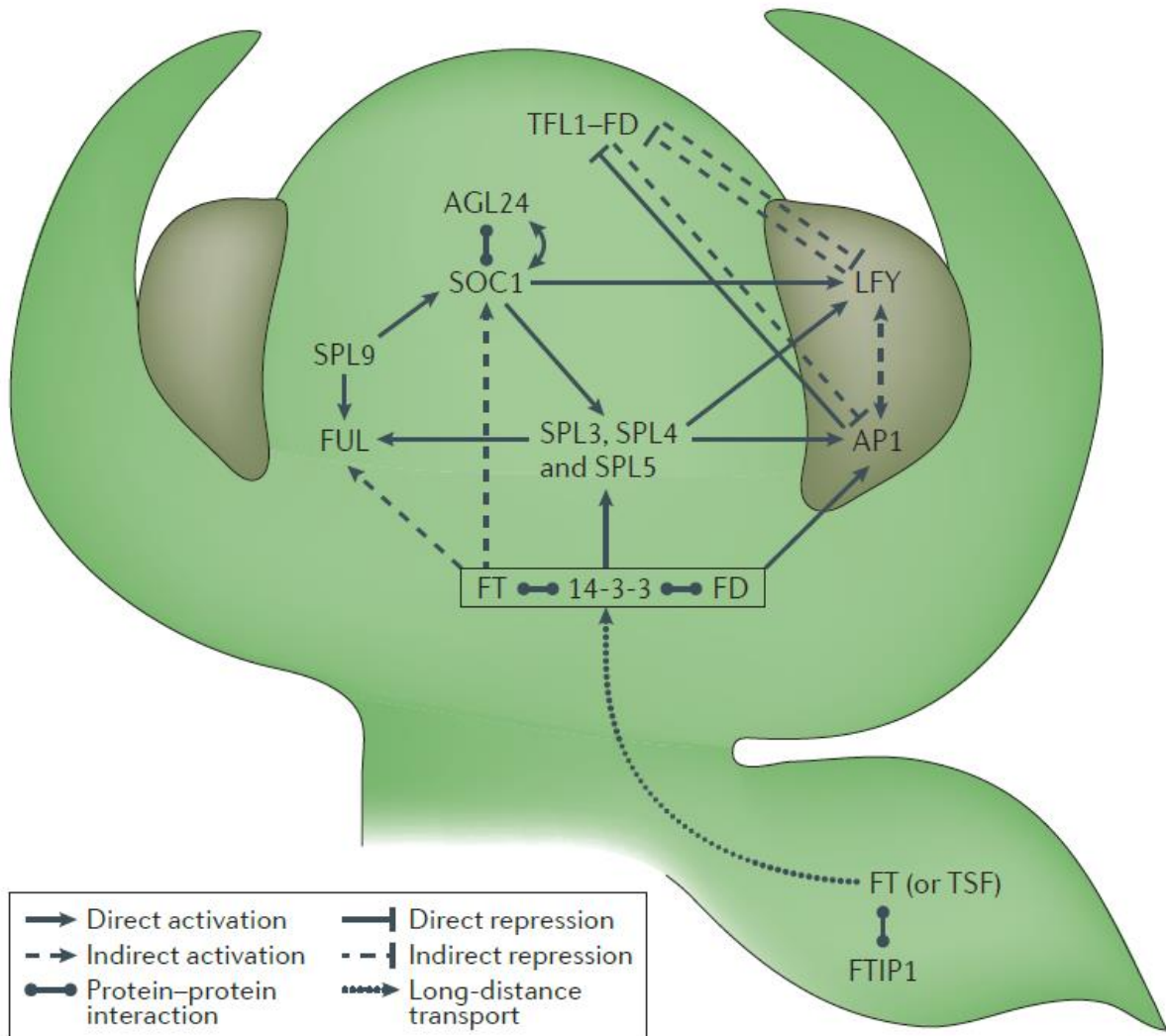
Figure 1. 2: Genetic network of floral transition at the shoot apex (modified from Andrés and Coupland, 2012). In Arabidopsis, FT that is expressed in leaves under long day is transported to the shoot apical meristem (SAM). In the SAM, it associates with the bZIP transcription factor, FD. This association, in turn, leads to the activation of floral identity genes such as *AP1*, *FUL*. On the other hand, TFL1 that is already present in the SAM can also associate with FD to repress the expression of floral identity genes.

These FD-like genes are essential for providing DNA binding specificity through recognition of ACGT-containing consensus sequences on the promoter of target genes such as *AP1* (Wigge *et al.*, 2005; Taoka *et al.*, 2011).
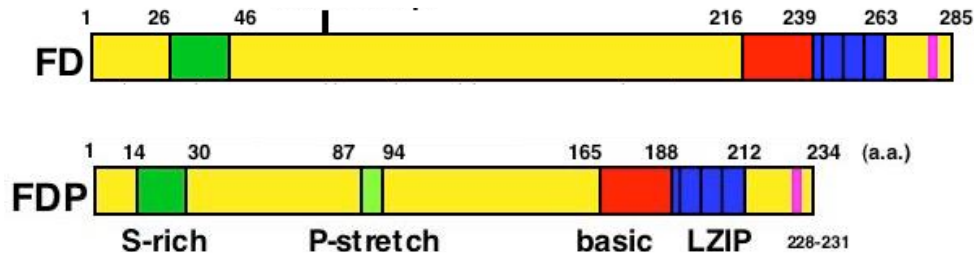
Figure 1. 3: The schematic representation of FD and FDP proteins (modified from Abe *et al*., 2005). S-rich shows serine residue stretch, proline residue by P-stretch, basic leucine zipper (LZIP) and CDPKs and 14-3-3s binding site at the C-terminus (in pink color).

1.3.4   Antagonism between FT and TFL1 fine-tunes the floral transition

FT and its closely related protein, TFL1, are key regulators of flowering time as well as plant shoot architecture, but in an opposite fashion. *TFL1* gene is expressed in the SAM, and *tfl1* mutants flower early with the rapid production of a terminal flower (Bradley *et al*., 1997). TFL1 suppresses the floral initiation and also keeps the SAM in vegetative state for a longer period by repressing floral identity genes. The gain-of-function studies demonstrated clear and opposing phenotypes of FT and TFL1, indicating that it is the protein sequence rather than expression pattern that causes their antagonistic functions *in vivo* (Kardailsky *et al*., 1999; Kobayashi *et al*., 1999). FT and TFL1 share approx. 59% identical amino acid residues and are closely related to phosphatidylethanolamine binding protein (PEBP; Pnueli *et al*., 2001). This led many groups to investigate the underlying differences between these proteins that cause their opposing functions in flowering time.

A single amino acid substitution, H88Y in TFL1 converts this protein into a floral inducer, and the corresponding Y85H in FT turns it into a floral repressor (Hanzawa *et al*., 2005). The crystal structure demonstrated that in TFL1, His-88 forms a hydrogen bond with Asp-144, while Tyr-85 and Gln-140 (which corresponds to Asp-144) in FT do not (Ahn *et al*., 2006). Besides, the fourth exon, which has highly variable segment B in TFL1, but almost invariant in FT, also seems to confer a biological specificity on two proteins (Ahn *et al*., 2006). However, the surface charge studies demonstrated that FD and FDP transcription factors and 14-3-3 proteins could not differentiate between TFL1 and FT (Ho and Weigel, 2014). The potential proteins, which have a

capability to discriminate between FT and TFL1 interaction belong to TCP (TEROSINTE BRANCHED1, CYCLOIDEA, PCF) transcription factors such as TCP17/18 (Niwa *et al.*, 2013; Ho and Weigel, 2014).

1.4 14-3-3 proteins

14-3-3 proteins are ubiquitously present in eukaryotes. The number of 14-3-3 genes varies with organisms, for example, humans typically have seven genes, and yeast has two. In *Arabidopsis thaliana*, there are 13 genes that are expressed; additional two are pseudogenes (Rosenquist *et al.*, 2001). They form either homo- or heterodimers. Crystal structure of plant 14-3-3 proteins show dimer formation containing two amphipathic grooves (Wurtele *et al.*, 2003). The grooves are the important sites where 14-3-3s bind to their phosphorylated targets. The interaction with target proteins is mostly phosphorylation dependent. These target proteins are phosphorylated on serine (S) or threonine (T) residues with a conserved binding motif and thus 14-3-3 proteins can be considered phospho-serine/threonine sensors. Three canonical 14-3-3 binding motifs have been defined so far. They are mode I – (R/K)SX(pS/pT)XP; mode II – PXY/FX(pS/pT)XP, and mode III – pS/pTX_{1-2}-COOH (Yaffe *et al.*, 1997; Ganguly *et al.*, 2005). The mode III has been best characterized from the plant plasma membrane H^+-ATPase pump, which has the YpTV-COOH (Svennelid *et al.*, 1999; Ottmann *et al.*, 2007). Moreover, some proteins also bind through non-canonical or nonphosphorylated motifs (Aitken *et al.*, 2002; Taoka *et al.*, 2011). The 14-3-3 proteins do not have any enzymatic activity, instead act by physical interaction. As a result of 14-3-3 association, target proteins can be modified in various ways such as their subcellular localization, ability to interact with other proteins and enzymatic activities.

1.4.1 14-3-3s in Arabidopsis

The *Arabidopsis* 14-3-3s are divided on basis of gene structure into epsilon and non-epsilon groups. They are highly functional redundant, which make it difficult to characterize the individual isoform's function and specificity. Many putative 14-3-3 client proteins have been identified in screening experiments (Jaspert *et al.*, 2011; Keicher *et al.*, 2017). This high number suggests that 14-3-3s could potentially be involved in several signaling pathways and

physiological processes in plants. However, *in vivo* validation of many of these clients and the underlying mechanisms are still lacking. The initial finding that the 14-3-3 proteins associate with metabolic enzymes such as nitrate reductase, glutamine synthetase gave an impression of their involvement in primary metabolism. But, later they were found to interact with membrane proteins that include proton-pumps, ATP-binding cassette (ABC) and aquaporins, suggesting role in ion homeostasis (Jaspert *et al*., 2011). Binding of 14-3-3s to the phosphorylated penultimate residue of H^+-ATPases results in release of auto-inhibition and thus activation of the proton pump (Svennelid *et al*., 1999).

Recent findings have revealed the involvement of 14-3-3s in many phytohormone signaling such as abscisic acid, brassinosteroid (BR), gibberellins, auxin (Jaspert *et al*., 2011). Dual role of 14-3-3 proteins in the regulation of BR signaling have been reported (Rue *et al*., 2007; Wang *et al*., 2011). In the absence of BR, the phosphorylated BRASSINAZOLE RESISTANT 1 (BZR1) transcription factor is retained by 14-3-3 binding in the cytoplasm, thus, inhibiting BR responses. By contrast, in the presence of BR, BR receptor, BRASSINOSTEROID INSENSITIVE 1 (BRI1), phosphorylates BRI1 KINASE INHIBITOR 1 (BKI1), causing its release into the cytoplasm where it associates with 14-3-3 proteins. This association between BRI1 and 14-3-3s takes place via an uncommon mode II motif, promoting the nuclear translocation of BZR1 and thus activating BR responses. Such dual role of 14-3-3 proteins seems to be crucial for a tight regulation of BR signaling.

In Auxin signaling, it has been demonstrated that IAA (Indole-3-acetic acid) promotes the phosphorylation of penultimate threonine residue of H^+-ATPases and subsequent 14-3-3 binding, which leads to the activation of pump activity (Takahashi *et al*., 2012). It has been recently shown that the members of 14-3-3epsilon protein family are involved in the alteration of polar distribution of IAA and production of IAA-transport-related phenotypes in *Arabidopsis* seedlings (Keicher *et al*., 2017).
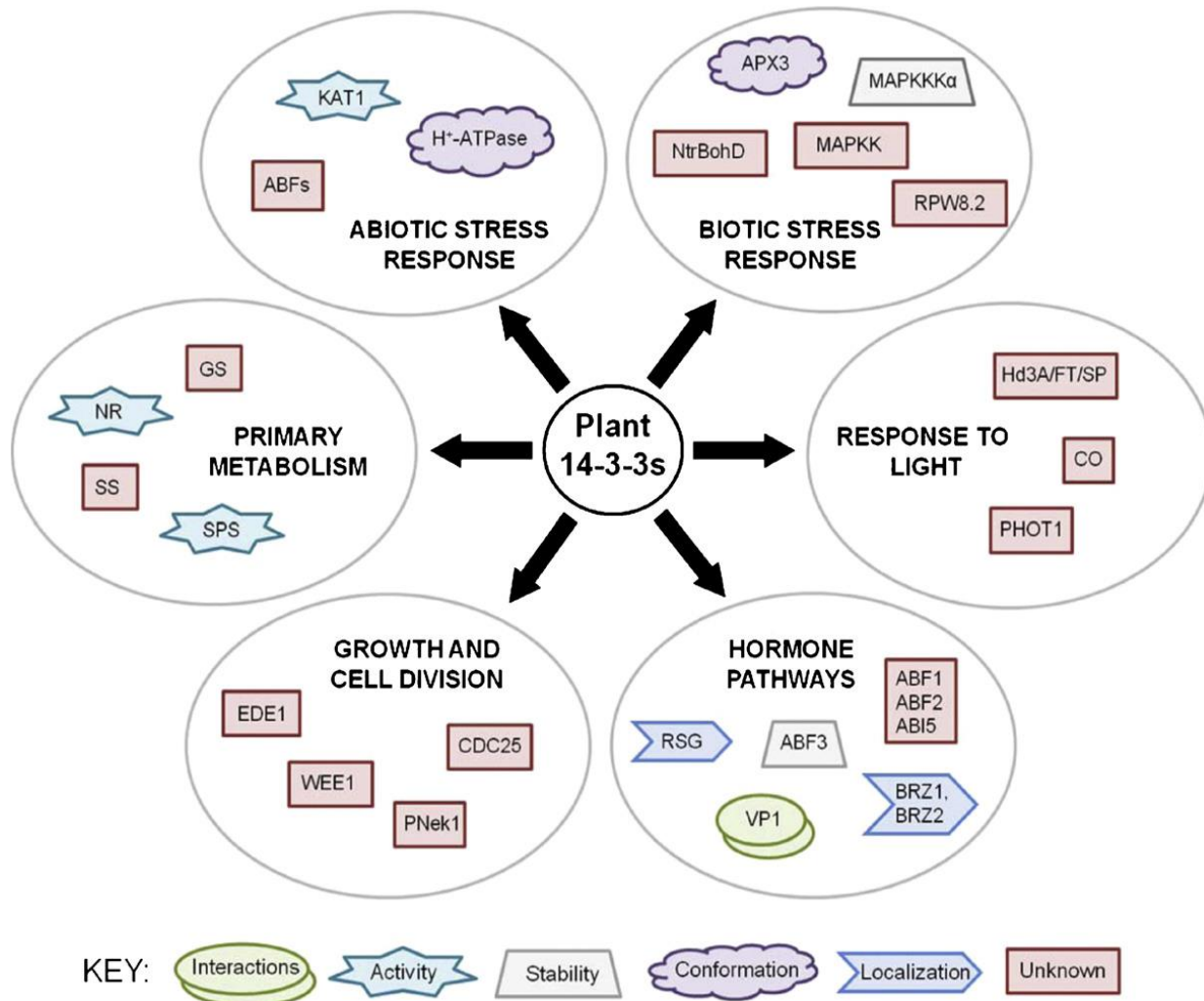
Figure 1. 4: Illustration showing diverse functions of plant 14-3-3s (modified from Denison *et al*., 2011). Involvement of 14-3-3 proteins in many important physiological processes is displayed. The key target proteins to which 14-3-3s bind for the regulation of these processes are shown. The different mechanism by which 14-3-3 binding alters the target is represented by the shape of the box.

1.4.2 14-3-3s in flowering regulation

14-3-3 proteins were found via yeast 2-hybrid (Y2H) assay as interacting partners of TFL1 and FT in tomato, suggesting their potential roles in shoot architecture and flowering (Pnueli *et al*., 2001). In *Arabidopsis*, 14-3-3mu and nu *knock-out* plants showed a delay in flowering and interaction with CONSTANS in Y2H experiments. However, others could not observe this delayed flowering phenotype, and the physiological significance of 14-3-3 and CONSTANS interaction needs further investigation. The crucial role of 14-3-3s in the regulation of

photoperiodic flowering was elegantly described in rice (Taoka *et al*., 2011; Fig. **1.5**). The author provided cell biological and biochemical evidence demonstrating 14-3-3 as a bridging protein for the interaction between Hd3a and OsFD1 (FT and FD homologs), which leads to the activation of floral identity genes such as *OsMADS15* (a homolog of *AP1*).
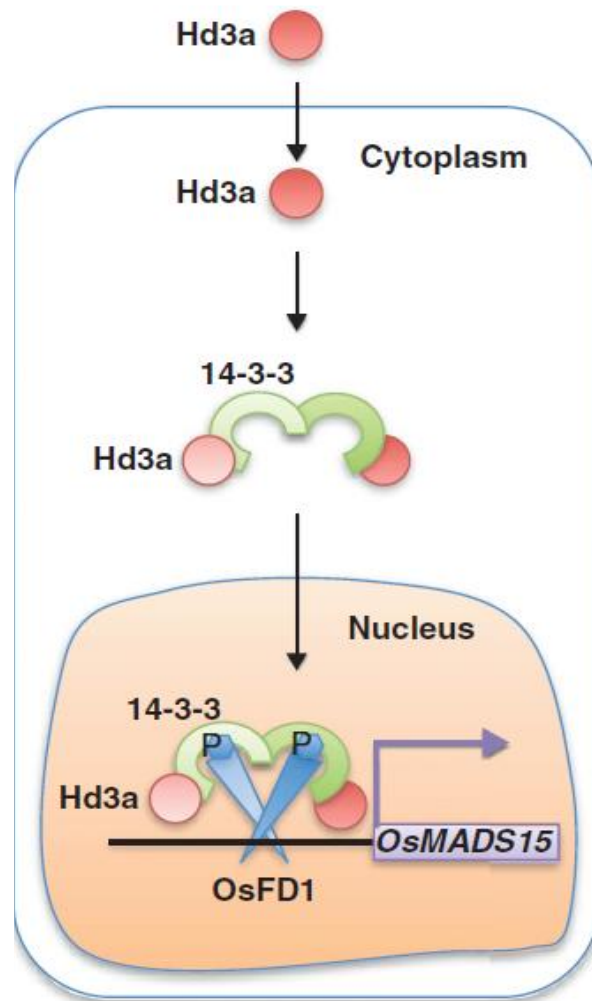
Figure 1. 5: Illustration showing the mechanism of 14-3-3 involvement in flowering regulation in rice (modified from Taoka *et al*., 2011). 14-3-3 proteins act as intracellular receptors of florigen, Hd3a (FT homolog). In the shoot apical meristem, Hd3a is received by 14-3-3s in the cytoplasm. Then the complex between Hd3a and 14-3-3 moves into the nucleus and interacts further with the bZIP transcription factor OsFD1 to form a florigen activation complex (FAC), leading to the activation of floral identify genes such as *OsMADS15*.

1.5 Objective of this work

Flowering is essential for reproduction in plants. For photoperiodic flowering, the important floral transition regulators in *Arabidopsis thaliana* are FLOWERING LOCUS T (FT, a floral activator) and its close homolog with antagonistic function, TERMINAL FLOWER1 (TFL1, a floral repressor) as well as the bZIP transcription factors - FD and the close homolog FDP. In a previous yeast two-hybrid (Y2H) screen our lab identified FD and FDP as interactors of 14-3-3s, which are eukaryotic proteins and interact commonly with phosphorylated target proteins. Furthermore, the Y2H assays showed that the phosphorylation of FDP is essential for association with 14-3-3. In rice, it has been shown that 14-3-3s mediate the interaction between FT and FD thus activating the floral transition. However, such a role of *Arabidopsis* 14-3-3 has not been studied. Moreover, the cell biological and biochemical information of FDP regarding the *in planta* connection of FDP with key floral regulators FT, TFL1 and 14-3-3 is largely unknown. The first objective was to investigate *in planta* relation of the transcription factor FDP with floral regulators.

The molecular basis behind the antagonism between FT and TFL1 remains unclear. Another major aim of this work was to understand the molecular basis of antagonism between these two proteins, which are crucial for the appropriate timing of flowering in plants.

2. Materials and Method

2.1 Materials

2.1.1 List of chemicals

Chemical	Company
Acetosyringone	Sigma Aldrich
Cyclohexylene dinitrilo tetraacetic acid (CDTA)	Sigma
Dithiothreitol (DTT)	Sigma Aldrich
Ethylene diamine tetraacetic acid (EDTA)	AppliChem
Glycerol	Roth
Glycin	Roth
Hydrochloric acid (HCl)	Sigma Aldrich
4-(hydroxyethyl)-1-piperazineethanesulfonic acid (HEPES)	Roth
Imidazol	Sigma Aldrich
Isopropyl β-D-1-thiogalactopyranoside (IPTG)	Roth
Luria-Bertani (LB)	Roth
Magnesium chloride (MgCl$_2$)	Merck
Methanol	Merck
2-(4-morpholino) ethanesulfonic acid (MES)	Roth
Phenylmethylsulfonyl fluoride (PMSF)	Sigma Aldrich
Potassium dihydrogen phosphate (KH$_2$PO$_4$)	Sigma Aldrich
Potassium hydroxide (KOH)	Roth
Silwet L-77	Lehle SEEDS
Sodium chloride (NaCl)	Merck
Sodium dodecyl sulfate (SDS)	Merck
Sodium hydrogen phosphate (Na$_2$HPO$_4$)	Roth
Sodium hydroxide (NaOH)	Merck
Tetramethylethylenediamine (TEMED)	Sigma Aldrich
Tris-base	Roth
Tween 20	Sigma Aldrich
X-gal	Promega

2.1.2   Abbreviation of Unit

mg   milligram

µg   microgram

ml   milliliter

µl   microliter

nm   nanometer

rpm   rotation per minute

%   percent

M   Molar

mM   Millimolar

pmol   picomole

+   Plus

sec   second

min   minute

kDa   kilodalton

mA   milliampere

2.1.3   Antibiotics working concentration

Antibiotics	Working concentration	Company
Ampicillin	100 µg/ml	Serva
Chloramphenicol	20 µg/ml	Sigma Chemie
Gentamycin	15 µg/ml	Duchefa Biochemie
Kanamycin	50 µg/ml	Roth
Rifampicin	5 to 50 µg/ml	Sigma Life Science
Spectinomycin	100 µg/ml	Duchefa Biochemie

2.1.4   Media

Plasmid isolation by Birnboin and Doly method

Solution I: 20 mM glucose, 10 mM CDTA, 25 mM Tris/HCl, pH8.0

Solution II: 1% SDS (fresh from 10% SDS stock solution), 0.2 M (2 M NaOH stock solution) and 7 µl RNaseI
(Thermoscientific, Germany)

Solution III: 3 M Potassium Acetate, 1.8 M Formic acid

SDS-PAGE (Sodium dodecyl- Polyachrylamide gel electrophoresis)

Resolving gel (12.5%) /per gel		Stacking gel (4%)
MilliQ H_2O	2.1 ml	3.3 ml
Resolving buffer, 1.5 M Tris/HCl (pH8.8)	1.67 ml	Stacking buffer,0.5 M Tris/HCl (pH6.8) = 1.25 ml
30% Acrylamide	2.78 ml	0.67 ml
10% SDS	66 µl	50 µl
10% ammonium persulfate	50 µl	26 µl
TEMED	5 µl	16 µl

10X running buffer for SDS-PAGE: 1.92 M Glycin, 0.25 M Tris base and 1% (w/v) SDS

Laemmli sample buffer

0.05 M Tris/HCl, pH6.8, 17.2% (v/v) Glycerin, 5% (v/v) Mercaptoethanol, 4% SDS, 0.005% (w/v) Bromophenolblue (Serva Blue G), with/without oComplete protease inhibitor

Coomassie staining: 40% (v/v) Methanol, 10% (v/v) Acetic acid, 0.1% (w/v)

Western blot

Blot transfer buffer: 20 mM Tris, 150 mM Glycin, 20% (v/v) Methanol/Ethanol, 0.01% (w/v) SDS

Ponceau S staining solution: 1% (w/v) Ponceau S and 2% (v/v) Acetic acid

Blocking solution: 2% (w/v) High Protein 90 powder (Powerplay Isostar, Germany) in 1XTBS

Washing buffer for western blot

TBS: 50 mM Tris/HCl, pH7.8, 150 mM NaCl and 1 mM $MgCl_2$

TBST: 0.2% (v/v) Tween-20 in TBS

Western blot detection reagents

Solution A: 0.1 M Tris/HCl, pH6.8 and 50 mg Luminol sodium salt (Sigma Aldrich, Germany)

Solution B: 11 mg p-Coumeric acid (Sigma Aldrich, Germany) in 10 ml DMSO

Mix solution A and B with 3 µl fresh 30% hydrogen peroxide.

Agarose gel electrophoresis

10X TAE (Tris-Acetate EDTA) running buffer: 0.4 M Tris/HAc, pH7.4-7.6, 0.2 M NaAc, 10 mM EDTA

6X DNA gel loading dye: 2% (w/v) EDTA, 51% (v/v) glycerin, 0.04% (w/v) Bromophenol blue, pH8.0 (KOH)

Affinity chromatography for His-tagged protein

Lysis Buffer: 20 mM Tris/HCl, pH7.8, 100 mM NaCl, 10 mM Imidazol

Washing buffer: 20 mM Tris/HCl, pH7.8, 100 mM NaCl, 20 mM Imidazol

Elution buffer: 20 mM Tris/HCl, pH7.8, 100 mM NaCl, 80/125/250 mM Imidazol

Phosphate buffered saline (PBS) for GST-tagged protein: 140 mM NaCl, 2.7 mM KCl, 10 mM Na_2HPO_4, 1.8 mM KH_2PO_4

Regeneration buffer for Glutathione Sepharose:

Solution A: 0.1 M Tris/HCl, pH8.5, 0.5 M NaCl

Solution B: 0.1 M Sodium-Acetat/HCl, pH4.5, 0.5 M NaCl

2.1.5 Plant materials and growth conditions

Seeds of T-DNA insertion line of FDP (SALK 200741C) was obtained from Arabidopsis Biological Resource Center (ABRC, USA). Columbia-0 (Col-0) was used as the wild type.

GS90 soil with 0.5% confidor was used. Plants were grown in growth chambers which have long-day (LD) conditions with 16 hours light and 8 hours dark at 22°C or short day (SD) with 8 hours light, 16 hours dark at 22°C. For *Agrobacterium*-mediated transient transformation, 3-5-week-old *Nicotiana benthamiana* plants were grown in greenhouse.

2.1.6 Equipment and Software

Equipment	Company
Gel Documentation	PeQLab Biotechnologie GmbH
Heidolph MR 3001K	Heidolph, Germany
Nanodrop ND-1000 spectrophotometer	Nanodrop, Germany
-80°C Freezer	GFL, Germany

pH Meter (FE20/EL20)	Mettler Tolerado, Germany
Polymax 1040	Heidolph, Germany
Sonicator UM-2070	Bandelin electronic, Germany
Thermostat plus	Eppendorf, Germany
TPM -2	Sarstedt
Vortex-2 GENIE	Scientific Industries, Germany
Ultrospec 3100 pro	Amersham Biosciences

PCR Machine:

Mastercycler personal, Eppendorf, Germany

96 Universat Gradient PeQStar, PeQLab Biotechnologie GmbH

Weighing Machine:

Kern PLJ 730-N

Kern ABT100-5NM

Incubator:

HettCube 600R, Hettich incubator, Germany

Eppendorf Innova® 44, ermany

Centrifuge:

Eppendorf centrifuge 5415 D, Germany

Eppendorf centrifuge 5415 R, Germany

Eppendorf centrifuge 5810 R, Germany

Micro-centrifuge, FugeOne, Germany

Sorvall RC6+ centrifuge, Thermo Scientific

Sorvall RC-5B Refrigerated Superspeed centrifuge, DuPont Instruments

Eletrophoresis:

Bio-RAD POWER PAC 300

CONSORT 1200V – 500mA E815

Tranfer tank, Amershem Biosciences

Software:

CLC Main Workbench 7 – A QIAGEN® Company

Adope Illustrator CS5 – Adobe systems, USA

Adobe Photoshop CS5 – Adobe systems, USA

ImageJ – Rasband, WS, US National Institutes of Health, Bethesda, USA

Leica Application Suite X – Leica Microsystems, Germany

Leica LAS AF Lite – Leica Microsystems, Germany

2.2 Method

2.2.1 Genotyping of T-DNA insertion line of FDP

2.2.1.1 TDNA-specific PCR

10-15 seeds of T-DNA insertion line of FDP were taken in 1.5ml EP tube and kept at -80°C overnight. Next day water was added to soak seed for 4-5 hours at 4°C. Later seeds were sown on soil in 10 individual pots. Then pots were transferred to growth chamber with LD conditions. On 28th day, leaf material was harvested from each 10 pots.

Genomic DNA was extracted from half leaf material by using Edward's buffer. Finally 70 µl MilliQ water was used to suspend DNA pellet and incubated at 37°C for 7 min. 1 µl was used as PCR template. PCR was performed for 35 cycles (as described in section 2.2.2.3) with primers: FDP-Bam-F and FDP-R-tdna. Annealing temperature was 53°C.

2.2.1.2 Wildtype-specific PCR

Genomic DNA extracted (in section 2.2.1.1) was used for performing wildtype-specific PCR. 1 µl was used as PCR template. PCR was performed for 35 cycles (as described in section 2.2.2.3) with primers: FDP-F- tdna and LBb1.3. Annealing temperature was 53°C.

2.2.1.3 Reverse transcription-PCR (RT-PCR)

Four homozygous plants of T-DNA insertion line of FDP was selected to test whether there is any *FDP* expression in these plants as compared to wild type Col-0 plant. For this, shoot apices were harvested from these plants and were stored at -80°C until further use. The RNA was extracted from these samples using Nucleospin RNAII kit (Macherey-Nagel, Germany). cDNA

synthesis with equal amount of RNA from all samples was performed using Oligo (dT) primer and Reverse transcriptase (Fermentas, Germany).

Gene expression was checked by carrying out PCR on cDNA. Loading control of cDNA samples was assured by checking actin. For this, 30 cycles of PCR was performed with Actin_F and Actin_R primers with annealing at 52°C. *FDP* mRNA was checked by performing 35cycles of PCR with FDP-F-tdna and FDP-R-tdna primers at 53°C for annealing.

2.2.2 Generation of FDP overexpression transgenic plants

The plasmid encoding GFP-FDP in binary vector pPTKan was kindly provided by Nina Jaspert, AG Oecking. This plasmid was used for alanine (A) and glutamic acid (E) substitution of Threonine (T) residue at the 231 position, which is located at C-terminus of FDP. To amplify the substituted version of FDP by PCR (as described in section 2.2.3.1), the modified reverse primer having base pair for either alanine or glutamic acid was used. PCR product was run on agarose gel and band specific to the size of GFP-FDP (ca. 1.5 Kilobase pair) was cut and cleaned by commercial kit. These fragments: GFP-FDP^{T231A} and GFP-FDP^{T231E} were cloned into pPTKan binary vector by restriction-based cloning. The presence of desired insert was confirmed by restriction digestion analysis and finally by sequencing.

The pPTKan plasmids encoding, GFP-FDP, GFP-FDP^{T231A} and GFP-FDP^{T231E} were transformed in *Agrobacterium* chemical competent strain, GV3101. Glycerol stock of *Agrobacterium* cells containing plasmid pGTKan, which encodes free GFP, was kindly provided by Christian Throm, AG Oecking). Approximately 200-300 ng of each plasmid was added to tube containing thawed competent cells on ice. The tube was incubated on ice for 5 min, followed by deep freezing in liquid Nitrogen for another 5 min. Then the cells were kept at 37°C for 5 min. Later 600-1000 µl of LB medium was added. The cells were then incubated at room temperature for 2-3 hours and afterwards plated on LB agar plate with appropriated antibiotics (in section 2.2.6). Plate was incubated at 28°C for 2 days.

A single colony for each construct was inoculated in 5 ml of LB with appropriated antibiotics and incubated for ca. 16 hours 28°C with rotation on rotor. 5 ml bacterial culture was inoculated into 1 liter flask containing 200 ml LB medium with antibiotics. The flask was incubated at 28°C overnight at 180 rpm for 16-20 hours.

Another day, bacterial culture was centrifuged at 4,000 rpm for 15 min. Pellet was washed with MilliQ H_2O by centrifugation for 15min. Then resuspended in Transformation medium (Half MS with basal salt mixture, 5% Saccharose, 150 µl/L Silwet L-77).

fdp knock-out plants were grown on pot with diameter 11 cm for each constructs. These plants were grown in growth chamber under LD conditions until there was many inflorescence stems. Floral dip method was performed to generate stable *Arabidopsis* transgenic plants (Clough & Bent, 1998). Inflorescences of plants were dipped in *Agrobacterium* suspension for 30 to 60 sec. Then plants were covered with plastic bags and kept in dark overnight and transferred to LD chamber. Plants were grown until seed were mature to harvest.

2.2.3 Preparation of DNA constructs

2.2.3.1 Amplification of gene of interest

Gene of interest was amplified with High fidelity Phusion polymerase (Thermofischer Scientific, Germany).

Component	50 µl reaction
5X Phusion HF buffer	10 µl
10 mM dNTPs	1 µl
10 pmol forward primer	1 µl
10 pmol reverse primer	1 µl
Phusion DNA polymerase	0.5 µl
Template DNA	1.5 µl
MilliQ H_2O	35 µl

The reaction mix was given a quick spin. Tubes were transferred from ice to PCR machine and begin thermocycling with following conditions:

Step	Temperature	Time
Initial denaturation	98°C	30 sec
35 cycles	98°C	10 sec
	50-65°C	30 sec
	72°C	30 sec/Kb
Final extension	72°C	10 min
Hold	20°C	

After thermocycling, 6X DNA gel loading dye was added. All reaction was loaded on agarose gel (0.8% agarose in TAE). Band corresponding to the size of gene of interest was cut from gel and purified by using PCR purification kit.

2.2.3.2 Ligation

Prior to use for ligation, vector and insert were digested by desired restriction enzymes and then cleaned PCR purification kit. 1 µl T4 DNA ligase (Thermofisher Scientific, Germany), 1 µl T4 DNA ligase buffer, vector and insert in molar ratio of 1:10. The reaction mixture was incubated at 14°C or 16°C overnight. 3-4 µl ligation reaction was transformed into XL-1B chemical competent cells by performing Heat-shock incubation at 42°C for 90 seconds. 1ml LB medium was added and incubated at 37°C for 1 hour. 500 µl was plated LB + Agar plate containing appropriate antibiotics. Presence of insert in clones was checked either by Colony PCR or restriction digestion. For restriction digestion, individual clones were incubated in LB medium with appropriate antibiotics at 37°C overnight. Another day, culture was suspended and plasmid was isolated either by applying Birnboin and Doly method (section 2.2.3.4) or by using manufacturer's plasmid miniprep kit (section 2.2.3.6). Isolated plasmid was incubated with specific restriction enzyme at 37°C for 1 hour and checked on agarose gel electrophoresis for specific band. Finally, the construct was sequenced to confirm the correctness of gene of interest. The sequencing was performed by a commercial supplier – GATC, Constance, Germany.

2.2.3.3 Gateway cloning

Adaptor PCR to generate PCR product containing *att*B sites

First PCR Components:

5X Phusion HF buffer – 10 µl, 10 mM dNTPs - 0.5 µl, 10 pmol *att*B forward primer_insert specific - 0.5 µl, 10 pmol *att*B reverse primer_insert specific - 0.5 µl, Phusion DNA polymerase – 0.5 µl, MilliQ H_2O – 36.5 µl, template – 1.5 µl

PCR program: 95°C (initial denaturation) – 2min, 10 cycles of (94°C – 15 sec, 62°C – 30 sec, 72°C – 30 sec)

Second PCR's components:

5X Phusion HF buffer – 40 µl, 10 mM dNTPs - 0.4 µl, 40 pmol *att*B forward primer - 0.4 µl, 40 pmol *att*B reverse primer - 0.4 µl, Phusion DNA polymerase – 0.4 µl, MilliQ H_2O – 30.4 µl, template – 10 µl of 1st PCR

Second PCR program: 95°C (Initial denaturation) – 1min, 5 cycles of (94°C – 15 sec, 45°C – 30 sec, 72°C – 30 sec), then 20 cycles of (94°C – 15 sec, 55°C – 30 sec, 72°C – 30 sec)

After thermocycling, 6X DNA gel loading dye was added. All reaction was loaded on agarose gel (0.8% agarose in TAE). Band corresponding to the size of gene of interest was cut from gel and purified by using PCR purification kit.

BP reaction

The BP recombination reaction was performed between insert flanking *att*B sites and appropriate *att*P-containing donor vector (pDONOR221 p1p4, pDONOR221 p3p2, or pDONOR201 p1p2) to generate an entry vector. This reaction was carried out using BP Clonase II Enzyme mix (Invitrogen, USA) as per manufacturer's instructions. The BP reaction:

Donor vector – 0.25 to 1.0 µl (75 ng)

*att*B-PCR product – 2 to 3 µl

BP Clonase II Enzyme mix – 0.5 to 1 µl

MilliQ H_2O – upto 3-5 µl

Reaction was incubated at 25°C for 1-2 hours. 0.5 µl of Proteinase K was added to terminate the reactions by incubating reaction at 37°C for 10 min.

3 µl of BP reaction was transformed into bacterial Top10 chemical competent cells by heat shock (42°C for 45 sec). 250 µl of LB medium was added and incubated at 37°C for 1 hour. All transformation was plated onto LB Agar plate containing appropriate antibiotic. Presence of insert and its correct orientation was first confirmed by ColonyPCR and then by sequencing.

LR reaction

LR recombination reaction was performed between one and two pEntry vectors and Gateway destination vector with one expression cassette and two expression cassettes containing 2in1 vectors, respectively. The reaction was carried out using LR clonase II plus Enzyme mix (Invitrogen, USA) to generate expression vector. Again, presence of insert and its correct orientation in expression vector was first confirmed by colony PCR and then by sequencing.

Entry vector – 0.5 µl (50 ng/µl)

Destination vector – 0.5 µl (100 ng/µl)

LR Clonase II Enzyme mix – 0.5 µl

MilliQ H$_2$O – 0.5 µl

Reaction was incubated at 25°C for 2 hours (for one entry vector) or at 16°C overnight (for two entry vectors). 0.5 µl of Proteinase K was added to terminate the reactions by incubating reaction at 37°C for 10 min. Transformation into bacterial Top10 chemical competent cells as described in BP reaction. All transformation was plated onto LB Agar with X-gal and appropriate antibiotics. Plate was incubated at 37°C overnight. White colonies were supposed to be transformed clones. Thus these clones were picked for presence of gene of interest.

2.2.3.4 Colony PCR

Clones from selection plate were picked and suspended in 20 µl MilliQ water. 5 µl suspension was used as template for PCR. PCR was performed with *Taq* polymerase (New England Biolabs, UK) as followed:

Component	25 µl reaction
10X Standard *Taq* buffer	2.5 µl
10 mM dNTPs	0.5 µl
10 pmol forward primer	0.5 µl
10 pmol reverse primer	0.5 µl
Taq DNA polymerase	0.125 µl
Template	5 µl
MilliQ H$_2$O	20 µl

The reaction mix was given a quick spin. Tubes were transferred from ice to PCR machine and begin thermocycling with following conditions:

Step	Temperature	Time
Initial denaturation	95°C	2 min
	95°C	30 sec
35 cycles	50-65°C	30 sec
	68°C	1 min/Kb
Final extension	68°C	5 min
Hold	20°C	

2.2.3.5 Plasmid extraction by Birnboin and Doly method

Overnight bacterial culture was centrifuged at 10,000 rpm for 1 min. Pellet was resuspended in Solution I, followed by addition of Solution II with RNase I and Solution III. Mix was centrifuged at 14,000 rpm for 15 min at 4°C. Supernatant was transferred to fresh EP tube and additional 700 µl 100% ethanol was added. EP tube was inverted up and down 5-6 times and centrifuged again at 14,000 rpm for 12 min at 4°C. P at the bottom was visible, which was washed with 70% ethanol at 14,000 rpm for 5 min at 4°C. DNA pellet was dried at 60°C for 5-6 min and resuspended in 50 µl MilliQ H_2O. For use as PCR template, plasmid was diluted in 1:500 and 1 µl was taken.

2.2.3.6 Plasmid cleaning by manufacturer's kit

DNA fragment and plasmid construct was cleaned to get rid of impurities by manufacturer's kit (Nucleospin Gel and PCR Clean, Macherey-Nagel, Germany).

2.2.3.7 Plasmid extraction by manufacturer's kit

For clean and grade plasmid, plasmid miniprep kit was used according to the instructions provided by manufacturer (Thermofisher Scientific, Germany).

2.2.4 Recombinant protein expression and purification

2.2.4.1 SDS-PAGE

Prepare the resolving gel with components in section 2.1.4. When the gel was solidified then stacking gel was casted on the top with comb to create wells. Cast gels were directly used or stored at 4°C until further use within a week. Protein samples were mixed with sample buffer (2x or 4x) and boiled, then loaded on gel with protein marker (Roti®-Marker Standard; Roth, Germany). The gel was dipped into the running buffer and was run at 20 mA (1 gel) or 40 mA (2 gels) for ca. 1 hour. Afterwards, either the gel was visualized by Coomassie blue staining or used for western blot analysis.

2.2.4.2 Western blot

For western blot, the protein was transferred from gel to the nitrocellulose membrane. For transfer, the gel was put on the top of membrane in blot transfer buffer and kept in transfer tank (Amersham Biosciences, Germany). The transfer was run at 200 mA for 90 min. Afterwards blot membrane was quickly checked for a successful transfer by Ponceau S staining. Then blot was was washed with water and blocked either with 1% BSA or 2% high protein powder at room temperature (RT) for 1 hour. This was followed by incubation with primary antibody either for 1 hour or at 4°C for overnight. Then the blot was washed 2 times with TBS buffer and the third time with TBST buffer. Blot was incubated with secondary antibody conjugated with HRP for 1 hour at RT. Blot was washed. The signal was detected by lab made detection reagents (section 2.1.4) by Amersham imager600 (GE Healthcare, Germany).

2.2.4.3 Expression of MBP-FDP fusion

The open reading frame (ORF) of FDP was codon-optimized by the commercial supplier (Life Technologies, Germany) for expression in *Escherichia coli*. The ORF was flanked by the unique restriction enzymes (BamHI and SalI) for cloning into the expression vector. The pET28-(His)$_8$-MBP expression vector was kindly provided by Michael Fitz, AG Schaff. The codon- optimized version of FDP was cloned into pET28-(His)$_8$-MBP by restriction based cloning. The presence of FDP and correct orientation was validated by sequencing.

This vector has allowed the expression of 8xHis-MBP fused to N-terminus of FDP (termed as MBP-FDP). The phosphomimic version FDP^{T231E} was generated using FDP as a template and primer pair allowing a single mutation. The gene of interest was amplified by PCR and PCR product was loaded on agarose gel. The band corresponding to the size of FDP was cut and cleaned by Gel Purification kit (section 2.2.2.5). The cleaned fragment was cloned into pET28-(His)$_8$-MBP vector by using unique restriction enzymes. The expression conditions of fusion protein were optimized.

The bacterial expression strain, BL21-CodonPlus RIL, was transformed with plasmid encoding FDP versions separately via heat shock incubation.

For optimized protein expression, a single colony was picked and inoculated in 5 ml LB medium with antibiotics. The colony was incubated overnight at 37°C at 180 rpm. Overnight bacterial culture was inoculated into 250-300 ml LB with appropriate antibiotics in a 1 liter flask. The bacteria were allowed to grow until OD600 of 0.5 to 0.8 was reached. Then culture was induced by 0.5 mM of IPTG and incubated at 16°C overnight. Another day the culture was centrifuged and either stored at -80°C until further use or used directly for protein extraction.

For protein extraction and purification, bacterial cell pellet was suspended in cold lysis buf (1:10) containing 1mg/ml lysozyme (section 2.1.4) and kept on ice for 25-30 min. The cell was further lysed by sonication. Afterwards, it was centrifuged at 15,000 rpm for 20-30 min at 4°C. Supernatant was mixed together with Ni-NTA resin (1 ml for 8-10 mg of protein; Qiagen, Germany) pre-equilibrated with lysis buffer without lysozyme and for a better protein binding; mix was rotated gently on rotor for 3-4 hours or overnight at 4°C. Then flow through was collected by gravity flow. The column was washed with washing buffer containing 10 mM imidazole. The desired protein was eluted subsequently with elution buffer containing 80 mM, 125 mM and 250 mM imidazole. The elution buffer of fusion protein was exchanged with storage buffer (50 mM Tris, pH7.5 and 100 mM KCl) and concentrated by using concentrator Vivaspin20 with 30 kDa cut-off (Sartorius, Germany). The concentrator was centrifuged at 1,000 to 2,500 rpm for several minutes (ca. 30 – 60 min) until the desired concentration was reached. The concentrated protein was either used freshly in pull-down assays or stored at -80°C until further use.

2.2.4.4 Expression and purification of 6xHis-T14.3c

6xHis-T14.3c in pQE30 vector was expressed in M15 chemical competent cells by Heat shock incubation and plated on LB agar plate with appropriate antibiotics and incubated overnight at 37°C.

For protein expression and purification, a single colony was picked and inoculated in LB medium with antibiotics. Rest was done as for the expression MBP-FDP fusion protein. Here, washing buffer has 20mM imidazole and elution buffer containing 125 mM and 250 mM imidazole was used. 100% glycerol was added to protein eluate in order to make a final concentration of 40%. Several aliquots were made and stored at -20°C until further use.

2.2.4.5 GST tagged protein expression and purification

GST, GST-FT and GST-TFL1, which were cloned in pGEX-4T vector, were kindly provided by Nina Jaspert, AG Oecking. These proteins were expressed as a GST-fusion protein in *E. coli* strain, BL21-CodonPlus RIL. The expression procedure was followed as done for MBP-FDP fusion expression.

For protein extraction and purification, the cell was lysed in PBS + lysozyme by incubating on ice for 30 min. The cells were further lysed by sonication (5-7times for 20 sec at 55% power) until cells were clear. Then cells were centrifuged at 15,000 rpm for 20-30 min at 4°C. The supernatant was loaded on Glutathione Sepharose T™ 4 Fast Flow resin (GE Healthcare, Germany), which was pre-equilibrated with PBS. The flow through was collected and resin was washed with PBS. The protein bound to resin was eluted with 10 mM reduced glutathione. The glutathione from purified protein was gotten rid of by exchanging against 50 mM Tris buffer with pH8.0 by using Vivaspin 20 concentrator with cut-off 30 kDa (Sartorius, Germany). For GST only, concentrator with cut-off 10 kDa was used. Concentration of proteins was measured by using Roti-Nanoquant reagent (Roth, Germany) as per manufacturer's instructions and proteins were stored in several aliquots at -80°C until further use.

2.2.5 *In vitro* pull-down Assays

For pull-down assays, recombinant proteins were expressed in *E. coli* expression strains. Proteins were purified, and the concentration of each fusion protein was determined using modified Bradford assays with Roti-Nanoquant reagents.

2.2.5.1 MBP pull-down assay

First the amylose resin (New England BioLabs, UK) was washed with 500 μl buffer. Then 4.5 nmol recombinant purified MBP-tagged proteins were incubated with 30 μl amylose resin for 30 min at 4°C on rotor. MBP tag alone was expressed, purified and used as a negative control. After 30 min, the resin was washed to get rid of unbound excess protein. This was followed by addition of incubation buffer (25 mM MOPS, 25 mM NaCl, 0.05% B-mercaptoethanol, 0.1% Triton X-100 and 5 mM $MgCl_2$) and 2.25 nmol 6xHis-T14.3c protein. Again, the resin was incubated for another 30 min at 4°C on rotor. Later the resin was washed 3times with 500 μl incubation buffer each time and fourth times with washing buffer (20 mM MOPS, pH6.5). 30 μl sample buffer (2X) was added to resin and boiled at 95°C for 5 min. The sample was loaded on SDS-PAGE gel and gel was transferred to nitrocellulose membrane (Portran BA 85; GE Healthcare Life Sciences Whatman, Germany). 6xHis-T14.3c was probed with anti-RGS-(His)$_6$ antibody (1:2000; Qiagen, Germany). Anti-Mouse-HRP (1:10,000 to 20,000) was used as secondary antibodies. Equal loading of MBP fusion protein was assured by Ponceau S staining.

2.2.5.2 Glutathione S-transferase (GST) pull-down assay

For GST pull-down, 25 μl Sepharose beads was taken and washed with buffer. Then 1.125 nmol recombinant purified GST-tagged proteins were incubated with beads for 30 min at 4°C on rotor. GST tag alone was expressed, purified and used as a negative control. After 30 min, the resin was washed to get rid of unbound excess protein. To avoid unspecific binding, beads were blocked by incubating with 5% BSA (Bovine Serum Albumin; Sigma Life Science, Germany) at RT, 10 min and another 20 min at 4°C. This was followed by addition of incubation buffer. 2.25 nmol RGS-(His)$_6$-T14.3c protein for two protein interaction investigation, while additional 4.5 nmol MBP-FDP^{T231E} was added to study ternary complex formation. Again, the resin was incubated for

another 30 min at 4°C on rotor. Later the resin was washed 4times with 500 µl wash buffer and fifth times with Tris buffer. 30 µl sample buffer (2X) was added to resin and boiled at 95°C for 5 min. The sample was loaded on SDS-PAGE gel and later gel was transferred to nitrocellulose membrane. 6xHis-T14.3c was probed with anti-RGS-(His)$_6$ antibody (1:2000; it binds exclusively to RGS epitope), while MBP-FDP^{T231E} was detected by anti-(His)$_6$ (1:1000; Roche, Germany) antibody. Anti-Mouse-HRP was used as secondary antibodies. Equal loading of GST fusion protein was assured by Ponceau S staining.

Incubation (TDM) buffer	Wash buffer	Last washing with buffer
10mM Tris/HCl, pH7.5	20mM MOPS, pH6.5	50mM Tris, pH6.5
1mM DTT	20% glycerin	
5mM MgCl2	1mM DTT	
5% BSA	100mM KCl	
---	0.05% Tween20	

2.2.6 Transient Agrobacterium transformation of *N. benthamiana*

Agrobacterium tumefaciens strain, GV3101 (Koncz and Schell, 1986) with binary vector or 2in1 rBiFC/colocalization/FRET vectors containing gene of interests was transformed (Grefen and Blatt, 2012). A single colony was picked and inoculated in 3-5 ml LB medium containing antibiotics: 15 µg/ml gentamycin, 5-10 µg/ml rifampicin and 100 µg/ml spectinomycin. Culture was grown at 28°C overnight with gentle rotation. Next day, 200-250 µl overnight culture was dispensed into 4-5 ml fresh LB medium having appropriate antibiotics and further incubated at 28°C for about 3.5 to 4 hours. Afterwards culture was centrifuged at 4,000 rpm for 5 min and followed by washing with MilliQ water at 4,000 rpm for 5 min. Washed culture was then re-suspended in Agroinfiltration medium (10 mM MES/KOH, pH5.6, 10 mM MgCl$_2$, 150 µM Acetosyringone) and final OD$_{600}$ was maintained to 0.2 for rBiFC and colocalization studies, and 0.15 for FRET-FLIM measurement. Then the culture was kept on ice for 40-60 min and infiltrated into leaves of 3- to 4-week-old *N. benthamiana* plants by using 1 ml syringe (Schoeb *et al*., 1997; Sparkes *et al*., 2006). Plants were kept in dark for overnight. Next day plants were moved to light in constant day chamber for 7 to 8 hours and then moved back to dark. Leaves were

observed under confocal laser scanning microscope SP8 (Leica Microsystems, Germany) for rBiFC and colocalization. For FRET-FLIM, the same confocal equipped with all the necessary additional FLIM setup was used.

2.2.7 Confocal microscopy for rBiFC, colocalization and FRET-FLIM

For all experiments, Confocal laser scanning microscope SP8 (Leica Microsystems, Germany) was used.

2.2.7.1 Ratiometric Bimolecular Fluorescence Complementation (rBiFC)

For rBiFC, genes of interests containing donor vectors were cloned into destination vector (V258, 2in1 vector) by LR reaction.

Figure 2. 1: A schematic representation of 2in1 rBiFC vector. pBiFCt-2in1-CN (V258) allows the C-terminus nYFP and N-terminus cYFP fusion to gene of interests under the control of constitutive 35S promoter. It encodes additional RFP under the same promoter.

These vectors were transformed into *N. benthamiana* leaves mediated by *Agrobacterium*. Approximately, 44 to 48 hours post-infiltration, two slices from two independent infiltrated tobacco leaves were observed under confocal microscope. For each experiment, confocal settings were kept identical for image acquisition – objective, laser power, zoom factor, gain setting. These settings were used – yellow fluorescent protein (YFP) was excited at 512 nm wavelength and detected in 520-545 nm emission range. Monomeric red fluorescent protein (RFP) was excited at 561 nm and emission range was 585-620 nm. The 40X objective for bigger image field and resonant scanner was used for faster image acquisition. For ratiometric analysis, each image was further exported as .tif format to be analyzed by Image J program. Since YFP reconstitution takes place in nucleus, nuclear intensity for YFP and RFP signal was measured in

nuclei by using ImageJ program. Each nucleus was selected as region of interest (ROI) to measure the intensity of fluorescence signal. The identical area of ROI was used for YFP and RFP to calculate YFP/RFP signal intensity ratio in Microsoft excel.

2.2.7.2 Colocalization and fluorescence intensity analysis

For colocalization studies, gene of interests containing donor vectors were cloned into destination vector (old V322, pFRETgc-2in1-CN) by LR reaction. The only difference in old V322 is the presence of enhanced green fluorescent protein (eGFP) instead of monomeric eGFP (mEGFP). These vectors were transformed into *N. benthamiana* leaves mediated by *Agrobacterium*. Approximately, 44 to 48 hours post-infiltration, two slices from two independent infiltrated tobacco leaves were observed under confocal microscope. For each experiment, confocal settings were kept identical for image acquisition - objective, laser power, zoom factor, detector gain. eGFP was excited at 488 nm wavelength and detected in 500-530 nm emission range. Fluorescent protein, mCherry, was excited at 561 nm and emission range was 585-625 nm. The 40X objective for bigger image field and resonant scanner was used for faster image acquisition. Scanning was performed in sequential mode to avoid bleed-through artefact. For nuclear accumulation analysis of 14-3-3-eGFP, FT-eGFP and TFL1-eGFP upon coexpression of mCherry fused to FDP and its substitution mutants, each confocal image was further exported as .tif format to be analyzed by Image J program. This analysis was done as described in Taoka *et al* (2011). A region of interest (ROI) was drawn around each nucleus and the mean fluorescence was measured for both GFP and mCherry channel. Additionally, the GFP and mCherry intensity of whole cell was measured. The obtained data were analyzed for box plot distribution and then subjected to a paired Student's t-test in Microsoft Excel.

Modification of subcellular localization of FT and TFL1 by 14-3-3 protein was analyzed by quantifying nuclear/cytoplasmic ratio, as described in Giska *et al.* (2013).

The pFRETgc-2in1-CN (V319) colocalization vector, containing FT-mEGFP or TFL1-mEGFP together either with 14-3-3-mCherry, NLS-mCherry or 14-3-3-NLS-mCherry were constructed by gateway cloning. These vectors containing specific pair each were transformed in

Agrobacterium, followed by infiltration in *N. benthamiana* leaves at the same day for direct comparison.
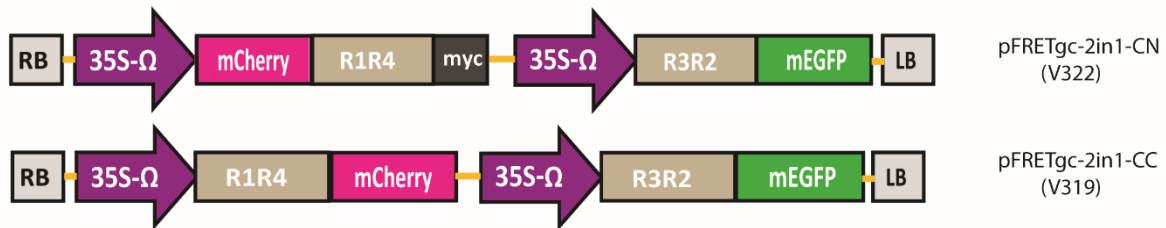
Figure 2. 2: A schematic representation of 2in1 colocalization and FRET vectors. pFRETgc-2in1-CN (V322) allows the N-terminus mCherry and C-terminus mEGFP fusion to gene of interests under the control of constitutive 35S promoter. pFRETgc-2in1-CN (V319) allows C-termini fusion to gene of interests under 35S promoter control.

Confocal images were acquired at identical settings and exported as .tif file for ImageJ analysis. In each cell, 3 ROIs each for nucleus, cytosol and background were selected for fluorescence intensity analysis. Average from 3 ROIs background fluorescence intensity was subtracted from nuclear and cytosolic intensity. Then nuclear and cytosolic intensity were averaged and nuclear/cytoplasmic ratio was obtained. These calculations were done in Microsoft Excel and result is shown as bar graph with standard deviation.

2.2.7.3 Förster Resonance Energy Transfer-Fluorescence Lifetime Imaging Microscopy (FRET-FLIM)

FRET-FLIM experiments were done as previously described in Hecker *et al*. (2015). Genes of interests containing donor vectors were cloned into destination vector (V322, 2in1 vector) by LR reaction. The V322 vector has mEGFP instead of eGFP. Monomeric eGFP was obtained by A206K substitution. It has advantages of not forming dimers and thus overcomes any possible artefacts coming from the interactions between probes themselves. This version was more suitable for FRET-FLIM measurement.

These vectors were transformed into *N. benthamiana* leaves mediated by *Agrobacterium*. Approximately, 42-48 hours post-infiltration, two slices from two independent infiltrated

tobacco leaves were observed under confocal microscope for lifetime measurement. For image acquisition and visualization, these confocal settings were used - mEGFP was excited at 488 nm wavelength and detected in emission range 500-530 nm. mCherry was excited at 561 nm and emission range was 585-625 nm. The 60X objective and normal scanner was used for image selection. The lifetime (ns) of either the donor only or donor-acceptor pairs expressing cells was measured with a pulsed laser as an excitation light source of 473 nm and with repetition rate of 40 MHz (PicoQuant Sepia Multichannel picosecond diode laser, PicoQuant Picoharp 300 TCSPC module, and Picosecond event timer). 500-530 nm Emission range was taken. The acquisition was performed until 500 photons in the brightest pixel were obtained. To obtain the donor (GFP) fluorescence lifetime, FLIM data was processed with SymPhoTime software (Picoquant, Germany). Biexponential curve fitting was calculated by taking measured instrument response function (IRF) for the correction and a fitting channel range from 0.03 to ≥ 20 nanoseconds.

2.2.7.4 For competition between FT and TFL1

Adaptor PCR was performed to create attB1 and attB2 sites for cloning in gateway donor vectors. FT and TFL1 flanking attB1 and attB2 sites were cloned each in donor vector, pDONR201-P1P2, by BP reaction. Presence of insert was confirmed by colony PCR and sequencing (GATC, Germany). Then this entry vector was used in LR reaction to transfer insert (FT or TFL1) into destination vector, pK7CWG2, having eCFP at the C-terminal (Karimi *et al.*, 2002). Presence of insert in destination was confirmed by colony PCR and sequencing. For competition between FT and TFL1, 2in1 vectors were used (Fig **2.2**). These vectors allow N-terminally fusion of mCherry to either FDP^{T231E} or FDP^{T231A} or NLS (nuclear localization signal, Hecker *et al.*, 2015) and mEGFP fused C-terminally to FT. 2in1 vectors were transformed in the absence or presence of FT- or TFL1-eCFP fusion in the *N. benthamiana* leaves and subjected to FRET-FLIM measurement as described above. For eCFP, excitation at 458 nm and emission range from 561-580 nm was set.

2.2.7.5 Heterotrimeric complex formation

The nuclear localization signal (NLS) was included to the 3' end of 14-3-3 by adding the amino acid sequence LQPKKKRKVGG with the help of modified PCR reverse primer (Genoud et al., 2008). 14-3-3-NLS version was cloned into pDonor vector and finally in 2in1 colocalization destination vector together with FT or TFL1. For heterotrimeric complex analysis by means of FRET-FLIM, this 2in1 vector in the presence of absence of eCFP-FDP was agroinfiltrated in *N. benthamiana* leaves. 42-46 hours post-infiltration, FRET-FLIM as well as Co-IP experiments were performed.

2.2.8 Co-immunoprecipitation (Co-IP) Assay

For Co-IP assay, *N. benthamiana* leaves transiently expressing constructs of choice were harvested 44-48 hours post infiltration. Leaf material was either stored at -80°C after freezing in liquid nitrogen (N$_2$) for later use or ground to fine powder in N$_2$ with mortar and pestle.

1 ml Extraction buf (50 mM HEPES, pH7.4, 50 mM NaCl, 10% glycerol, 1 mM PMSF, 2mM DTT, 1% NP-40 (IEGPAL), protease inhibitor cocktail (oComplete Roche, 1 tablet/50 ml) per mg of plant material was added directly in mortar. The powder was mixed thoroughly in buffer and let it thaw for around 15-20 min in cool room with temperature 4°C to 10°C. The extract was transferred to 2 ml Eppendorf (EP) tubes and centrifuged for 15 min at 13,200 rpm at 4°C. Supernatant was transferred to new 2 ml EP tube and centrifuged again at the same speed for 10 min to get rid of any remaining big particles. Then 2 ml supernatant was incubated with 20 µl pre-washed GFP trap or RFP trap (Chromotek, Germany) for immunoprecipitation. This was incubated for 2 hours at 4°C with gentle rotation. Immunoprecipitates were washed three times with wash buffer (= extraction buffer without PMSF) and once with extraction buffer with only HEPES, NaCl and glycerol.

The sample was loaded on SDS-PAGE gel and later gel was transferred to nitrocellulose membrane. IP and Co-IP was probed with primary antibodies: anti-RFP-Rat (1:1100; Chromotek, Germany), anti-HA-Rat (1:2000; Roche) and anti-GFP (1:5000; Torrey pines). Secondary antibodies conjugated to horseradish peroxidase (HRP): anti-Rabbit (1:10,000; Promega, Madison, USA). Some images for immunoprecipitates were enhanced using Adobe Photoshop

software for improved signal visualization and for thesis pictures were organised using Adobe illustrator.

3. Results

The FLOWERING LOCUS T (FT) is the florigenic component and is crucial for the photoperiodic flowering regulation (Corbesier *et al.*, 2007). In *Arabidopsis*, it requires the basic zipper (bZIP) transcription factor, FD, in the shoot apical meristem (SAM) to activate the floral identity genes such as *APETALA1* (Abe *et al.*, 2005; Wigge; *et al.*, 2005). Besides *FD*, its paralog, *FDP*, is genetically important in FT signaling (Jaeger *et al.*, 2013). In rice, it has been demonstrated that 14-3-3 protein mediates the interaction between HEADING DATE 3a and OsFD1, orthologs of FT and FD, respectively (Taoka *et al.*, 2011). However, it is unclear whether 14-3-3 also mediates interaction between *Arabidopsis* FT and FD/FDP. Also the molecular mechanism of TERMINAL FLOWER 1 (TFL1), which is closely related to FT, during floral transition remains unknown. Here, I present the cell biological and biochemical evidences showing complex formation among floral regulators - FDP, 14-3-3 and FT or TFL1. Altogether, this provides evidence, which gives first insights into the differential molecular mechanisms of FT and TFL1.

3.1 FDP interacts with floral regulators - 14-3-3, FT and TFL1 in a phosphorylation-dependent manner

It has been demonstrated by Abe *et al.* (2005) that both FD and FDP have a conserved 'STAPF-COOH' motif at the C-terminus and Threonine (T) in this motif is the site of potential phosphorylation by kinases such as calcium-dependent protein kinases (CPKs). Furthermore, they found that the substitution of T by a non-phosphorylatable amino acid, Alanine (A), abolished the interaction between FD and FLOWERING LOCUS T (FT) suggesting the importance of phosphorylation for FD interaction. Recently the calcium-dependent protein kinase, CPK33, which phosphorylates Threonine within the STAPF motif of FD and FDP, was described (Kawamoto *et al.*, 2015a; Kawamoto *et al.*, 2015b). The yeast two-hybrid (Y2H) screen in our lab has isolated FD and FDP as the potential interaction partners of 14-3-3 proteins. A further Y2H assay has demonstrated that the threonine substitution for alanine disrupted the interaction of FD and FDP with 14-3-3. However, the replacement with a phosphomimic amino acid, glutamic acid (E), allows for the interaction (data not shown here). This assay demonstrates that the

'STAPF' motif is crucial for 14-3-3 binding in yeast. This STAPF motif represents the canonical 14-3-3 binding mode I - (R/K)SX(pS/pT)XP (Yaffe *et al.*, 1997).

To validate whether the protein-protein interaction of FDP and 14-3-3 proteins is detectable *in planta*, I approached ratiometric Bimolecular Fluorescence Complementation (rBiFC) assay. This assay is based on a novel gateway compatible '2in1 cloning vector,' developed and described by Grefen and Blatt (2012). The 2in1 rBiFC vector comprises two expression cassettes, each driven by *Cauliflower mosaic virus* (*CaMV*) *35S* promoter. This vector allows the expression of two proteins fused to N- and C- terminal eYFP (enhanced yellow fluorescent protein) halves on a single vector backbone (Fig. **2.1**). Furthermore, it facilitates additional expression of red fluorescent protein (RFP) under the same promoter. This vector ensures the equal gene dosage and provides RFP signal for internal expression control and ratiometric/quantitative analysis. This increases the credibility of result in comparison to the classical BiFC assay (Grefen and Blatt, 2012). Y2H experiments in our lab could show the interaction of 14-3-3omega (14-3-3Ω, a 14-3-3 protein) with FDP and FT. The rBiFC vector expressing the C-terminal eYFP half fused to the N-terminus of FDP (cYFP-FDP) and its mutants, and the N-terminal eYFP half fused to the C-terminus of 14-3-3Ω (14-3-3Ω-nYFP) was transiently coexpressed in *Nicotiana benthamiana* leaves via *Agrobacterium*-mediated transformation. The reconstitution of YFP fluorescence was observed in the nucleus upon expression of 14-3-3Ω-nYFP together with wild-type cYFP-FDP and the phosphomimic version cYFP-FDP^{T231E}. However, no YFP signal was visible upon coexpression with a non-phosphorylatable cYFP-FDP^{T231A} mutant, which is a biological negative control (Fig. **3.1.1A**). Furthermore, the YFP fluorescence signal was quantified relative to the nuclear expression of RFP signal (Fig. **3.1.1B**). It is displayed as graph in term of 'relative fluorescence intensity (YFP/RFP)' and the mean was obtained from more than 27 nuclei of epidermal cells from two independent leaves. The mean relative fluorescence intensity for combinations of FDP–14-3-3Ω (mean ± sd = *81.5 ± 18.4%*) and FDP^{T231E}–14-3-3Ω (*121.2 ± 26.5%*) is significantly higher as compared to FDP^{T231A}–14-3-3Ω (*10.5 ± 4.4%*) (Fig. **3.1.1B**). In addition, the YFP/RFP fluorescence for the 14-3-3Ω association to FDP^{T231E} is higher as compared to wild-type FDP. This is consistent with the observation that 14-3-3 proteins interact mostly with the phosphorylated target proteins. It can also be possible that the respective kinase in *N. benthamiana* is unable to phosphorylate all the target FDP protein molecules.
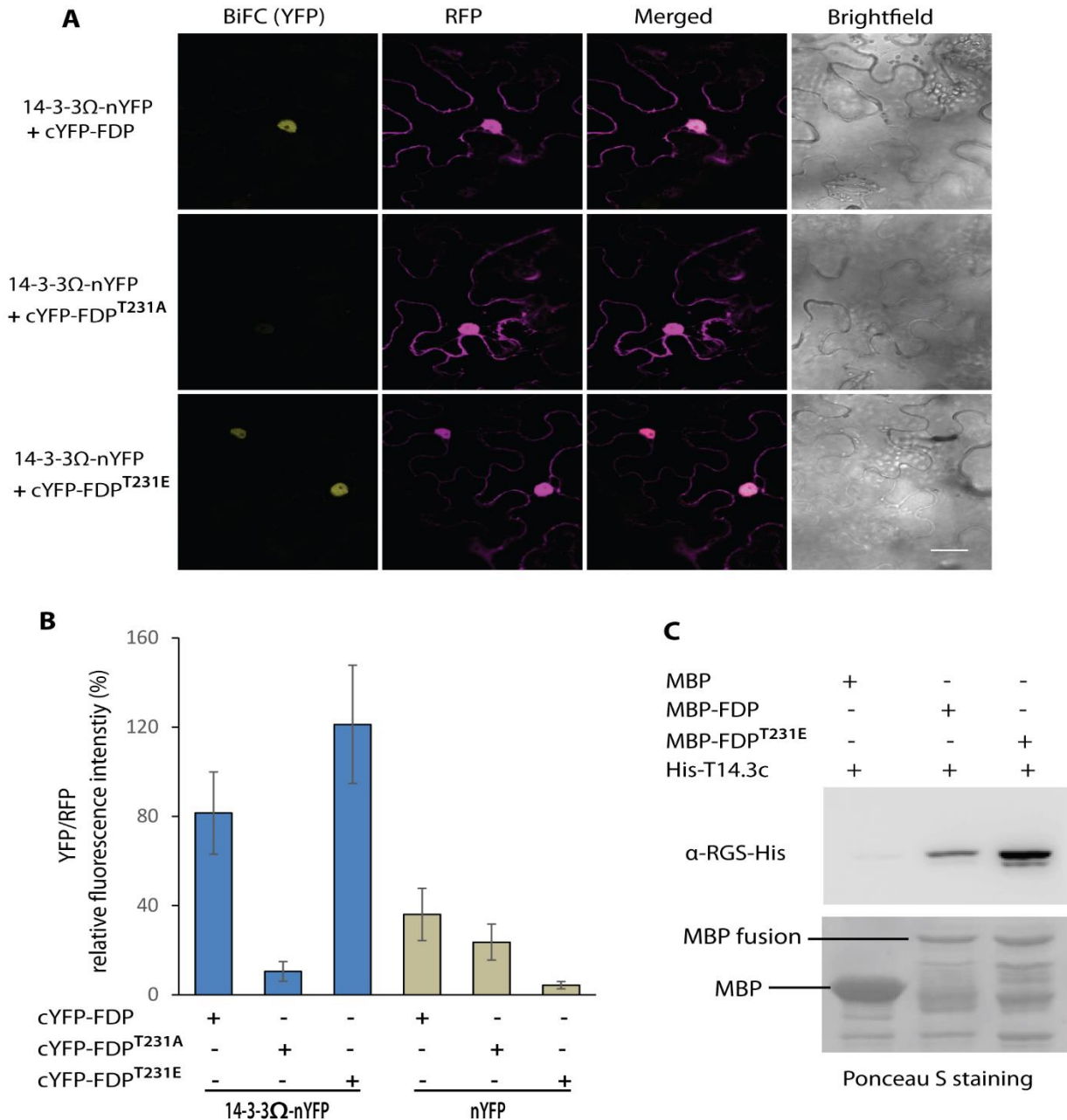
Figure 3.1. 1: Interaction studies of FDP and 14-3-3 *in vivo* and *in vitro*. **A,** confocal images depicting the BiFC fluorescence signal in the nucleus of leaf epidermal cells of *N. benthamiana* 2days after *Agrobacterium*-infiltration of FDP wildtype, its substitution mutants, FDP^T231A or FDP^T231E, with 14-3-3omega (14-3-3Ω). RFP fluorescence was used as expression control and for ratiometric analysis. Scale bar, 25 μm. **B,** Bar chart illustrating the relative fluorescence intensity of YFP ratioed to RFP signal against the constructs shown in **A**. Data shows mean ± sd (standard deviation) obtained from ≥ 27 nuclei from two independent infiltrated leaves. For image acquisition, settings at confocal microscope were kept identical. Three independent experiments showed similar results. **C,** *In vitro* MBP pull-down assay illustrating the amount of 14-3-3 (T14.3c) pull-downed is highly increased in MBP-FDP^T231E compared to non-phosphorylated MBP-FDP. Anti-RGS-(His)$_6$ antibody was used to detect His-T14.3c. Ponceau S staining shows the loading control for MBP tag and MBP fusion proteins.

For negative controls, the rBiFC vector encoding either cYFP fused to FDP or its two mutants, and nYFP alone in the second expression cassette (Fig. 3.1.1B). In these cases, the mean relative fluorescence intensity is comparable to the biological control, FDP^{T231A}. The rBiFC experiment confirms that the physical association of 14-3-3 *in planta* depends on the phosphorylation status of FDP.

To further investigate the requirement of FDP phosphorylation for 14-3-3 association, *in vitro* MBP (Maltose binding protein) pull-down experiment was performed. For this experiment, the sufficient amount of purified recombinant FDP protein in native form was prerequisite. It was, however, difficult to obtain the FDP protein in a soluble form. I checked several different conditions for protein expression such as different bacterial expression strains, growth temperature, and codon optimization for bacterial expression. Finally, the decision was taken to use the 8xhistidine-MBP (8xHis-MBP) tag fused to the N-terminal of codon optimized full-length FDP and FDP^{T231E}. It is known from the literature that a MBP tag enhances the solubility and yield of fusion protein (Kapust and Waugh, 1999).

This approach has worked well for FDP protein expression in *Escherichia coli* strain (*E.coli* BL21-CodonPlus RIL) in a soluble form, however, the removal of the 8xHis-MBP tag was not successful. So, the full-length protein fused to 8xHis-MBP tag was used for *in vitro* pull-down assays. Besides, RGS-6xHis-tagged tobacco 14-3-3c (His-T14.3c) isoform, which has a higher solubility and yield in *E. coli,* was used (Jelich-Ottmann *et al.*, 2001). As expected, MBP pull-down assay shows that the phosphomimic version, MBP-FDP^{T231E}, has bound the higher amount of 14-3-3 protein, as compared to MBP-FDP, which is not phosphorylated in the *E. coli* expression system because of lack of such machinery (Fig. **3.1.1C**). As a negative control, MBP protein alone was used and is not able to precipitate the 14-3-3 protein. Altogether, these experiments support that the phosphorylation of threonine within STAPF motif of FDP is essential for the interaction of 14-3-3Ω and FDP.

The floral activator, FLOWERING LOCUS T (FT), promotes flowering in *A. thaliana*, while the closely related protein, TERMINAL FLOWER1 (TFL1) acts as a repressor (Kardailsky *et al.*, 1999; Kobayashi *et al.*, 1999). However, the underlying differential molecular mechanism of FT and TFL1 remains an important question for the plant scientific community.
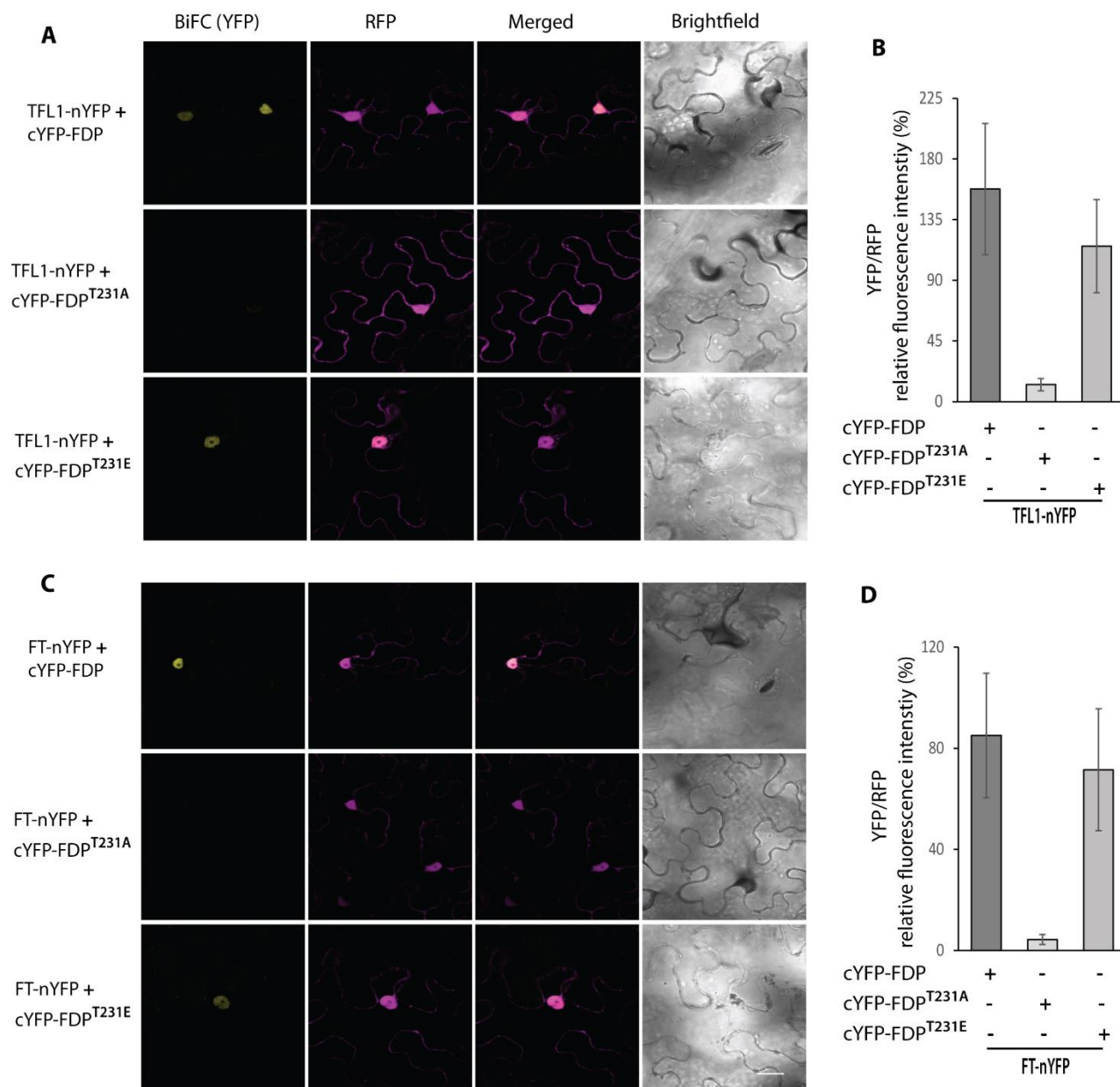
Figure 3.1. 2: Ratiometric biomolecular fluorescence complementation (rBiFC) analysis for *in planta* interaction of FDP with FT and TFL1. Exemplary confocal images exhibiting the BiFC (YFP) signal for FDP, FDP[T231A] or FDP[T231E] with FT (**A**) and TFL1 (**C**) in the nuclei of leaf epidermal cells of *N. benthamiana* 2 days after *Agrobacterium*-infiltration. RFP fluorescence was used as expression control and for ratiometric analysis. Scale bar, 25 µm. **B** and **D**, Bar chart illustrating the relative fluorescence intensity of YFP ratioed to RFP signal (%) against the constructs shown in **A** and **C**, respectively. Data shows mean ± sd (standard deviation) obtained from ≥ 27 nuclei from two independent leaves. For image acquisition, settings at confocal microscopy were kept identical. Three independent experiments have similar results.

What is the molecular basis of antagonistic activities of these proteins? The yeast two-hybrid (Y2H) based interaction studies of FDP with FT and TFL1 are controversial. Previous Y2H assays showed that FDP could interact with FT, not TFL1 (Jang *et al.*, 2009), showed a stronger interaction with FT than TFL1 (Abe *et al.*, 2005; Hanano and Goto, 2011) and comparable interaction with FT and TFL1 (Wigge *et al.*, 2005). In our lab, Y2H experiment also displayed that FDP interacted with FT and TFL1 in a comparable strength (data not shown here). Such discrepancies demonstrate the limitation of applying Y2H assay to investigate the interaction between plant proteins. The BiFC studies have previously demonstrated the *in planta* interaction of FD with FT and TFL1 occurs in the nucleus (Abe *et al.*, 2005; Hanano and Goto, 2011). In the first approach, the rBiFC approach was employed to check the *in vivo* physical interaction of FDP and its two mutants with FT as well as TFL1. The idea was to verify the *in vivo* interaction scenario between FDP and FT or TFL1, but also to test the mediating role of 14-3-3 via FDP substitution mutants, as reported in rice (Taoka *et al.*, 2011). For this, the rBiFC vectors expressing cYFP fused to FDP or its mutants, and nYFP fused either to FT (FT-nYFP) or TFL1 (TFL1-nYFP) were transiently transformed in *N. benthamiana* leaves. The YFP reconstitution was observed in the nucleus for FT together with wild-type FDP or FDP^{T231E}, while no YFP signal was observed with the non-phosphorylatable FDP^{T231A} mutant coexpression (Fig. **3.1.2C**). Interestingly, TFL1 also shows the same interaction tendency as FT and 14-3-3 protein (Fig **3.1.2A**).

Moreover, the BiFC signal was quantified relative to the nuclear expression of RFP signal as relative fluorescence intensity (as mentioned above for FDP and 14-3-3 interaction). It was obtained by averaging the YFP/RFP intensity from more than 27 nuclei of epidermal cells. The bar graph shows that the relative fluorescence intensity for TFL1 and FT is significantly higher upon coexpression of either FDP or FDP^{T231E} in comparison to a biological control, FDP^{T231A} mutant (Fig. **3.1.2C** and **3.1.2D**, respectively). The YFP/RFP signal for FDP together with TFL1 and FT is *157.7 ± 48.7%* and *85.1 ± 24.6%,* respectively. Taken together, these experiments show that FT and TFL1 do not differ in the interaction capability with FDP. Furthermore, these findings also indicate the significance of FDP phosphorylation and the possible role of 14-3-3s in establishing the association with either FT or TFL1.

3.2 Phosphorylation of FDP drives the nuclear accumulation of 14-3-3, FT and TFL1

14-3-3 proteins are known to regulate signaling output by altering the subcellular localization of target proteins. Upon phosphorylation, transcription factors such as REPRESSION OF SHOOT GROWTH (RSG) in gibberellic acid signaling and BRASSINAZOLE-RESISTANT 1 (BZR1) in brassinosteroid signaling are confined in the cytoplasm through 14-3-3 binding (Igarashi *et al.*, 2001; Rue *et al.*, 2007; Gampala *et al.*, 2007). It is likely that 14-3-3 proteins target FDP in a similar manner to modulate its transcriptional activity. Initially, I checked the subcellular localization of 14-3-3 proteins as well as FDP and its mutant versions - T231A and T231E. I observed that 14-3-3Ω-GFP localizes mostly to the cytosol and weakly to the nucleus, when expressed in *N. benthamiana* leaf epidermal cells (Supplementary Fig. **S5**; Taoka *et al.*, 2011). On the other hand, FDP and its mutants all localize to the nucleus of *Arabidopsis* protoplast (Supplementary Fig. **S4**). FDP^{T231A} mutant shows a tendency to localize in the nuclear speckles. Such nuclear speckles localization has also been observed for FD^{T282A} substitution mutant (Abe *et al.*, 2005).

Then I addressed the questions whether 14-3-3s modify the distribution of FDP in the plant cell and if this is affected by the phosphorylation status of FDP. I used '2in1 colocalization vectors' containing two expression cassettes, each under the control of *35S* promoter on a single plasmid. The enhanced green fluorescent protein fused to the C-terminus of 14-3-3Ω (14-3-3Ω-eGFP) was co-expressed with monomeric Cherry (mCherry) fused to the N-terminus of FDP or its mutant versions - T231A and T231E. From coexpression studies in transformed *N. benthamiana* leaves, it is evident that there is no change in nuclear localization of FDP, irrespective of the 14-3-3 binding mutation (**Fig. 3.2.1A**). But, 14-3-3-eGFP concentrates in the nucleus with FDP and FDP^{T231E}. In case of the non-phosphorylatable and non-interacting mutant, mCherry-FDP^{T231A}, the 14-3-3 proteins predominantly exhibit the cytosolic localization (Fig. **3.2.1A**). This observation mirrors a predominant cytosolic localization of 14-3-3s alone (Supplementary Fig. **S5**).

Moreover, I quantified these microscopic observations for nuclear accumulation. The mean fluorescence intensities were analyzed from at least 12 or more nuclei from two independently transformed *N. benthamiana* leaves.

Figure 3.2. 1: Enhanced nuclear accumulation of 14-3-3omega and FT is dependent on co-expression of FDP or FDP^{T231E}. **A** and **C,** exemplary confocal colocalization images of FDP and its substitution mutants – FDP^{T231A} and FDP^{T231E} together with 14-3-3omega (14-3-3Ω) and FT, respectively, in the nuclei of epidermal cells of *Agrobacterium*-infiltrated *N. benthamiana* leaf. Scale bar, 30 μm. **B** and **D**, Box plot representations of nuclear accumulation of 14-3-3Ω and FT, respectively, when co-expressed with FDP and its two mutants. These plots illustrate the mean of GFP fluorescence intensity of 14-3-3 (**B**) and FT (**D**) in the nucleus as median, 1st and 3rd quartiles, minimum and maximum. *** shows P value ≤ 0.009 on basis of paired Student's t-test. a.u., Arbitrary unit. n, is the number of nuclei taken for mean calculation. Two independent experiments have similar results.
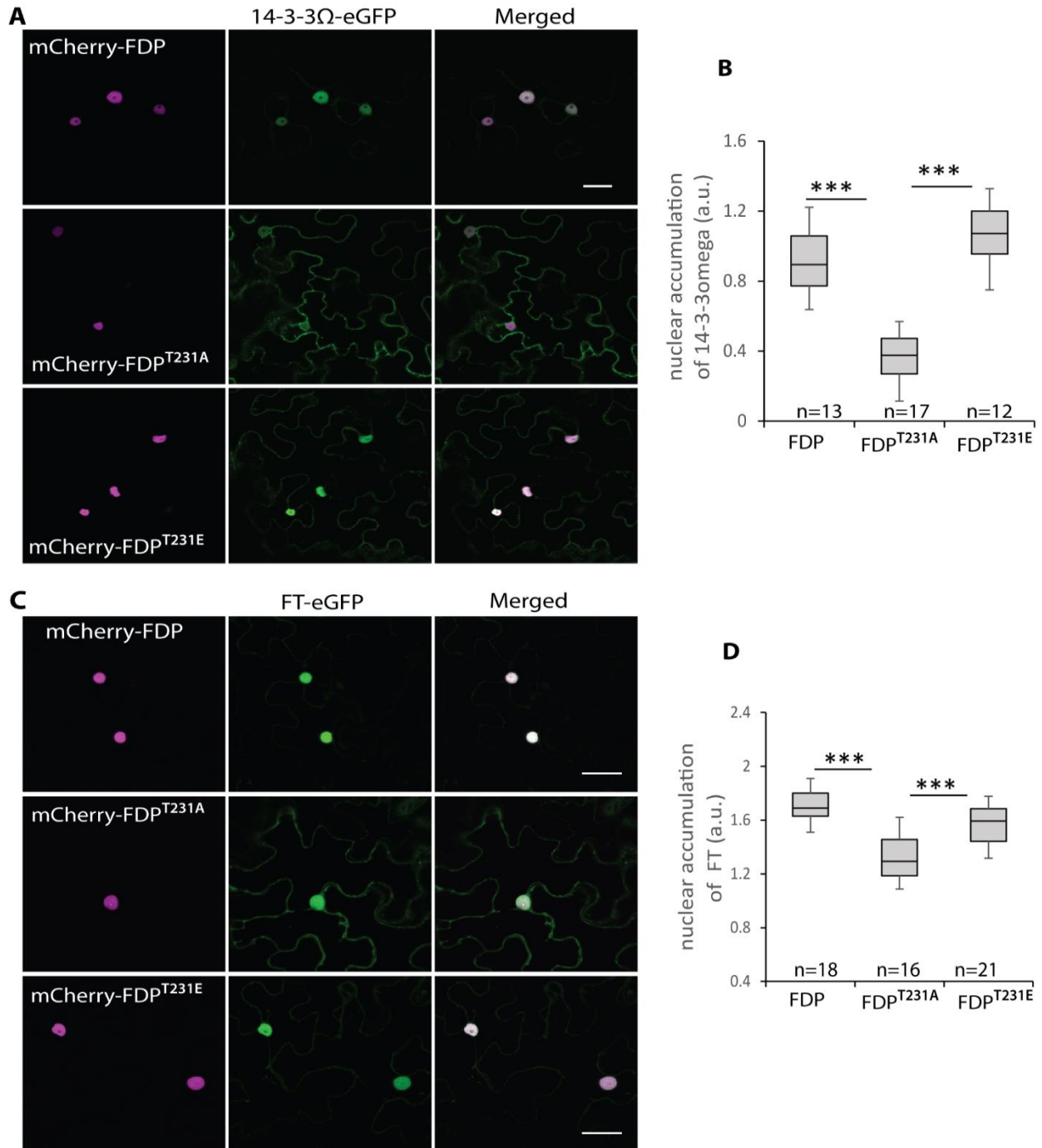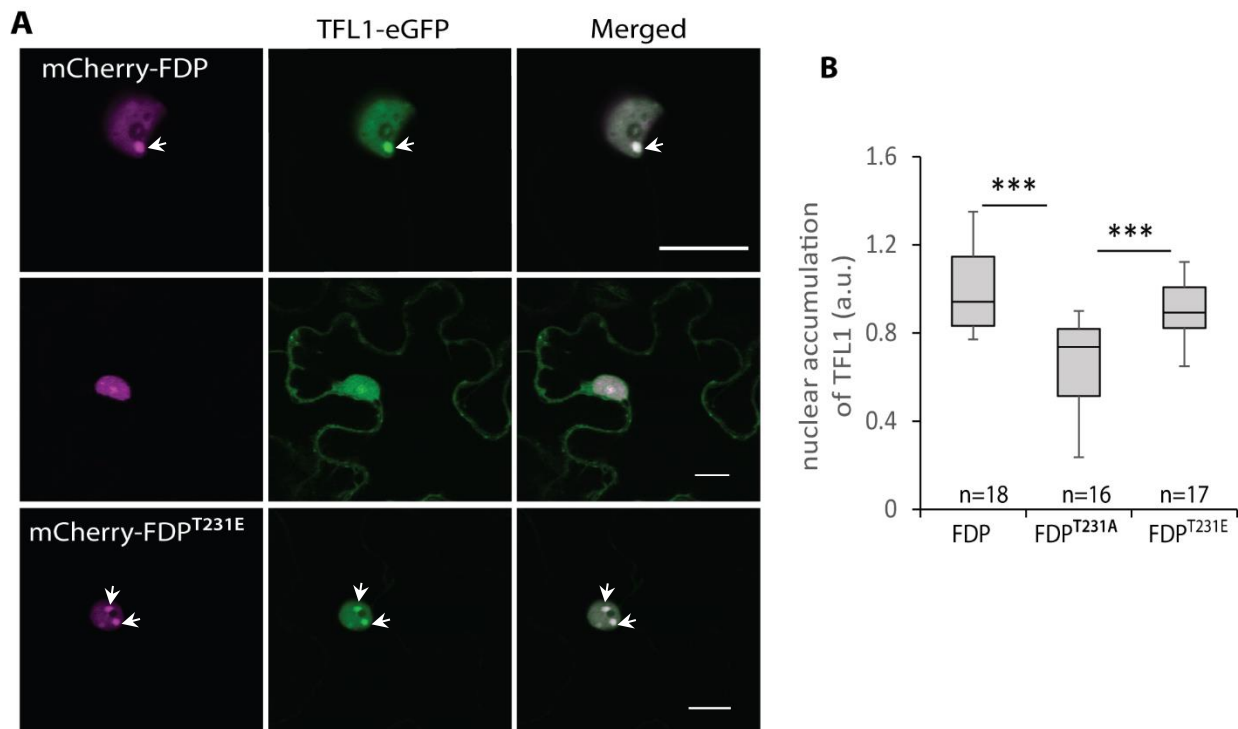
Figure 3.2. 2: Enhanced nuclear accumulation of TFL1 is dependent on co-expression of FDP or FDP[T231E]. **A,** exemplary confocal images of colocalization of TFL1 with wild type, FDP and its substitution mutants, T231A and T231E, in leaf epidermal cells of *N. benthamiana* after 2 days of the *Agrobacterium* infiltration. White arrow indicates nuclear speckles. Scale bar, 15 μm. **B,** Box plot representation of nuclear accumulation of TFL1 with FDP and its two mutants. It illustrates the mean of TFL1-GFP fluorescence intensity in the nucleus as median, 1st and 3rd quartiles, minimum and maximum. *** shows P value ≤ 0.001 on basis of Student's t-test. a.u., Arbitrary unit. n, is the number of nuclei taken for mean calculation. Two independent experiments have similar results.

The ratio of nuclear eGFP to nuclear mCherry was normalized to the ratio of whole cell eGFP fluorescence to whole cell mCherry fluorescence (as described in Taoka *et al*., 2011). It is termed as 'nuclear accumulation' and displayed as a box-plot diagram (Fig. **3.2.1B**). The box-plot illustrates that there is a highly significant nuclear accumulation of 14-3-3 upon coexpression with FDP and its phosphomimic substitution, T231E, in comparison to non-phosphorylatable, T231A. This is in agreement with the role of 14-3-3s as a phosphosensor and thus it moves into the nucleus to facilitate the role of FDP in the flowering regulation (Taoka *et al*., 2011; Boer *et al*., 2013). Overall, this suggests that FDP execute its role in the nucleus.
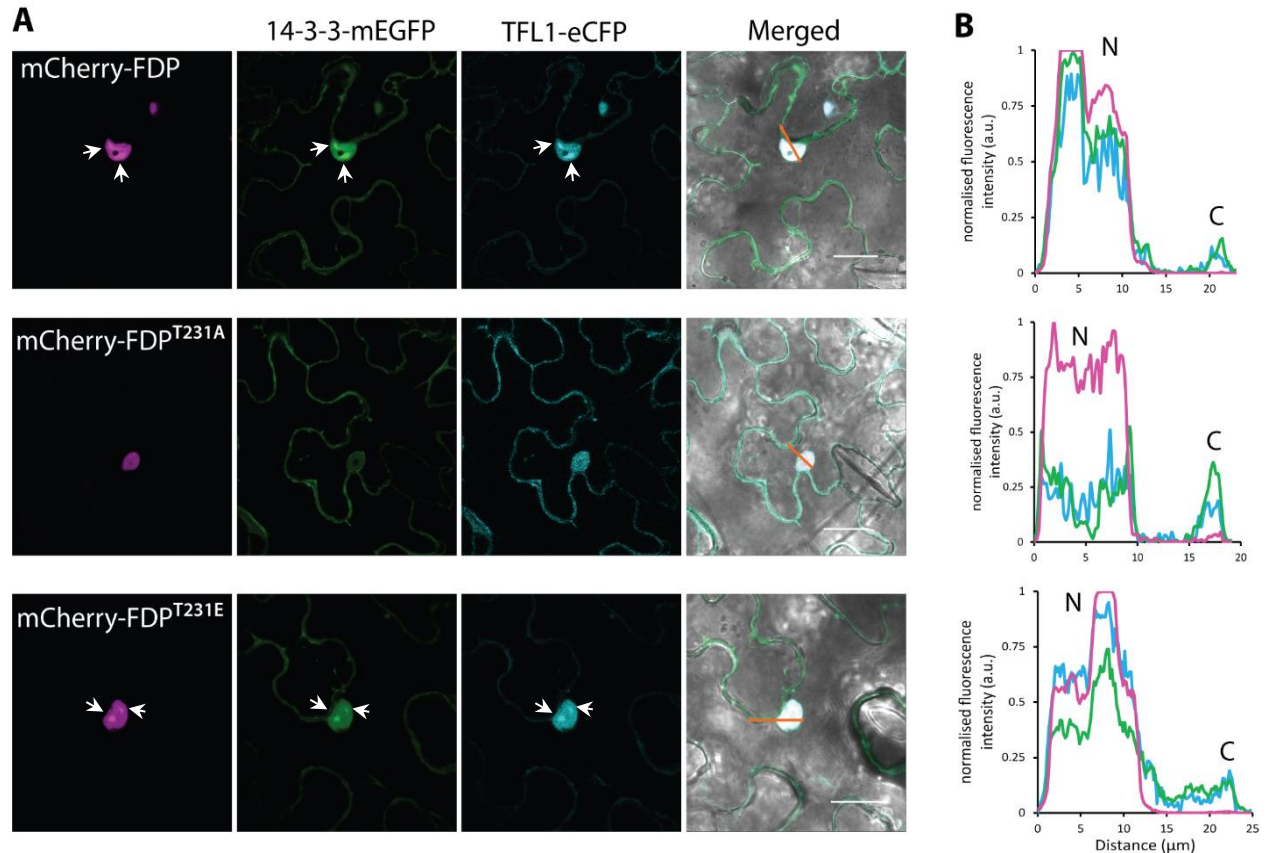
Figure 3.2. 3: Phosphorylation of FDP drives the nuclear accumulation of 14-3-3 and TFL1. **A,** confocal images demonstrating colocalization of three proteins by cotransformation in *N. benthamiana* leaves after 2 days. 2in1 vectors expressing either mCherry fused to FDP or FDP^T231A or FDP^T231E, together with 14-3-3Ω-eGFP. This was combined with TFL1-eCFP as a third protein. White arrow points to the presence of nuclear speckles. Scale bar, 25 μm. **B,** normalised intensity graph illustrating the fluorescence intensity of mCherry-FDP, 14-3-3-eGFP and TFL1-eCFP along arrow line drawn on the merged image. N - nucleus, C - cytoplasm

The molecular basis of the antagonistic activity of florigen, FT, and the closely related protein, TFL1, is still puzzling. In rice, 14-3-3 mediates the interaction between FT and FD (Taoka *et al.*, 2011). Therefore, I addressed the question whether expression of FDP and its two mutants – T231A and T231E affect the subcellular localization of FT and TFL1 as well as their antagonistic activities. As mentioned above for 14-3-3 proteins, colocalization studies of FT and TFL1 with FDP and its mutants were performed. Upon coexpression of either mCherry-FDP or mCherry-FDP^T231E in *N. benthamiana* leaves, FT-eGFP (Fig. **3.2.1C**) and TFL1-eGFP (Fig. **3.2.2A**) get concentrated in the nucleus. In case of the non-interacting mCherry-FDP^T231A, both FT and TFL1 were detected in the cytoplasm and nucleus (Fig. **3.2.1C** and **3.2.2A**). This microscopic

observation is consistent with the quantification of the nuclear accumulation for FT and TFL1 (Fig. **3.2.1D** and **3.2.2B**, respectively).

The major difference between FT and TFL1 in these colocalization studies is the presence of nuclear speckles exclusively in case of TFL1, which is observed only with wild-type FDP and its phosphomimic version (Fig. **3.2.2A**). The nuclear speckles are distinct compartments without membranes, thus allowing free exchanges of components between speckles and surrounding nucleoplasm. Such speckles may contain protein-protein or protein-RNA complexes, which regulate biological processes (Shaw and Brown, 2004; Dundr, 2012). This tendency of TFL1 nuclear speckles localization is potential avenues for further research, which might provide additional clues about its floral repressing activity. Overall, the colocalization studies support that FT and TFL1 more or less behave the same in their subcellular distributions with FDP, and the phosphorylation of FDP within the STAPF motif is a driving factor for their nuclear accumulation.

To further investigate the differences in subcellular distribution between FT and TFL1, I also performed the colocalization studies with three proteins - FDP, 14-3-3 and FT or TFL1. For this, enhanced cyan fluorescent protein (eCFP) fused either to FT (FT-eCFP) or TFL1 (TFL1-eCFP) in a binary vector was established. Then FT- or TFL1-eCFP was coexpressed with 2in1 vector carrying mCherry fused either to FDP or its substitution mutants, together with 14-3-3-mEGFP in *N. benthamiana* leaf epidermal cells. The colocalization of three proteins illustrates that FDP as well as phosphomimic version FDP^{T231E} led to the nuclear accumulation of 14-3-3-mEGFP and FT-eCFP (Supplementary Fig. **S6**). Whereas in combination with FDP^{T231A} version, they were clearly present both in the cytoplasm and nucleus. The similar colocalization tendency has been observed, when TFL1-eCFP was coexpressed (Fig. **3.2.3A** and **3.2.3B**). Consistent with the colocalization of FDP/FDP^{T231E} –TFL1 (Fig. **3.2.2A**), the localization of TFL1–14-3-3–FDP/FDP^{T231E} in nuclear speckles was also obvious. Overall, these findings suggest that the phosphorylation of FDP is crucial for the nuclear accumulation of 14-3-3, FT and TFL1.

3.3 14-3-3s interact with FT and TFL1 in the cytoplasm and might piggyback them into the nucleus

Interestingly, in this study a similar colocalization and interaction tendency of the antagonistic proteins FT and TFL1 were observed, and there is an indication that 14-3-3 might influence their interaction with FDP. It was reported that in rice, 14-3-3 interacts with FT in the cytoplasm. Moreover, the structural studies demonstrated that unphosphorylated FT binds to the outer surface of 14-3-3, away from the amphipathic groove site where usually a phosphorylated transcription factor such as FD strongly binds (Taoka *et al.*, 2011). In our lab, *Arabidopsis* FT has been shown to interact with 14-3-3 in a similar fashion by *in vitro* experiments.

According to Y2H studies, both FT and TFL1 interact with 14-3-3 protein (Pnueli *et al*., 2001). Based on quantitative Y2H and qualitative biomolecular luminescence complementation assays, it was reported that 14-3-3 proteins do not discriminate between FT and TFL1 (Ho and Weigel, 2014). This however does not tell anything about the location of the 14-3-3 interaction with TFL1, and whether FT and TFL1 bind to 14-3-3 with different affinities, which would then explain their opposite functions in flowering regulation. To address these questions, I applied GST pull-down and quantitative FRET-FLIM experiments.

In vitro glutathione S-transferase (GST) pull-down assays were performed with equal molar amounts (1.125 nmol) of recombinant GST-FT, GST-TFL1 and GST proteins, which were immobilized on glutathione beads. Then two times higher amounts (2.25 nmol) of His-T14.3c were used to saturate the GST dimers and test for protein binding. The pull-down results show that in case of GST-FT and GST-TFL1, the amount of pulled-down 14-3-3 proteins (T14.3c, a tobacco 14-3-3 protein) is evidently higher as compared to GST alone, which acts a negative control (Fig. **3.4.1**). The signal strength of 14-3-3 binding either to GST-FT or GST-TFL1 was quantified relative to that in GST. The relative amount of pulled-down 14-3-3 protein is 4.7 and 19.0 fold higher for GST-FT and GST-TFL1, respectively, as compared to GST alone (Fig. **3.4.1**). These values also indicate that 14-3-3 might bind to TFL1 with a stronger affinity than to FT, which requires further quantitative evidence. Interestingly, the pull-down clearly demonstrates that 14-3-3 proteins, in addition to FT, do interact with non-phosphorylated TFL1.
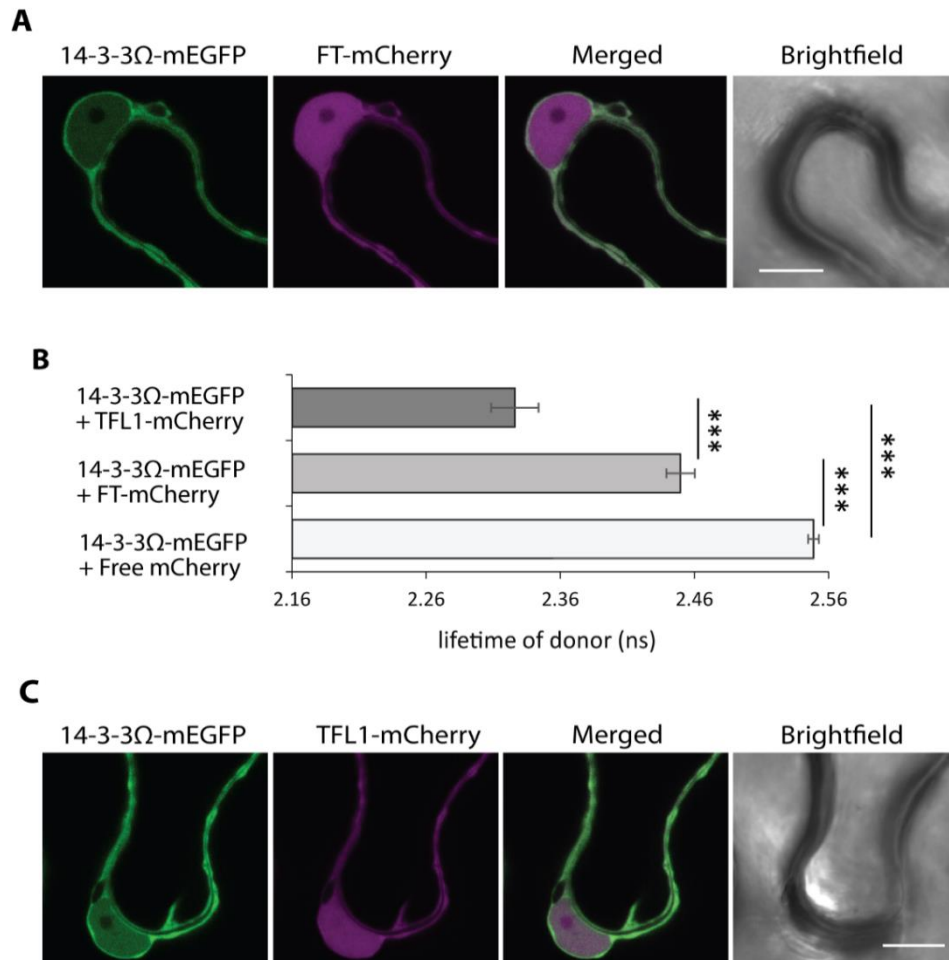
Figure 3.3. 1: 14-3-3 interacts with both FT and TFL1 in the cytoplasm. **A** and **C,** depict confocal images of the subcellular localization of 14-3-3Ω co-expressed in transformed tobacco cells with FT and TFL1, respectively. Scale bar, 10 µm. **B**, displays the FRET-FLIM results. Significant reduction of the 14-3-3Ω-mEGFP lifetime in presence of either TFL1 or FT, compared to that of free mCherry as a negative control. Error bar represents the SE from ≥9 number of cells from two independent transformed leaves. *** shows P value ≤ 0.001. For direct comparison, FRET-FLIM was performed for FT and TFL1 at the same time. At least two independent FRET-FLIM experiments have similar results.

Further investigations in our lab have shown that TFL1, similar to FT, binds to the outer surface of 14-3-3 protein, away from its amphipathic groove (Data not shown).

To further investigate the location of the TFL1–14-3-3 interaction, Förster Resonance Energy Transfer - Fluorescence Lifetime Imaging Microscopy (FRET-FLIM) technique was employed. The measurement was performed in *Agrobacterium* transformed *N. benthamiana* epidermal cells.

This method has been applied to understand not only the protein-protein interaction, but also the protein complex dynamics as a result of either competition or dissociation events (Bücherl *et al.*, 2013; Randoux *et al.*, 2014; Sheerin *et al.*, 2015). FRET means energy transfer from fluorescently tagged donor molecules to fluorescently tagged acceptor molecules (a FRET pair), when their distance is below 10 nm. The FRET event can be most reliably measured by FLIM method (Hecker *et al.*, 2015). For this, the lifetime of the donor fluorescence (here: monomeric eGFP, mEGFP) is measured either in the absence or presence of an acceptor fluorophore (here: mCherry).

The lifetime of the donor fluorescence is significantly reduced in the presence of a suitable acceptor. This lifetime reduction is indicative of a physical interaction between two proteins. Monomeric eGFP (mEGFP) is a superior donor because it is unsusceptible to dimerization related quenching as compared to eGFP version (Tramier *et al.*, 2006). The 2in1 vectors encoding FT- or TFL1-mEGFP and 14-3-3Ω-mCherry were established and transiently expressed in *N. benthamiana*. The colocalization studies clearly indicate that both FT and TFL1 are present both in the nucleus and cytoplasm, while 14-3-3 is present predominantly in the cytosol (Fig. **3.3.2A** and **3.3.2C**, respectively). Such colocalization patterns have also been observed for FT and 14-3-3 orthologs in rice and tomato (Taoka *et al.*, 2011; Park *et al.*, 2014).

Hence, it was logical to perform the FRET-FLIM measurement in the cytosol. The measurements demonstrate that the lifetime of TFL1-mEGFP in the presence of 14-3-3-mCherry was significantly reduced as compared to TFL1-mEGFP alone (Supplementary Fig. **S7B**). This suggests that TFL1−14-3-3 interaction takes place in the cytosol. In a similar experiment, no reduction in the lifetime of FT-mEGFP with 14-3-3 as compared to FT-mEGFP alone was observed, indicating that there is no interaction between two proteins (Supplementary Fig. **S7A**).

This was a surprising fact and there could be two possible explanations. First, the two fluorophores (FRET pair – mEGFP and mCherry) are not in the obligatory proximity (below 10nm distance). Second, the 14-3-3 association causes different protein conformation in FT as compared to TFL1 resulting in a stronger lifetime reduction of TFL1-mEGFP than that of FT-mEGFP. A second approach was taken to clearly separate the 14-3-3s association with FT and TFL1 proteins. This time, 14-3-3Ω-mEGFP fusion as a donor in combinations with either TFL1- or FT-mCherry as an acceptor were constructed.
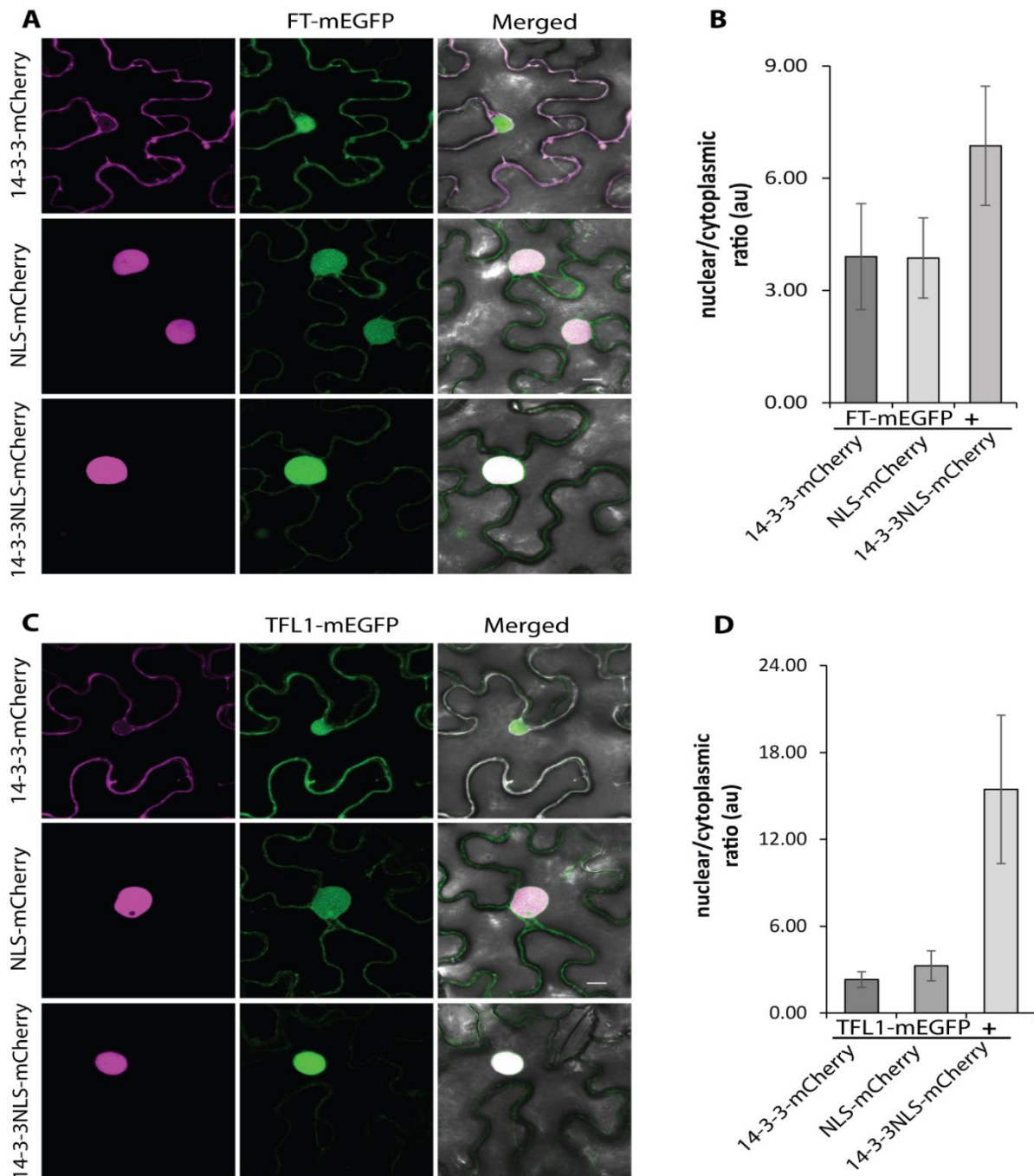
Figure 3.3. 2: 14-3-3 modifies the subcellular localization of both FT and TFL1 and might move its interaction partner into the nucleus. **A** and **C,** confocal images illustrating subcellular localizations of FT-mEGFP and TFL1-mEGFP, respectively, in transformed leaf epidermal cells of *N. benthamiana*. FT and TFL1 were coexpressed either with 14-3-3-NLS-mCherry, 14-3-3-mCherry or NLS-mCherry. Scale bar 10 μm. **B** and **D,** bar graph representation demonstrating the nuclear/cytoplasmic ratio for FT and TFL1, respectively. This ratio was calculated by averaging the nuclear/cytoplasmic intensity from ≥16 epidermal cells from two independent cotransformed *N. benthamiana* leaves. au – arbitrary unit. The experiment was repeated twice and yielded similar results.

The coexpression of either TFL1- or FT-mCherry with 14-3-3Ω-mEGFP showed the identical colocalization pattern observed previously (Fig. **3.3.1A** and **3.3.1C**). The FRET-FLIM was measured in the cytosol; and for the direct comparison, it was performed for both FT and TFL1 at the same day. The results revealed that the lifetime of the donor 14-3-3Ω-mEGFP is *2.45 ± 0.04 ns* (mean ± SE) in the presence of FT-mCherry, as compared to *2.55 ± 0.01 ns* for donor alone (Fig. **3.3B**). This indicates that the interaction between FT and 14-3-3 proteins takes place in the cytosol. In comparison, the lifetime of 14-3-3Ω-mEGFP has strongly dropped to *2.33 ± 0.06 ns* in the presence of TFL1-mCherry (Fig. **3.3B**). This higher reduction in lifetime could be due to different conformational changes in the FT and TFL1 molecules resulted through 14-3-3 binding, which needs further validation. The FRET-FLIM analyses suggest the association of 14-3-3 proteins with FT and TFL1 take place in the cytosol.

In this study, I demonstrated that the phosphorylation of FDP drives the accumulation of interacting proteins − 14-3-3, FT and TFL1 into the nucleus (Fig. **3.2.1** and **3.2.2**). This raises another important question whether the nuclear import of FT and TFL1 is dependent on the association with 14-3-3s. In this regard, it was shown that rice 14-3-3 proteins act as the cytoplasmic receptor for FT protein; and then both proteins were transported as binary complex in the nucleus of rice protoplast (Taoka *et al*., 2011). This finding is based on the experiment in which the Hd3a−14-3-3 BiFC complex moves to the nucleus upon coexpression of the transcription factor, OsFD1. However, the facts that the BiFC leads to the formation of an irreversible stable complex, and the higher affinity of 14-3-3 proteins for a phosphorylated transcription factor compared to an unphosphorylated target demand a further clarification of 14-3-3's role in FT import. Because in this scenario, as 14-3-3s move to the nucleus where phosphorylated OsFD1 is localized, the irreversibility of Hd3a−14-3-3 BiFC complex could likely force Hd3a to the nucleus as well.

To address the role of 14-3-3s in mediating the import of FT to the nucleus, I took a different approach in which FT protein was free. Since the molecular basis for the import of TFL1, a floral repressor, to the nucleus has not been studied before, I investigated both FT and TFL1 in the anticipation of unfolding differences between these antagonistic proteins. A nuclear localization signal (NLS) was included to the C- terminus of 14-3-3Ω (14-3-3Ω-NLS) and finally cloned into a 2in1 vector together either with FT or TFL1. The colocalization studies in tobacco leaf epidermal

cells exhibited that both FT and TFL1 were concentrated in the nucleus (Fig. **3.3.2A** and **3.3.2C**, respectively). 14-3-3Ω-NLS-mCherry fusion protein was, as expected, exclusively detected in the nucleus. This indicates that 14-3-3s are influencing the subcellular localization of FT and TFL1. Such a mode of action of 14-3-3 proteins is so far only known for the regulation of transcription factors such as RSG and BZR1, which are retained in the cytoplasm upon phosphorylation (Igarashi *et al*., 2001; Wang *et al*., 2011).

Moreover, the nuclear-cytoplasmic fluorescence intensity of FT-mEGFP and TFL1-mEGFP were quantified when coexpressed either with 14-3-3-mCherry, NLS-mCherry or 14-3-3-NLS-mCherry in *N. benthamiana*. This quantification exhibited that the nuclear/cytoplasmic ratio for FT is about two times higher upon coexpression with 14-3-3-NLS-mCherry than that with 14-3-3-mCherry and NLS-mCherry (Fig. **3.3.2B**). For TFL1, this ratio is about 5-6 fold higher (Fig. **3.3.2D**). At this point, it remains unclear whether 14-3-3s are capable of differentiating between these antagonistic proteins. According to the previous studies, the 14-3-3 proteins are described to act both positively and negatively in the brassinosteroid signaling pathway (Wang *et al*., 2011). Thus, it is likely that 14-3-3 interaction with antagonistic proteins, FT and TFL1, is essential to fine-tune the photoperiodic flowering regulation. Altogether, these experiments suggest that 14-3-3 alters the subcellular localization of FT and TFL1, which might be piggybacked to the nucleus.

3.4 Presence of pFDP reveals differences in the organization of protein complex of 14-3-3s with FT and TFL1

The dynamics of protein complex is vital for the spatio-temporal regulation of plant growth and development. The tight regulation of floral initiation might rely on such spatio-temporal protein complex formation. In rice, it has been well-characterized that 14-3-3s act as an intermolecular bridge enabling the interaction between Hd3a and OsFD1, orthologs of FT and FD in *Arabidopsis*. 14-3-3s thus mediate a tripartite complex formation, termed 'Florigen Activation complex (FAC),' leading to the activation of the floral identity gene, *OsMADS15* - ortholog of *AP1* gene in *Arabidopsis* (Taoka *et al*., 2011). From my findings, it is evident that 14-3-3 interacts *in planta* with FT as well as TFL1, and all these three proteins interact with FDP in the nucleus.
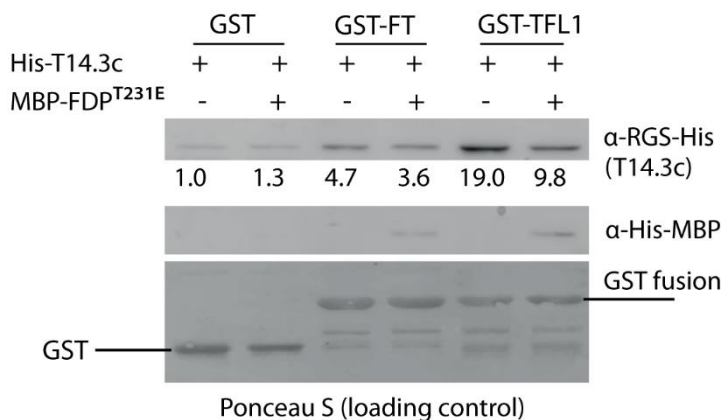
Figure 3.4. 1: *In vitro* GST pull-down assays demonstrating the interaction of GST-FT and GST-TFL1 with 14-3-3 protein, in the absence or presence of MBP-FDP^{T231E}. This assay was performed with purified recombinant proteins expressed in *E. coli*. GST-FT and GST-TFL1 bound proteins were subjected to SDS-PAGE, followed by western blot analysis. Anti-RGS-(His)$_6$ and (His)$_6$ antibodies were used to detect His-T14.3c and MBP fusion proteins, respectively. Ponceau S staining shows the loading control for GST tag and GST fusion proteins. The values below the top gel indicate the relative strength levels of signals after standardization using Ponceau S staining of GST, GST-FT and GST-TFL1 as a loading control. The value of GST as a negative control was set to 1. At least two experiments were performed and yielded similar results.

This observation raises an important question how the FT–14-3-3 and TFL1–14-3-3 complexes influence the bZIP transcription factor, FDP. In *Arabidopsis*, the direct evidence for such a large complex formation among FT, 14-3-3 and FD or FDP is lacking. It also remains unknown whether 14-3-3 proteins play the mediating role between FDP and TFL1. I addressed the possibility of the complex formation among three proteins - FDP, 14-3-3, FT or TFL1 by employing FRET-FLIM approach. The visualization of hetero-trimeric protein complexes in living cells is technically limited. However, new progresses in the FRET-FLIM method has made it possible to investigate at least certain protein complex dynamics. Most of such studies have analyzed the binary complex formation and its dynamics via FRET-FLIM approach (Bücherl *et al.*, 2014). Moreover, some researchers have applied a combination of BiFC and FRET-FLIM approaches to demonstrate a trimeric complex formation in living plant cells (Kawaaitaal *et al.*, 2010; Taoka *et al.*, 2011). Here, they performed FRET-FLIM measurements on a YFP reconstitution resulting from BiFC between two proteins as an acceptor fluorophore and a third potential interaction

protein fused to cyan fluorescent protein (CFP) acting as a donor molecule. However, since it is known that BiFC results in an irreversible stable complex formation, this system can limit the complex formation dynamics in living cells. To my knowledge, there are few publications showing ternary complex formation by using the direct FRET-FLIM approach. For example, in the mammalian field, scientists have used FRET-FLIM by employing two proteins - one fused to donor and the other to acceptor FPs, respectively, combined with a third protein fused to a small tag (e.g. c-Myc) or without a tag (Kinoshita *et al*., 2007; Gibbs *et al*., 2012). 14-3-3 interacts with FT as well as TFL1 in the cytosol, while upon additional co-expression of FDP there is a shift in the subcellular localization of 14-3-3, FT and TFL1 to the nucleus.

For FLIM studies, the issue of different compartmentation of the proteins was solved by including a nuclear localization signal (NLS) to 14-3-3 protein (14-3-3-NLS), which leads to the nuclear accumulation of FT and TFL1 (Fig **3.3.2**). This approach allows for measurement of FRET-FLIM in the nucleus and the effect of eCFP-FDP on the complex formation can be examined. Different combinations of constructs encoding three proteins were tested to find clear evidence whether there is any difference between FT and TFL1 (Supplementary Table **4**). The combinations of FT or TFL1 with 14-3-3-NLS in the absence or presence of eCFP-FDP worked well, which are described below in the sections 3.4.1 and 3.4.2.

3.4.1 FDP positively affects FT–14-3-3 complex formation

To clarify whether the association between FT and FDP is direct or not, I performed *in vitro* GST pull-down experiments with a phosphomimic version of the full-length FDP protein fused to MBP (MBP-FDP^{T231E}), and no direct binding between these two proteins was observed (data not shown). This finding is consistent with the similar observation made in rice between FT and FD, in which 14-3-3 proteins act as a scaffold (Taoka *et al*., 2011).

Then, I addressed the possible mediating role of 14-3-3 in *Arabidopsis* by further GST pull-down experiments. As mentioned before (section **3.3**), the results from pull-down demonstrated the binding of 14-3-3 to FT protein (Fig. **3.4.1**).
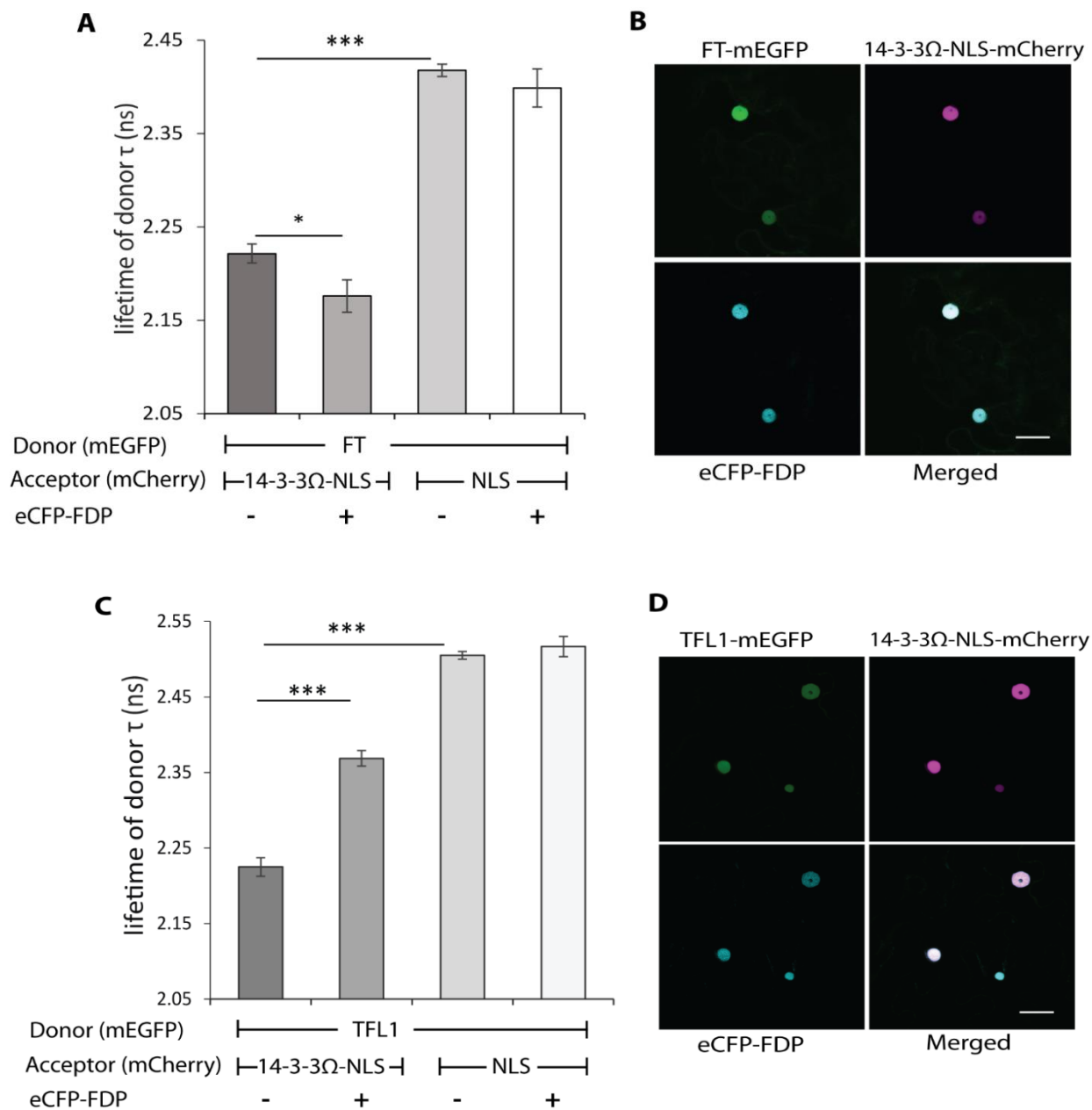
Figure 3.4. 2: FRET-FLIM analysis of FDP's effect on the *in vivo* interaction of 14-3-3 with FT and TFL1. **A** and **C**, FRET-FLIM analyses demonstrate the influence of eCFP-FDP expression as a third protein on the lifetimes of FT-mEGFP and TFL1-mEGFP, respectively, either with 14-3-3Ω-NLS-mCherry or NLS-mCherry. For FT, three independent experiments were performed – one presented here has a further decrease in FT-mEGFP lifetime in the presence 14-3-3Ω-NLS and eCFP-FDP, while the other two show neither decrease nor increase in lifetimes. For TFL1, three independent experiments yielded similar result. Error bar represents the SE from ≥11 number of nuclei from two independent transformed leaves. * and *** indicate P value equal to 0.03 and ≤ 0.001, respectively. **B** and **D**, exemplary confocal images of the expression of three proteins in the nuclei of tobacco epidermal cells comparing FT and TFL1, respectively. Scale bar, 30 µm.

In the same pull-down experiment, I included the phosphomimic mutant MBP-FDP[T231E] to investigate its capability to associate with FT–14-3-3 complex to form a large protein complex. For this GST assay, equal molar amounts (1.125 nmol) of purified GST alone and GST-FT proteins were immobilized on glutathione-agarose beads. Then 2.25 nmol of His-T14.3c and 4.5 nmol of MBP-FDP[T231E] were incubated to allow a saturation of protein complex and to test for protein-protein binding. According to the pull-down results in the presence of MBP-FDP[T231E], it is obvious that not only the amount of 14-3-3 protein remained unchanged, but also MBP-FDP[T231E] was detectable as a third component of the protein complex (Fig. **3.4.1**). Furthermore, this observation is clearly supported by the signal strength of 14-3-3 binding to GST-FT, which is 4.7 and 3.6 fold higher compared to GST in the absence or presence of MBP- FDP[T231E], respectively (Fig. **3.4.1**). These findings suggest the stable binding among FDP, FT and 14-3-3 proteins. It is likely that these three proteins form a heterotrimeric complex similar to the florigen activation complex described in rice (Taoka *et al.*, 2011).

The formation of this heterotrimer also assembles in living plant cells, further investigations were carried out by FRET-FLIM experiments. The 2in1 vector expressing FT-mEGFP with NLS-mCherry or 14-3-3Ω-NLS-mCherry was transformed in tobacco leaves in the absence or presence of a plasmid expressing eCFP-FDP fusion protein. The use of eCFP fusion also facilitated the direct visualization of protein in the right compartment during the FRET-FLIM measurements. The lifetime analyses displayed that in the presence of 14-3-3Ω-NLS-mCherry, the lifetime of FT-mEGFP significantly decreased to *2.22 ± 0.05* ns from *2.42 ± 0.02* ns with NLS-mCherry as a control acceptor. This reduction indicates the interaction of FT and 14-3-3 as expected (Fig **3.4.2A**). Upon additional eCFP-FDP coexpression, there was a further significant decrease in FT-mEGFP lifetime to *2.18 ± 0.06* ns. No significant change was observed for NLS-mCherry as a control acceptor (lifetime: *2.40 ± 0.07* ns), showing that the eCFP fusion did not cause any unwanted lifetime quenching/reduction (Fig **3.4.2A**; Supplementary Table **3.1**). This specific further reduction of lifetime of FT-mEGFP indicates a stronger association or more stable binding among FT, 14-3-3 and FDP. However, this phenomenon of further lifetime reduction upon eCFP-FDP expression was observed only in one experiment. The other two experiments resulted in neither significant reduction nor increase of the lifetime (Supplementary Table **3.1**). The possible reasons for no further decrease could be the

rearrangement and a conformational change of the complex in such a way that does not lead to a further proximity of FRET pairs, and thus no further lifetime reduction is possible. However, the binding of FDP to FT−14-3-3 complex is clear from GST pull-down results, suggesting that the FDP is capable of forming a larger protein complex with FT and 14-3-3 (Fig. **3.4.1**).

To address that FDP protein is also stable in plant cells and participates in a heterotrimeric complex as a third component, which was observed in GST pull-down and FRET-FLIM experiments, Co-IP assays were performed. For this assay, the same vector, which was used for FRET-FLIM experiment, was taken. For the expression of the third partner, 3x hemagglutinin (HA) tagged N-terminally to FDP (3xHA-FDP), which allowed a distinct detection, was used. The cell lysates were obtained from transformed tobacco leaves with and without 3xHA-FDP expression. FT-mEGFP was immunoprecipitated by GFP trap and subjected to western blot analysis for the detection of bound proteins by specific antibodies. The amount of FT-mEGFP immunoprecipitate (IP) was used as a loading control and detected by anti-GFP antibody. Co-immunoprecipitation of 14-3-3Ω-NLS-mCherry and 3xHA-FDP were detected by anti-RFP and anti-HA antibodies, respectively. This assay demonstrates that FT can co-immunoprecipitate both 14-3-3 and FDP (Fig **3.4.3B**). This suggests that it is very likely that there is a heterotrimeric complex formation among FDP, 14-3-3 and FT, consistent with GST pull-down and FRET-FLIM findings. Taken together, these experiments demonstrate that FDP has a positive effect on the FT and 14-3-3 complex formation. These findings also indicate that in *Arabidopsis* 14-3-3 proteins can act as a scaffold to mediate the interaction between FDP and FT in plant cells.

3.4.2   FDP negatively affects the TFL1−14-3-3 complex formation

Based on my experiments, it is evident that TFL1 does not differ from FT with respect to its subcellular localization and interaction capability with the bZIP transcription factor, FDP. Together with the knowledge about the ability of FT protein to participate in the FAC-like complex, one would speculate about the possibility of such complex formation among TFL1, FDP and 14-3-3s, which would then act as a floral repressor to counteract FT signaling. It has been reported that FD participates in TFL1-mediated transcriptional repression of floral transition (Hanano and Goto, 2011).
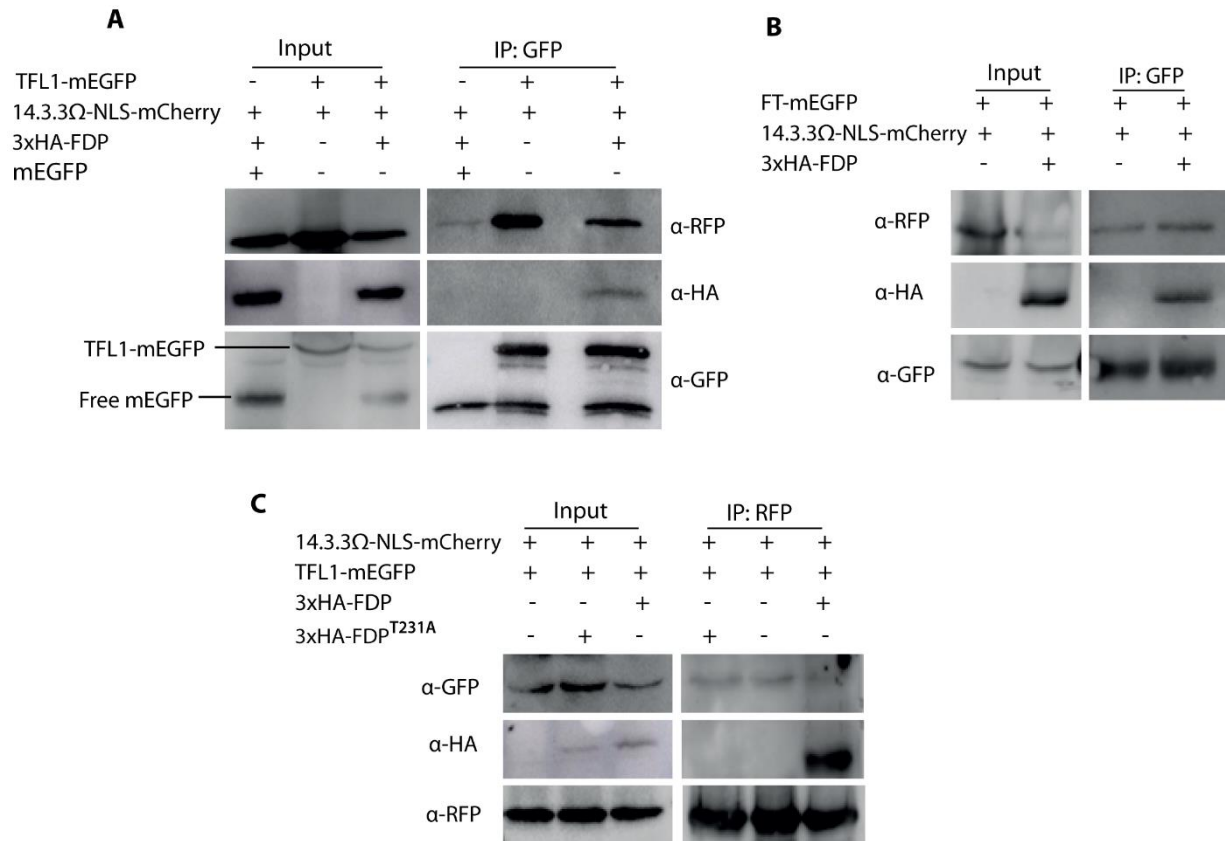
Figure 3.4. 3: Co-immunoprecipitation assays illustrating the differences caused by FDP expression on FT and TFL1. **A**, Co-immunoprecipitation (Co-IP) experiment showing that FT-mEGFP co-precipitates both 14-3-3Ω and FDP. **B**, Co-IP experiment showing that TFL1-mEGFP strongly co-precipitates 14-3-3Ω, while upon 3xHA-FDP coexpression, the amount 14-3-3 protein is clearly reduced. **C**, Another Co-IP of 14-3-3Ω-NLS-mCherry by using RFP trap demonstrates the dissociation effect (observed in **C**). The effect of FDP[T231E] and FDP[T231A] on the interaction of 14-3-3 and TFL1 have been demonstrated. All Co-IP assays were carried out by transient *Agrobacterium* transformation of leaves of ca. 4-week-old *N. benthamiana*. Input, IP and Co-IP were detected by GFP, HA and RFP antibodies. At least two experiments were performed and yielded similar results.

It is possible that FDP might also participate in a similar floral repressing mechanism. Moreover, the role of 14-3-3 proteins as an intermolecular bridge between TFL1 and FD/FDP has not been explored. To investigate if there is any differential mechanism of FT and TFL1 proteins, GST pull-down, FRET-FLIM and Co-IP experiments were carried out.

For GST pull-down experiments, 1.125 nmol of purified GST and GST-TFL1 proteins were immobilized on glutathione-agarose beads and incubated with 2.25 nmol of His-T14.3c and 4.5 nmol of MBP-FDP[T231E] proteins. The direct interaction between TFL1 and MBP-FDP [T231E] was not detected, but a weak interaction cannot be excluded (data not shown). From pull-down results,

it is evident that 14-3-3 (T14.3c) proteins specifically bind to GST-TFL1 compared to GST alone (Fig. **3.4.1**). Amazingly, in the presence of the phosphomimic version, MBP-FDP^{T231E}, the 14-3-3 binding is clearly reduced. This observation is in agreement with the signal strength of 14-3-3 binding to GST-TFL1, which is reduced from 19.0 fold to 9.8 in the absence and presence of MBP-FDP^{T231E}, respectively (Fig. **3.4.1**). These results suggest that the phosphorylated FDP (pFDP) negatively affects the stable binding of TFL1–14-3-3 complex. Remarkably, this is in contrast to the effect that could not be observed with respect to the interaction of FT and 14-3-3s (Fig. **3.4.1**).

To understand whether this negative effect of FDP is also detectable *in planta*, FRET-FLIM experiments were performed. For this experiment, 2in1 vector encoding TFL1-mEGFP either with NLS-mCherry or 14-3-3Ω-NLS-mCherry, in the absence or presence of a plasmid expressing eCFP-FDP fusion were cotransformed in tobacco leaf epidermal cells. The lifetime analyses exhibited that TFL1-mEGFP lifetime has significantly decreased from *2.50 ± 0.03* ns to *2.22 ± 0.04* ns in the presence of NLS-mCherry and 14-3-3Ω-NLS-mCherry as acceptors, respectively (Fig **3.4.2C**). This suggests the physical interaction of TFL1 and 14-3-3 as expected. Moreover, in the presence of eCFP-FDP together with 14-3-3Ω-NLS-mCherry, the TFL1-mEGFP lifetime was significantly increased to *2.32 ± 0.06* ns. While control measurement of eCFP-FDP together with NLS-mCherry yielded a lifetime of *2.51 ± 0.09* ns, showing that eCFP fusion did not cause adverse effects on donor lifetime (Fig **3.4.2C**; Supplementary Table **3.2**). This additional increase in lifetime indicates that FDP negatively affects the formation of TFL1–14-3-3 complex *in planta*. To avoid any unknown influence of eCFP fusion on donor lifetime measurements, another vector expressing 3xHA tagged to FDP (3xHA-FDP) was assembled. A similar FRET-FLIM experiment was performed in the absence and presence of 3xHA-FDP, and lifetime analyses gave the similar outcome (Supplementary Table **3.2**). The FRET-FLIM experiments provide *in planta* evidences supporting the *in vitro* observation of FDP's negative influence on TFL1 and 14-3-3 complex formation.

For additional *in vivo* validation of the negative effect of FDP, Co-IP assays were performed. For Co-IP assays, the same 2in1 vector that was used for FRET-FLIM experiments was employed. To observe the influence of FDP coexpression as a third partner, 3xHA-FDP expressing vector was used. The cell lysates were obtained from transformed tobacco leaves expressing the 2in1

vector. As a control, the 2in1 vector allowing the expression of free mEGFP with 14-3-3Ω-NLS-mCherry was transformed in tobacco leaves, in the absence or presence of 3xHA-FDP. Free mEGFP and TFL1-mEGFP were immunoprecipitated using GFP trap and subjected to western blot analysis. The immunoprecipitate detected by anti-GFP antibody was used as loading control. The Co-IP of 14-3-3Ω-NLS-mCherry and 3xHA-FDP were detected by anti-RFP and anti-HA antibody, respectively. This assay demonstrates that TFL1 can strongly co-immunoprecipitate 14-3-3 proteins. But in the presence of 3xHA-FDP expression, the strength of 14-3-3 signal is clearly reduced, suggesting the disruption or weakening of TFL1–14-3-3 complexes (Fig **3.4.3A**). As a negative control, free mEGFP was unable to show any Co-IP, indicating the TFL1-specific Co-IP observations. These findings support the weakening of TFL1–14-3-3 interaction by FDP *in planta*, consistent with GST pull-down and FRET-FLIM experiments.

To clarify if this negative effect is caused by phosphorylated FDP, another Co-IP experiment was performed with the same constructs where 14-3-3Ω-NLS-mCherry was immunoprecipitated by using RFP trap. As a biological negative control for this assay, the 3xHA fused to non-phosphomimic mutant, FDP^{T231A}, expressing vector was assembled. To get immunoprecipitate the cell lysates from transformed tobacco leaf epidermal cells was incubated with RFP trap. Then the immunoprecipitate was subjected to western blot analysis and detected by anti-RFP antibody. Co-immunoprecipitation of TFL1-mEGFP and 3xHA-FDP or -FDP^{T231A} were detected by anti-GFP and anti-HA antibody, respectively. The Co-IP results illustrated that, as expected, 14-3-3 proteins strongly bind to the endogenously phosphorylated FDP, but not to FDP^{T231A} (Fig **3.4.3C**). Furthermore, they were able to co-immunoprecipitate TFL1 proteins both in the absence and presence of the FDP^{T231A} mutant. But, only in the presence of 3xHA-FDP, the binding of 14-3-3 to TFL1 was significantly reduced (Fig **3.4.3C**). Together with GST pull-down and FRET-FLIM assays, Co-IP experiments provide strong evidences that support the negative influence of FDP on the TFL1 and 14-3-3 association *in planta*. It is not completely clear whether these three proteins also form a tripartite complex. These findings give a first insight into the differential mechanisms of the antagonistic proteins - FT and TFL1.

3.5 FT and TFL1 compete for the phosphorylated FDP

From colocalization studies, it is apparent that both FT, the floral activator, and its closely related protein with antagonistic function, TFL1, are attracted to the nucleus in the presence of phosphorylated FDP. Consistent with this, rBiFC and FRET-FLIM assays provide evidences that both FT and TFL1 interact with FDP and its phosphomimic mutant FDP^{T231E} in the nucleus.

Despite their antagonistic properties, FT and TFL1 exhibit the similar tendency of nuclear accumulation and interaction behaviour. This led to the hypothesis that these proteins might compete for pFDP in the nucleus. Jaeger *et al*. (2013) have demonstrated that both *FD* and its paralogue, *FDP*, are genetically required for *FT* signaling in promoting flowering, as well as for *TFL1* signaling in repressing flowering in *A. thaliana*. This scenario suggests that a potential competition may occur between FT and TFL1 to fine-tune the initiation of the reproductive phase of the flowering plant. To address this hypothesis of competition *in vivo*, a tool that allows studying the protein-protein interaction dynamics was vital. For FRET-FLIM experiments, the 2in1 vector encoding mCherry fused to FDP^{T231E} (mCherry-FDP^{T231E}) or FDP^{T231A} (mCherry-FDP^{T231A}) together with either FT- or TFL1-mEGFP fusions was transiently expressed in *N. benthamiana*. As a third protein, enhanced cyan fluorescent protein (eCFP) fused either to FT (FT-eCFP) or TFL1 (TFL1-eCFP) was used. FRET-FLIM analyses exhibited that the donor (FT-mEGFP) lifetime is reduced to *2.31 ± 0.05 ns* (mean ± SE) in the presence of mCherry-FDP^{T231E} as an acceptor, as compared to *2.49 ± 0.01 ns* lifetime in the presence of mCherry-FDP^{T231A} (Fig. **3.5B**). Besides, the combination of FT-mEGFP and mCherry-FDP^{T231A} as a biological negative control, 2in1 vector expressing FT-mEGFP and NLS-mCherry combination was also included for additional control measurements in which the donor lifetime was also higher (Supplementary Table **2**). This implies that the lifetime reduction is specific to FT–FDP^{T231E} interaction *in planta*, which is consistent with the rBiFC results (Fig. **3.1.2A**).
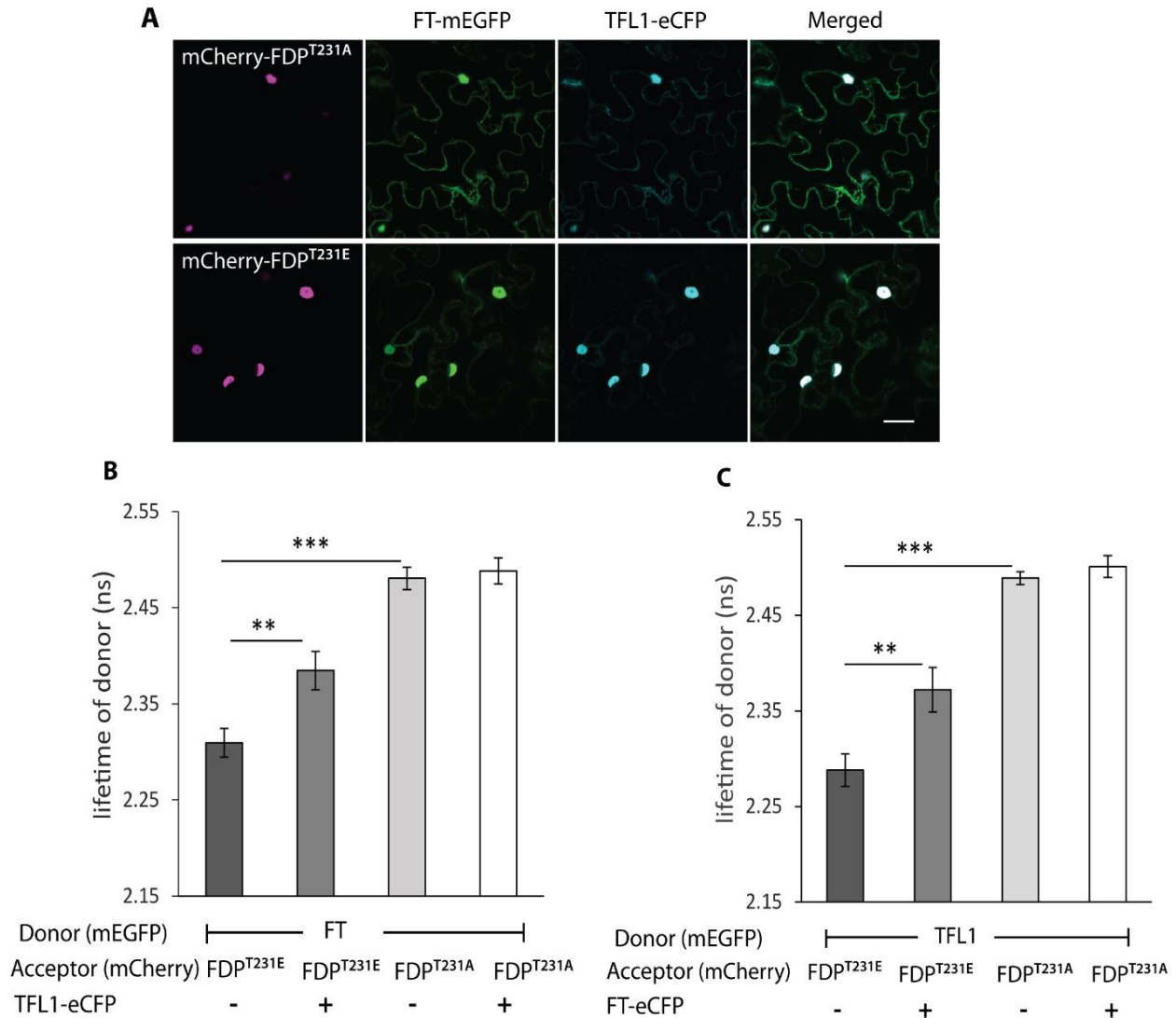
Figure 3.5. 1: Competition between FT and TFL1 *in planta* for a common partner, phosphorylated FDP. **A**, exemplary confocal colocalization images of FT, TFL1 and FDP[T231A] or FDP[T231E] in epidermal cells of *N. benthamiana* leaves. Co-transformation of the 2in1 vector expressing FT and FDP[T231A] or FDP[T231E], together with or without a vector expressing TFL1-eCFP. Scale bar, 30 μm. **B** and **C**, FRET-FLIM measurements were performed in the nuclei of transformed *N. benthamiana* epidermal cells. **B**, mean fluorescence lifetime (ns) of FT-mEGFP in the presence mCherry-FDP[T231E] or FDP[T231A] combined with the absence or presence of TFL1-eCFP. **C**, mean fluorescence lifetime (ns) of TFL1-mEGFP in presence of mCherry-FDP[T231E] or mCherry-FDP[T231A], together with or without FT-eCFP expression. Asterisk ** and *** indicate P value of ≤ 0.01 and ≤ 0.001, respectively and a significant difference on basis of Student's paired t-test. Error bar represents the SE from ≥10 number of nuclei from two independent transformed leaves. Three independent experiments have similar results.

However, in the presence of mCherry-FDP^{T231E} as well as TFL1-eCFP, a significant increase in the FT-mEGFP lifetime to *2.38 ± 0.07 ns* could be observed (Fig. **3.1.2A**). The lifetime of donor showed no decrease or increase in the presence of TFL1-eCFP with controls, indicating that eCFP fusion did not cause any undesirable reduction in donor lifetime. The FRET-FLIM experiment suggests a negative influence of TFL1 protein on FT–FDP complex formation. This finding reflects a scenario where FT and TFL1 *in planta* might compete out for the association with the phosphorylated FDP.

The similar FRET-FLIM experiments were carried out in vice-versa scenario, i.e. additional FT-eCFP was coexpressed, to analyse the negative influence on the complex formation between TFL1 and FDP^{T231E}. The FRET-FLIM analyses showed that the lifetime of TFL1-mEGFP donor alone is *2.49 ± 0.01 ns*, while there was a significant drop in the lifetime to *2.29 ± 0.06 ns* in the presence of mCherry-FDP^{T231E} (Fig. **3.5C**), confirming the TFL1–FDP^{T231E} interaction in agreement with the rBiFC results (Fig. **3.1.2C**). But, in the presence of FT-eCFP, the lifetime for TFL1-mEGFP and mCherry-FDP^{T231E} significantly increased to *2.37 ± 0.09 ns*. In agreement to my observations, it has been demonstrated by applying FRET-FLIM experiments in transformed tobacco leaf epidermal cells that there is a competition between FT and TFL1 orthologs in rose for FD association (Randoux *et al*., 2014). Altogether, the FRET-FLIM experiments reflect that FT and TFL1 could compete in planta for interaction with pFDP.

4. Discussion

FT and TFL1 are key floral regulators, which fine-tune the appropriate flowering onset. In Arabidopsis, FT is expressed in leaves under long-day (LD) conditions and moves to the shoot apical meristem (SAM), while TFL1 is already present in the SAM. These antagonistic proteins have been shown via yeast 2-hybrid assay to interact with the bZIP transcription factors FD and FDP, which are locally expressed in the SAM (Abe *et al*., 2005; Wigge *et al*., 2005). Under LD conditions, both FD and FDP promote the expression of floral identity genes such as *AP1* and *SOC1*. Furthermore, in rice, which responds to inductive short-day conditions, the interaction between FT and FD is not direct. Instead the interaction is mediated by 14-3-3 proteins, leading to the formation of the tripartite complex called 'florigen activation complex' (FAC; Taoka *et al*., 2011). In this study, I analyzed the relation of FDP with important floral regulators FT, TFL1 and 14-3-3 *in planta* using the cell biological and biochemical methods. I could show that the phosphorylation of FDP is the determining factor for the *in planta* interaction with 14-3-3s, FT and TFL1. Moreover, I demonstrated that 14-3-3 proteins play opposing roles in flowering time by regulating both FT and TFL1 signaling pathways. Several lines of evidence reported in this study provide the first hint to the molecular basis of antagonistic activity of FT and TFL1 dependent on 14-3-3.

4.1 Phosphorylation of FDP is a key factor for interaction with floral regulators

The activity of transcription factors including basic zipper (bZIP) transcription factors is modified by various mechanisms, one of which is phosphorylation. Phosphorylation of target proteins can create 14-3-3 binding sites, thus allowing association of these phosphosensors. This association, in turn, can modify target proteins' activity by changing their subcellular localization, stability or ability to interact with other proteins (Gampala *et al*., 2007; Sirichandra *et al*., 2010; Taoka *et al*., 2011). The transcription factors FD and FDP belong to the bZIP Group A. Both have a conserved STAPF-COOH motif, which is a phosphorylation site for calcium-dependent kinases (CPKs; Abe *et al*., 2005). For example, Arabidopsis CPK6 and CPK33 have been shown to efficiently phosphorylate threonine (T) within this motif (Kawamoto *et al*., 2015a). However, it is not yet clear which among the different CPK kinases has the strong effect because single and

even double *knock-outs* of these kinases in plants showed only slightly delayed flowering, probably due to a high functional redundancy within the family (Kawamoto *et al.*, 2015b). The regulation of phosphorylation status of FDP by these kinases seems to be important for an accurate determination of flowering responses.

To demonstrate the significance of phosphorylation of FDP for the interaction with 14-3-3, FT and TFL1, threonine (T) residue within STAPF motif of FDP has been substituted by glutamic acid (E) and alanine (A). First, I could show via MBP pull-down experiments using the phosphomimic FDP protein version (MBP-FDP^{T231E}) that the phosphorylation of threonine within the STAPF-COOH motif of FDP is crucial for 14-3-3 binding. It is thus possible that the phosphorylation of FDP by CPKs facilitates the binding of 14-3-3 proteins. A further *in vitro* experiment could clarify whether the recombinant FDP protein phosphorylated by CPK6/33 is indeed capable of binding to 14-3-3 proteins.

For *in vivo* interaction study, the rBiFC method that is based on 2in1 vector was applied. This novel rBiFC vector allows the introduction of two genes of interest and additional RFP on a single plasmid backbone. This approach ensures equal gene dosage as well as ratiometric analysis via additional free RFP expression. These attributes of rBiFC vector increase the credibility of protein interaction study compared to a classical BiFC (Grefen and Blatt, 2012). For such assay, normally nYFP in combination with the protein of interest is used as control. Here the FDP^{T231A} mutant version, which shows a subcellular localization comparable to wild-type (FDP)/FDP^{231E} version, was used as a biological negative control. In this study, the rBiFC studies demonstrated the *in planta* interaction of 14-3-3s with wild-type FDP and its phosphomimic version FDP^{T231E}, but not with the non-phosphorylatable mutant FDP^{T231A} (Fig. **3.1.1**). This indicates that the phosphorylation of FDP is a crucial factor for FDP−14-3-3 *in vivo* interaction and results in complex formation in the nucleus where the transcription factor is present regardless of T231A or T231E substitution.

FD/FDP interaction with FT and TFL1 has previously been demonstrated, but mostly by yeast two-hybrid (Y2H) assays. Notably these published results agree only partially with each other. For example, it has been proposed that FD/FDP interacts with FT, but not with TFL1 (Jang *et al.*, 2009). Other labs could show a stronger interaction with FT than with TFL1 (Abe *et al.*, 2005; Hanano and Goto, 2011) and a comparable interaction with both FT and TFL1 (Wigge *et al.*,

74

2005). In our lab, Y2H experiments displayed that FDP interacts comparably with FT and TFL1, while FD interacts exclusively with FT and did not or very weakly associate with TFL1 (data not shown).

The *in vivo* physical interaction of FD with FT and TFL1 that takes place in the nucleus has been shown via classical BiFC assays (Abe *et al*., 2005; Hanano and Goto, 2011). However, it was unclear until now whether the interaction of FT and TFL1 with FDP *in planta* depends on the phosphorylation of FDP. By means of rBiFC studies, I could show that both FT and TFL1 interacted with wild-type FDP or its phosphomimic version in the nucleus. By contrast, non-phosphorylatable mutant, FDP[T231A], was incapable of interacting with either floral regulator (Fig. **3.1.2**). It appears that the phosphorylation of FDP is also a crucial factor for the FT–FDP and TFL1–FDP *in vivo* interactions. Remarkably, the antagonistic proteins FT and TFL1 do not differ in their interaction capabilities with FDP.

The phosphorylated target proteins can be modified by 14-3-3s in many ways. It has been described that one of the modes of actions of 14-3-3 proteins is the indirect modulation of target proteins' activity by nucleocytoplasmic shuttling. For example, upon phosphorylation, the transcription factors such as REPRESSION OF SHOOT GROWTH (RSG) that is involved in gibberellic acid signaling and BRASSINAZOLE-RESISTANT 1 (BZR1) that is crucial for brassinosteroid signaling, are retained in the cytoplasm through 14-3-3 binding (Igarashi *et al*., 2001; Rue *et al*., 2007; Gampala *et al*., 2007). The subcellular localization in *N. benthamiana*, performed in this work, showed that 14-3-3s are present highly in the cytoplasm and weakly in the nucleus. And all versions of transcription factor FDP have been observed exclusively in the nucleus. Furthermore, the colocalization studies in this work demonstrate the nuclear accumulation of 14-3-3 proteins upon coexpression with FDP and its phosphomimic version FDP[T231E]. By contrast, 14-3-3s do not accumulate in the nucleus upon coexpression of the non-phosphorylatable version FDP[T231A]. This indicates that the phosphorylated FDP attracts 14-3-3s to the nucleus. This is in agreement with the dynamic capability of 14-3-3 proteins to detect phosphorylated target proteins (Taoka *et al*., 2011; Boer *et al*., 2013).

This further indicates that 14-3-3 proteins can move to the nucleus where the phosphorylated transcription factors such as FDP are present. This is supported by an indirect observation in the regulation of abscisic acid (ABA) signaling (Sirichandra *et al*., 2010). In ABA signaling, the bZIP

transcription factor ABF3 is phosphorylated by OST1 kinase in the nucleus (open stomata 1 - a Snf1-Related Kinases 2; SnRK2), allowing its association with 14-3-3s. The binding of 14-3-3s results in the stabilization of the ABF3 proteins, which in turn regulate long-term responses in ABA signaling (Sirichandra *et al.*, 2010). However, the author did not provide colocalization data for ABF3 and 14-3-3. It is clear that another mode of action of 14-3-3 proteins is the stabilization of target proteins, which play important regulatory role in plant growth and development. This is not the scenario between the transcription factor FDP and 14-3-3. Because the colocalization data demonstrate that FDP^{T231A} version is comparatively stable like wildtype and the phosphomimic version (Fig. **3.2.1A**). It seems that the association of 14-3-3 proteins modifies the capability of the phosphorylated FDP in the nucleus to interact with other proteins such as floral regulators FT and TFL1 (Taoka *et al.*, 2011).

Remarkably the colocalization studies show the similar localization tendency of antagonistic floral regulators FT and TFL1 with FDP. Upon the coexpression of wild-type FDP and FDP^{T231E}, FT as well as TFL1 that are normally present both in the cytoplasm and the nucleus, became highly concentrated in the nucleus. In contrast, the distribution of both floral regulators in the presence of FDP^{T231A} substitution version could be observed in the cytoplasm as well as in the nucleus. These findings show that the antagonistic proteins FT and TFL1 do not differ in their subcellular distributions in living plant cells. Strikingly, nuclear speckles localization of TFL1 was observed exclusively upon coexpression of FDP and FDP^{T231E}. It is possible that the localization of TFL1−FDP complex in nuclear speckles might be essential for the transcriptional repression of floral identity genes like *AP1* (Hanano and Goto, 2011). Moreover, the subcellular localization of TFL1 protein alone is a matter of debate in the literature. I observed TFL1-GFP fluorescence in the cytoplasm and the nucleus, which is consistent with the finding of Hanano and Goto (2011). In contrast, the other scientists reported that TFL1 localizes exclusively to the cytosol (Conti and Bradley, 2007), or associated with the plasma membrane, tonoplast, and vesicles (Sohn *et al.*, 2007). The latter authors proposed that TFL1 (as a floral repressor) would cause the removal of binding partners such as FD/FDP from the nucleus to protein storage vacuoles and thus inhibit the FD/FDP-dependent transcription (Sohn *et al.*, 2007). Further investigation of nuclear speckles localization and its significance in regard to TFL1−FDP function could reveal more about the floral repressing properties of TFL1.

4.2 14-3-3 proteins show dual role in floral transition by interacting with FT and TFL1

FT and TFL1 are key players of photoperiodic flowering pathways in many plant species including *A. thaliana*. The ectopic overexpression of FT (a floral activator) causes an early flowering, but such plants are determined to growth termination with fewer leaves and flowers (Kardailsky *et al*., 1999; Kobayashi *et al*., 1999). This suggests that an uncontrolled FT signaling can cause a drastic reduction in plant biomass. In contrast, constitutive overexpression of TFL1 (a floral repressor) results in significantly delayed flowering and the plant stays in vegetative stage for a long period with a higher number of rosette leaves (Kardailsky *et al*., 1999; Kobayashi *et al*., 1999). Therefore, the fine balance of these antagonistic proteins is critical for a plant to achieve optimal reproduction (Lifschitz *et al*., 2014).

The 14-3-3 proteins are capable of interacting with both FT and TFL1 proteins as shown previously in the Y2H assays and qualitative luciferase complementation assays performed in tobacco (Pnueli *et al*., 2001; Ho and Weigel, 2014). These assays, however, did not tell whether the interaction is phosphorylation dependent. In this study, I have provided evidence using GST pull-down assays with bacterially expressed proteins that 14-3-3 proteins interacted directly with FT as well as with TFL1 proteins in phosphorylation-independent manner (Fig. **3.4.1**). According to quantitative *in vitro* experiments such as microscale thermophoresis (MST), 14-3-3s seem to exhibit a low affinity for the floral antagonists, while the phosphopeptide containing 14-3-3 binding motif of FD/FDP is bound with higher affinity (Nina Jaspert – personal communication). The binding sites in 14-3-3 for FDP and floral antagonists are separated. It has been shown via mutation analysis that *Arabidopsis* FT and TFL1 bind on the outer surface of 14-3-3s away from an amphipathic groove (Nina Jaspert – personal communication), as described for rice FT and 14-3-3 by Taoka *et al*. (2011). The amphipathic grooves of 14-3-3 proteins are preferentially the sites of high affinity binding to the phosphorylated target proteins including transcription factors. In this regard, our lab determined the crystal structure, which shows that FD/FDP phosphopeptide binds in the grooves of 14-3-3s (Christian Ottmann – unpublished data). This is also supported by studies on the crystal structure determined for rice 14-3-3 protein together with Hd3a (FT homolog) and the OsFD1 phosphopeptide (Taoka *et al*., 2011).

Moreover, I could show by applying FRET-FLIM method that 14-3-3 interacts with FT as well as TFL1 in the cytosol where most of the 14-3-3 proteins are present (Fig. **3.3.1**). It was clear from colocalization studies that FT, TFL1 and 14-3-3 all accumulate highly into the nucleus upon phosphorylation of FDP. 14-3-3 proteins are known as scaffold proteins and act as sensors for phosphorylated target proteins including transcription factors. The question was asked whether 14-3-3s have a role in the nuclear import of the unphosphorylated antagonistic proteins, FT or TFL1. It was suggested that rice 14-3-3 acts as an intracellular receptor for Hd3a, based on the movement of 14-3-3−Hd3a BiFC complex into the nucleus upon coexpression of OsFD1 (FD homolog; Taoka *et al.*, 2011). However, one has to keep in mind that irreversible complex formation between two proteins in a BiFC approach may produce an unreliable result. Together with the fact that OsFD1 is a stronger 14-3-3 partner, 14-3-3s would translocate as 14-3-3−Hd3a BiFC complexes into the nucleus thus compelling Hd3a along as a part of the irreversible complex.

The role of 14-3-3 in the import of FT was clarified by using constructs expressing 14-3-3-NLS together with FT, which would allow a free movement of each protein. The colocalization studies exhibited that FT-mEGFP was highly accumulated in the nucleus upon coexpression with 14-3-3-NLS-mCherry (Fig. **3.3.2**). Surprisingly, the floral repressor TFL1 also exhibited the similar tendency of nuclear accumulation with the coexpression of 14-3-3-NLS. This supports the mechanism in which 14-3-3 proteins determine the subcellular localization of these unphosphorylated antagonistic proteins. The modification of subcellular localization of target proteins by 14-3-3 proteins is so far known in the regulation of transcription factors such as RSG and BZR1. This also demonstrates that by interacting with floral antagonists 14-3-3 proteins are possibly involved both in the activation and repression of floral transition in *Arabidopsis*. Interestingly, the dual role of 14-3-3 proteins has been observed in other signaling pathways such as in the regulation of BR signaling (Wang *et al.*, 2011). They act as a positive regulator in the presence of BR by keeping the phosphorylated BRI1 KINASE INHIBITOR 1 (BKI1; a plasma membrane protein) in the cytoplasm. In the absence of BR, as a negative regulator by the cytoplasmic retention of the phosphorylated BZR1 transcription factor and thus inhibiting BR

responses. Such a dual role of 14-3-3 seems to be crucial for a tight regulation of signaling pathways including floral transition.

4.3 Presence of FDP causes different complex assemblies of 14-3-3 with FT and TFL1

The evidence for a larger complex formation among *A. thaliana* FT, 14-3-3 and FDP proteins is lacking. In rice, no direct interaction between Hd3a and OsFD1 (a phosphomimic version) was observed by *in vitro* experiments such as GST pull-down. They could only interact in the presence of 14-3-3 proteins, thus suggesting the existence of a tripartite complex. This points to a crucial role of 14-3-3 proteins in the floral induction. In this work, I showed via GST pull-down assays that *Arabidopsis* FT and the phosphomimic FDP version (FDP^{T231E}) did not interact directly, but an extremely weak interaction could not be excluded. The binding of FDP^{T231E} was detected only in the presence of GST-FT and 14-3-3 proteins, indicating the intermolecular bridging role of 14-3-3 proteins. This suggests that there is a large complex formation among FDP, FT and 14-3-3. A further experiment based on MBP pull-down to test the interaction between MBP-FDP^{T231E} and GST-FT in the absence or presence of His-14-3-3 proteins was not successful (data not shown). A direct weak interaction between Arabidopsis FT and FD had previously been reported using pull-down experiment, which could be due to excessive amounts of these proteins used in the experiments (Abe *et al.*, 2005; Jang *et al.*, 2017). A further investigation of the direct FT-FD/FDP interaction by quantitative experiments such as MST with the full-length FD/FDP proteins tagged to a small tag (e.g. 6xhistidine) would be highly desirable. The possibilities of higher-order complex assemblies *in planta* among FDP, 14-3-3 and FT or TFL1 proteins were investigated by FRET-FLIM technique. The FRET-FLIM is a powerful method to demonstrate a protein-protein interaction in living cells. Using this technique, only a few studies have demonstrated the interaction or stable association among three proteins, indicating the formation of the tripartite complex (Kinoshita *et al.*, 2007; Gibbs *et al.*, 2012). In this work, I employed the FRET-FLIM technique, which has demonstrated that the lifetime of mEGFP-FT has either further reduced or not reduced in the presence of 14-3-3-NLS and FDP as compared to the lifetime of FT−14-3-3-NLS. The lifetime reduction was not observed in all experiments. This might be due to the fact that native 14-3-3 proteins, which are highly abundant, could lead to

the pre-formation of FT−14-3-3−FDP complex in plant cells. This lifetime analysis indicates the positive effect of FDP on the complex formation of FT−14-3-3-NLS. This means that there is the formation of higher-order complexes among FT, FDP and 14-3-3 in living plant cells. Furthermore, the *in vivo* pull-down of three proteins FDP, FT and 14-3-3 has been validated by co-immunoprecipitation (Co-IP) assays. Taken together, GST pull-down, FRET-FLIM, and CO-IP experiments support that the *Arabidopsis* 14-3-3 proteins act as a mediator between FT and FDP for floral activation (Fig. **4.1**). These results are consistent with the florigen complex formation (FAC), reported in rice. However, the important information as to how FT influences the FD-like proteins is still lacking from known crystal structure where phosphopeptide containing 14-3-3 motif of FD has been used (Taoka *et al*., 2011). Surprisingly, this crystal structure does not show any contact of FT with the transcription factor, then how the activity of FDP is modified. Besides, there are other important questions that need further investigation. First, what is the molecular specificity of the transcription factors FD/FDP and 14-3-3 proteins, which are already present in the SAM? Second, what kind of specificities is conferred to FD/FDP after the arrival of FT protein, which leads to its binding to the promoter and thus the activation of floral identity genes such as *AP1*? Therefore, to study these questions the determination of the crystal structure containing FT and 14-3-3 proteins with full-length FD/FDP, ideally in the presence of DNA target sequence, would be imperative. This approach could provide more insights into the structural details of the complex, explaining the specificities conferred to FD/FDP by an upstream signal from FT and 14-3-3.

The floral repressor TFL1 has displayed the subcellular localization and interaction capabilities similar to that of the floral activator FT. I also investigated the *in vivo* connection among TFL1, 14-3-3 and FDP in *N. benthamiana* by performing FRET-FLIM. Remarkably, in this experiment, the TFL1-mEGFP showed higher lifetime in the presence of FDP and 14-3-3-NLS as compared to that of TFL1−14-3-3-NLS. This lifetime analysis suggests that FDP has a strong negative effect on TFL1−14-3-3 complex formation in living plant cells. This *in planta* observation was further validated by Co-IP assays. Even in GST pull-down assays, the presence of MBP-FDP[T231E] showed the similar negative effect on the TFL1−14-3-3 complex formation. Altogether, these results gave the first indication of mechanistic differences between floral antagonistic proteins FT and

TFL1. This negative effect of FDP can be explained in two ways (Fig. **3.4.2**). First, TFL1 and 14-3-3 proteins compete out for the association with phosphorylated FDP.
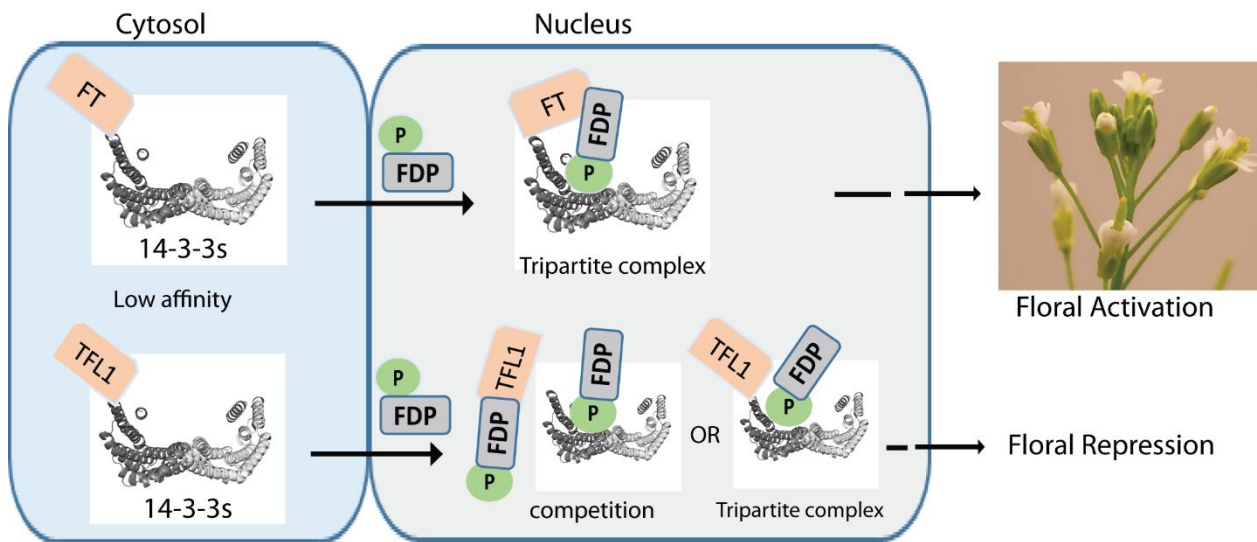

Figure 4. 1: A proposed working model for FDP, 14-3-3, FT and TFL1 in floral transition. 14-3-3 proteins interact with FT and TFL1 in the cytoplasm with low affinity. Upon the phosphorylation of FDP in the nucleus, the complex between 14-3-3s and FT or TFL1 moves to the nucleus. In this scenario, 14-3-3 proteins likely mediate the nuclear import of FT and TFL1 proteins. In the nucleus, the FT–14-3-3 subcomplex associates further with FDP, leading to the formation and stabilization of a tripartite complex. The tripartite complex then promotes the floral activation by enhancing the expression of floral identity genes such as *AP1*. By contrast, FDP negatively affects the TFL1–14-3-3 complex, suggesting two possibilities – either competition between TFL1 and 14-3-3 for FDP association, or a tripartite complex in which TFL1 is located away from FDP. As a result, there is an inhibition of the expression of *AP1* and thus a floral repression.

This would suggest that TFL1 is able to directly bind FDP, but as tested by GST pull-down assays this is not the case, eliminating this possibility. Another explanation is that the presence of phosphorylated FDP might cause such a conformational change and thus different reorganization of resulting tripartite complex with TFL1 and 14-3-3 (Fig. **4**). It was reported that a single amino acid substitution Y85H can change FT into a floral repressor and vice-versa in TFL1 (H88Y) into a floral inducer (Hanzawa *et al*., 2005). Moreover, the crystal structure demonstrated that the residue His-88 in TFL1 forms a hydrogen bond with Asp-144 suggesting rigidity. In contrast, Tyr-85 and Gln-140 (corresponding to Asp-144) in FT do not form such

bond, indicating more flexibility (Ahn *et al*., 2006). This flexibility might explain the ability of FT to stabilize the complex with FDP and 14-3-3 and form a ternary complex, which would then induce the expression of floral identity genes and finally to the onset of flowering (Fig. **4**). On the other hand, TFL1 is oriented in such a manner in complex with FDP and 14-3-3, which would result in repression of the transcriptional activity of FDP. This would thus lead in the repression of floral transition (Fig. **4**). It is known that the same transcription factor may act either as an activator or a repressor, depending on which protein it interacts with. Recently, it was reported that rice TFL1 homolog, RCN, might replace Hd3a in FAC complex turning the complex into a floral repressing complex (Kaneko-Suzuki *et al*., 2018). However, the findings in my study demonstrate that *Arabidopsis* TFL1 do not form FAC-like complex. Therefore, the structural arrangement of TFL1 with FDP and 14-3-3 need to be studied further for understanding of the molecular basis between FT and TFL1. For this, the determination of crystal structure of TFL1 and 14-3-3 proteins with the full-length FD/FDP protein is vital. This could provide answer to the important question - what kind of effects do the antagonistic proteins have on the FD/FDP transcription factor.

The similar interaction as well as localization capabilities of FT and TFL1 with FDP and 14-3-3 proteins suggests a competition for association with these common partners. My FRET-FLIM experiments demonstrated that FT and TFL1 indeed compete for the association with the phosphorylated FDP *in planta*. This competition explains the significance of why the equilibrium between FT and TFL1 proteins are required. This is important for adaption to various environmental changes in order to achieve the optimal reproductive success by the plants. It was shown in tomato that the fine balance between FT and TFL1 proteins is required to achieve optimal reproduction (Lifschitz *et al*., 2014). It has been further demonstrated how the balance between these antagonistic proteins are good targets to optimize and enhance the crop productivity. This knowledge has been applied to many other crop systems, besides tomato, to improve the crop yield (Park *et al*., 2014).

4.4 Multiple roles of florigen in plants

In my hand, the *fdp* knock-out lines did show a slight difference in flowering rate, but no difference in term of rosette leaf number as compared to Col-0 (Supplementary Fig. **S1**). As expected, the *fd mutants* exhibited a stronger flowering delay phenotype compared to *fdp* mutant (Jaeger *et al*., 2013; Supplementary Fig. **S1E**). The overexpression of *FDP* as well as of 14-3-3 binding mutations - *FDP^{T231A}* and *FDP^{T231E}* under the control of *35S* promoter in *fdp* background flowered more or less like Col-0 and empty vector expression (Supplementary Fig. **S2B**). In this study, the overexpression of phosphomimic mutant *FDP^{T231E}*, however, exhibited a predominant flat leaves phenotype as compared to wild-type Col-0, and the plant lines overexpressing free GFP, FDP and *FDP^{T231A}* (Supplementary Fig. **S2A**)*.* This phenotype demonstrates the significance of the phosphorylation status of FDP and suggests that the regulation of FDP phosphorylation is important in *Arabidopsis*. Furthermore, this phenotype indicates an additional role of FDP overexpression, possibly together with FT and 14-3-3s, in the leaf development. A previous study reported that the loss of FD fully suppressed leaf curling and leaf-size reduction of constitutive *FT* expressing plants. This suggests the involvement of *Arabidopsis* FT together with FD in the leaf development and curling (Teper-Bamnolker and Samach, 2005). It seems that bZIP proteins are capable of forming homo- and/or heterodimers, thus, it is thus likely that ectopic expression of these proteins induce novel phenotypes by disrupting original interactions and/or forming de novo interactions, which result in transcriptional modifications in the plant cells.

Another study in rice have demonstrated that *OsFD1* and *OsFD2,* which are Poaceae-specific FD homologs, have been diversified to have a distinct function in plants, even though their interacting partners remain identical (Tsuji *et al*., 2013). The plants expressing phosphomimic version *OsFD1^{S192E}* under ubiquitin promoter had accelerated flowering, while overexpression of *OsFD2* produced smaller leaf suggesting its role in the leaf development. Furthermore, the authors showed that OsFD2 interacted with both 14-3-3 and Hd3a, which are interacting partners of OsFD1, suggesting the possibility that OsFD2 could replace OsFD1 in the florigen activation complex (FAC; Tsuji *et al*., 2013). It appears that besides flowering, the involvement of FDP and FD in the leaf development could be owing to the interaction with FT and 14-3-3.

This supports the possibility of other role for Arabidopsis FD homologs, besides flowering, in the other developmental processes such as leaf development.

This also might indicate the additional involvement of FT, besides flowering, in other developmental processes, possibly via interacting with many different proteins such as transcription factors. To this end, many roles of FT homologs have been reported such as tuberization in potato (Navarro *et al*., 2011; Teo *et al*., 2017), growth cessation and bud set in Populus (Hsu *et al*., 2011), leaf shape and inflorescence architecture in tomato (Park *et al*., 2014), leaf curling (Teper-Bamnolker and Samach, 2005) and stomatal opening in *Arabidopsis* (Kinoshita *et al*., 2011). It is evident that FT is localized both in the nucleus and cytoplasm. However, the purpose of the cytoplasmic localization of FT protein in plant cells remains unknown. It has been reported that FT regulates the stomatal opening via an unidentified component that modulates the activity plasma membrane localized H^+-ATPase (Kinoshita *et al*., 2011).

Both FDP and H^+-ATPase are 14-3-3 interaction partners whose binding motifs differ from the canonical 14-3-3 motifs. Thus there remains a gap in the typical 14-3-3 binding groove, which might accommodate a surface exposed FT domain. It is further supported by the fact that the presence of Tyr-85 in FT confers the flexibility thus allowing FT to fill the gap in 14-3-3 binding groove. This scenario then leads to the stabilization of the complex among FT, 14-3-3 and H^+-ATPases , similar to FT–13-3-3–FD complex. In line with this assumption, I explored this aspect of FT and could show that FT is able to interact with the plasma membrane localized H^+-ATPases - AHA1 and AHA2 by means of FRET-FLIM experiments (Supplementary Fig. **S3A;** data not shown for AHA2). It is well-known that 14-3-3s regulate these proton ATPases through binding to the phosphorylated YpTV-COOH motif (Ottmann *et al*., 2007). Therefore, I checked whether the phosphorylation of threonine within this motif is also crucial for the FT association.

The FRET-FLIM data showed that the alanine substitution version, AHA1[T953A], has reduced interaction capability with FT as compared to wild-type AHA1 (Supplementary Fig. **S3A**). Furthermore, this mutant was unable to interact with 14-3-3s in similar experiments (Supplementary Fig. **S3C**). Altogether, these findings support our hypothesis that FT might act as an endogenous stabilizer for the interaction of H^+-ATPases and 14-3-3 proteins, which then modulates the opening of stomata. Furthermore, these data suggest the cytosolic function of FT

in the regulation of stomatal opening via the regulation of AHAs in a 14-3-3 dependent manner. This finding also supports the multi-functionality of FT and its importance in regulation of several developmental processes, the evidence for which is growing in the scientific community. In conclusion, I demonstrated that 14-3-3s are capable of binding to the antagonistic proteins FT and TFL1 in the cytoplasm in a phosphorylation-independent manner. Upon the phosphorylation of FDP in the nucleus, 14-3-3s facilitate the translocation of FT and TFL1 from the cytoplasm to the nucleus. Once in the nucleus, the interaction of FT and FDP is mediated by 14-3-3s, resulting in the formation of tripartite complex in which FT might boost the transcriptional activity of FDP. This in turn enhances the expression of *AP1* leading to floral activation. By contrast, FDP negatively affects the complex formation between TFL1 and 14-3-3, indicating the inability of TFL1 to stabilize the tripartite complex. This complex with TFL1 might then suppress the transcriptional activity of FDP, reducing the expression of *AP1*. In fact, TFL1 competes with stable FT–14-3-3–FDP for the association with the phosphorylated FDP. The 14-3-3s show a dual role in floral transition by interacting with floral antagonists FT and TFL1. Altogether there is an indication of differential mechanism for antagonistic proteins. Such a complex regulation is crucial for integrating various internal and external cues for the precise timing of flowering in plants. This knowledge offers a further ways to manipulate FT and TFL1 signaling, which would increase the repertoire of tools necessary for boosting the agricultural productivity.

5. References

Abe M, Kobayashi Y, Yamamoto S, Daimon Y, Yamaguchi A, Ikeda Y, Ichinoki H, Notaguchi M, Goto K, Araki T (2005) FD, a bZIP Protein Mediating Signals from the Floral Pathway Integrator FT at the Shoot Apex. Science **309:** 1052-1056

Ahn JH, Miller D, Winter VJ, Banfield MJ, Lee JH, Yoo SY, Henz SR, Brady RL, Weigel D (2006) A divergent external loop confers antagonistic activity on floral regulators FT and TFL1. The Embo J **25**: 605-614

Aitken A (2002) Functional specificity in 14-3-3 isoform interactions through dimer formation and phosphorylation. Chromosome location of mammalian isoforms and variants. Plant Mol Biol **50**: 993-1010

Bradley DJ, Ratcliffe OJ, Vincent C, Carpenter R and Coen ES (1997) Inflorescence commitment and architecture in Arabidopsis. Science **275**: 80-83

Bucherl CA, Bader A, Westphal AH, Laptenok SP, Borst JW (2014) FRET-FLIM applications in plant systems. Protoplasma **251:** 383-394

Bucherl CA, van Esse GW, Kruis A, Luchtenberg J, Westphal AH, Aker J, van Hoek A, Albrecht C, Borst JW, de Vries SC (2013) Visualization of BRI1 and BAK1(SERK3) membrane receptor heterooligomers during brassinosteroid signaling. Plant Physiol **162:** 1911-1925

Clough SJ, Bent AF (1998) Floral dip: a simplified method for Agrobaterium-mediated transformation of Arabidopsis thaliana. Plant J 16(6): 735-743

Conti L, Bradley D (2007) TERMINAL FLOWER1 is a mobile signal controlling Arabidopsis architecture. The Plant Cell **19:** 767-778

Corbesier L, Vincent C, Jang S, Fornara F, Fan Q, Searle I, Giakountis A, Farrona S, Gissot L, Turnbull C, Coupland G (2007) FT protein movement contributes to long-distance signaling in floral induction of *Arabidopsis*. Science **316**: 1030-1033

de Boer AH, van Kleeff PJ, Gao J (2013) Plant 14-3-3 proteins as spiders in a web of phosphorylation. Protoplasma **250:** 425-440

Denison FC, Paul A-L, Zupanska AK, Ferl RJ (2011) 14-3-3 proteins in plant physiology. Seminars in Cell & Development Biol **22**: 720-727

Dundr M (2012) Nuclear bodies: multifunctional companions of the genome. Curr Opin Cell Biol **24**: 415-422

Fernandez V, Takahashi Y, Le Gourrierec J, Coupland G (2016) Photoperiodic and thermosensory pathways interact through CONSTANS to promote flowering at high temperature under short days. Plant J **86:** 426-440

Fornara F, Panigrahi KC, Gissot L, Sauerbrunn N, Rühl M, Jarillo JA, Coupland G (2009) *Arabidopsis* DOF transcription factors act redundantly to reduce *CONSTANS* expression and are essential for a photoperiodic flowering response. Dev Cell **17**: 75-86

Gampala SS, Kim T-W, He J-X, Tang W, Deng Z, Bai M, Guan S, Lalonde S, Sun Y, Gendron JM, *et al.* (2007) An Essential Role for 14-3-3 Proteins in Brassinosteroid Signal Transduction in Arabidopsis. Dev Cell **13(2)**: 177-189

Ganguly S, Weller JL, Ho A, Chemineau P, Malpaux B, Klein DC (2005) Melatonin synthesis: 14-3-3-dependent activation and inhibition of arylalkylamine N-acetyltransferase mediated by phosphoserine-205. Proc Natl Acad Sci USA **102**: 1222-1227

Genoud T, Schweizer F, Tscheuschler A, Debrieux D, Casal JJ, Schäfer E, Hiltbrunner A, Frankhauser C (2008) FHY1 mediates nuclear import of the light-activated phytochrome A photoreceptor. PLoS Genet 4: e1000143

Gibbs PEM, Miralem T, Lerner-Marmarosh N, Tudor C, Maines MD (2012) Formation of Ternary Complex of Human Biliverdin Reductase-Protein Kinase C -ERK2 Protein Is Essential for ERK2-mediated Activation of Elk1 Protein, Nuclear Factor- B, and Inducible Nitric-oxidase Synthase (iNOS). J Biol Chem **287**: 1066-1079

Grefen C, Blatt MR (2012) A 2in1 cloning system enables ratiometric bimolecular fluorescence complementation (rBiFC). BioTechniques Rapid Dispatches

Guo Y, Hans H, Christian J, Molina C (2014) Mutations in single FT- and TFL1-paralogs of rapeseed (Brassica napus L.) and their impact on flowering time and yield components. Front Plant Sci **5:** 282

Hanano S, Goto K (2011) Arabidopsis TERMINAL FLOWER1 Is Involved in the Regulation of Flowering Time and Inflorescence Development through Transcriptional Repression. The Plant Cell **23**: 3172-3184

Hanzawa Y, Money T, Bradley D (2005) A single amino acid converts a repressor to an activator of flowering. Proc Natl Acad Sci USA **102**: 7748-7753

Hecker A, Wallmeroth N, Peter S, Blatt MR, Harter K, Grefen C (2015) Binary 2in1 Vectors Improve in Planta (Co)localization and Dynamic Protein Interaction Studies. Plant Physiol **168:** 776-787

Ho WW, Weigel D (2014) Structural features determining flower-promoting activity of Arabidopsis FLOWERING LOCUS T. The Plant Cell **26:** 552-564

Hsu C-Y, Adams JP, Kim H, No K, Ma C, Strauss SH, Drnevich J, Vandervelde L, Ellis JD, Rice BM, *et al.* (2011) *FLOWERING LOCUS T* duplication coordinates reproductive and vegetative growth in perennial poplar. Proc Natl Acad Sci USA **108(26)**: 10756-10761

Igarashi D, Ishida S, Fukazawa J, Takahashi Y (2001) 14-3-3 Proteins Regulate Intracellular Localization of the bZIP Transcriptional Activator RSG. The Plant Cell **13**: 2483-2497

Imaizumi T, Schultz TF, Harmon FG, Ho LA, Kay SA. (2005) FKF1 F-box protein mediates cyclic degradation of a repressor of *CONSTANS* in *Arabidopsis*. Science **309**: 293-297

Ito T, Nakata M, Fukazawa J, Ishida S, Takahashi Y (2014) Scaffold Function of Ca2+-Dependent Protein Kinase: Tobacco Ca2+-DEPENDENT PROTEIN KINASE1 Transfers 14-3-3 to the Substrate REPRESSION OF SHOOT GROWTH after Phosphorylation. Plant Physiol **165**: 1737-1750

Jaeger KE, Wigge PA (2007) FT protein acts as a long-range signal in Arabidopsis. Curr Biol **17**: 1050-1054

Jaeger KE, Pullen N, Lamzin S, Morris RJ, Wigge PA (2013) Interlocking feedback loops govern the dynamic behavior of the floral transition in Arabidopsis. The Plant Cell **25:** 820-833

Jang S, Li S-Y, Kuo M-L (2017) Ectopic expression of Arabidopsis FD and FD PARALOGUE in rice results in dwarfism with size reduction of spikelets. Sci Rep **7**: 44477

Jang S, Torti S, Coupland G (2009) Genetic and spatial interactions between FT, TSF and SVP during the early stages of floral induction in Arabidopsis. The Plant Journal **60**: 614-625

Jaspert N, Throm C, Oecking C (2011) *Arabidopsis* 14-3-3 proteins: fascinating and less fascinating aspects. Front Plant Sci **2**: 1-8

Jelich-Ottmann C, Weiler EW, Oecking C (2001) Binding of regulatory 14-3-3 proteins to the C-terminus of the plant plasma membrane H$^+$-ATPase involves part of its autoinhibitory region. J Biol Chem **276**: 39852-39857

Kardailsky I, Shukla VK, Ahn JH, Dagenais N, Christensen SK, Nguyen JT, Chory J, Harrison MJ, Weigel D (1999) Activation Tagging of the Floral Inducer *FT*. Science **286**: 1962-1965

Kaneko-Suzuki M, Kurihara-Ishikawa R, Okushita-Terakawa C, Kojima C, Nagano-Fujiwara M, Ohki I, Tshuji H, Shimamoto K, Taoka KI (2018) TFL1-like proteins in rice antagonize rice FT-like protein in inflorescence development by competition for complex formation with 14-3-3 and FD. Plant Cell Physiol **59**: 458-468

Karimi M, Inzé D, Depicker A (2002) GATEWAY vectors for Agrobacterium-mediated plant transformation. Trends Plant Sci **7**: 193-195

Kawamoto N, Sasabe M, Endo M, Machida Y, Araki T (2015a) Calcium-dependent protein kinases responsible for the phosphorylation of a bZIP transcription factor FD crucial for the florigen complex formation. Sci Rep **5**: 8341

Kawamoto N, Endo M, Araki T (2015b) expression of a kinase-dead form of CPK33 involved in florigen complex formation causes delayed flowering. Plant Signal Behav **10**(12)

Keicher J, Jaspert N, Weckermann K, Möller C, Throm C, Kintzi A, Oecking C (2017) Arabidopsis 14-3-3 epsilon members contribute to polarity of PIN auxin carrier and auxin transport-related development. Elife **6**: e24336

Kinoshita K, Goryo K, Takada M, Tomokuni Y, Aso T, Okuda H, Shuin T, Fukumura H, Sogawa K (2007) Ternary complex formation of pVHL, elongin B and elongin C visualized in living cells by a fluorescence resonance energy transfer–fluorescence lifetime imaging microscopy technique. the FEBS Journal **274**: 5567-5575

Kobayashi Y, Kaya H, Goto K, Iwabuchi M, Araki T (1999) A Pair of Related Genes with Antagonistic Roles in Mediating Flowering Signals. Science **286**: 1960-1962

Kobayashi Y, Weigel D (2007) Move on up, it's time for change – mobile signals controlling photoperiod-dependent flowering. Genes Dev **21**: 2371-2384

Koncz C, Schell J (1986) The promoter of TI-DNA gene 5 controls the tissue-specific expression of chimeric genes carried by a novel type of Agrobacterium binary vector. Mol Gen Genet **204**: 383-396

Koornneef M, Hanhart CJ, van der Veen JH (1991) A genetic and physiological analysis of late flowering mutants in Arabidopsis thaliana. Mol Gen Genet **229:** 57-66

Kwaaitaal M, Keinath NF, Pajonk S, Biskup C, Panstruga R (2010) Combined Biomolecular Fluorescence Complementation and Förster Resonance Energy Transfer Reveals Ternary SNARE Complex Formation in Living Plant Cells. Plant Physiol **152**: 1135-1147

Laubinger S, Marchal V, Gentilhomme J, Wenkel S, Adrian J, Jang S, Kulajta C, Braum H, Coupland G, Hoecker U (2006) *Arabidopsis* SPA proteins regulate photoperiodic flowering and interact with the floral inducer CONSTANS to regulate its stability. Development **133**: 3213-3222

Lichocka M, Schmelzer E (2014) Subcellular Localization Experiments and FRET-FLIM Measurements in Plants. *Bio-protocol* 4(1): e1018. DOI: 10.21769/BioProtoc.1018.

Lifschitz E, Ayre BG, Eshed Y (2014) Florigen and anti-florigen - a systemic mechanism for coordinating growth and termination in flowering plants. Front Plant Sci **5:** 465

Liu L, Liu C, Hou X, Xi W, Shen L, Tao Z, Wang Y, Yu H (2012) FTIP1 is an essential regulator required for florigen transport. PLOS Biol **10**: e1001313

Liu Y, Li X, Li K, Liu H, Lin C (2013) Multiple bHLH proteins form heterodimers to mediate CRY2-dependent regulation of flowering-time in Arabidopsis. PLOS Genet **9**: e1003861

Liu H, Yu X, Li K, Klejnot J, Yang H, Lisiero D, Lin C (2008) Photoexcited CRY2 interacts with CIB1 to regulate transcription and floral initiation in *Arabidopsis*. Science 322: 1535-1539

Muszynski MG, Dam T, Li B, Shirbroun DM, Hou Z, Bruggemann E, Archibald R, Ananiev EV, Danilevskaya ON (2006) delayed flowering 1 Encodes a basic leucine zipper protein that mediates floral inductive signals at the shoot apex in maize. Plant Physiol **142**: 1523-1536

Navarro C, Abelenda JA, Cruz-Oró E, Cuéllar CA, Tamaki S, Silva J, Shimamoto K, Prat S (2011) Control of flowering and storage organ formation in potato by FLOWERING LOCUS T. Nature **478**: 119-122

Niwa M, Daimon Y, Kurotani K, Higo A, Pruneda-Paz JL, Breton G, Mitsuda N, Kay SA, Ohme-Takagi M, Endo M, Araki T (2013) BRANCHED1 interacts with FLOWERING LOCUS T to repress the floral transition of the axillary meristems in Arabidopsis. The Plant Cell **25:** 1228-1242

Ottmann C, Marco S, Jaspert N, Marcon C, Schauer N, Weyand M, Vandermeeren C, Duby G, Boutry M, Wittinghofer A, Rigaud J-L, Oecking C (2007) Structure of a 14-3-3Coordinated Hexamer of the Plant Plasma Membrane H^+-ATPase by Combining X-Ray Crystallography and Electron Cryomicroscopy. Molecular Cell **25**: 427-440

Park SJ, Jiang K, Tal L, Yichie Y, Gar O, Zamir D, Eshed Y, Lippman ZB (2014) Optimization of crop productivity in tomato using induced mutations in the florigen pathway. Nat Genet **46:** 1337-1342

Pnueli L, Gutfinger T, Hareven D, Ben-Naim O, Ron N, Adir N, Lifschitz E (2001) Tomato SP-Interacting Proteins Define a Conserved Signaling System That Regulates Shoot Architecture and Flowering. The Plant Cell **13**: 2687-2702

Putterill J, Robson F, Lee K, Simon R, Coupland G (1995) The *CONSTANS* gene of *Arabidopsis* promotes flowering and encodes a protein showing similarities to zinc finger transcription factors. Cell **80**: 847-857

Purwestri YA, Ogaki Y, Tamaki S, Tsuji H, Shimamoto K (2009) The 14-3-3 protein GF14c acts as a negative regulator of flowering in rice by interacting with the florigen Hd3a. Plant Cell Physiol **50:** 429-438

Randoux M, Daviere JM, Jeauffre J, Thouroude T, Pierre S, Toualbia Y, Perrotte J, Reynoird J-P, Jammes M-J, Oyant L H-S, Foucher F (2014) RoKSN, a floral repressor, forms protein complexes with RoFD and RoFT to regulate vegetative and reproductive development in rose. New Phytol **202:** 161-173

Rosenquist M, Alsterfjord M, Larsson C, Sommarin M (2001) Data mining the *Arabidopsis* genome reveals fifteen 14-3-3 genes. Expression is demonstrated for two out of five novel genes. Plant Physiol **127**: 142-149

Ryu H, Kim K, Cho H, Park J, Choe S, Hwanga I (2007) Nucleocytoplasmic Shuttling of BZR1 Mediated by Phosphorylation Is Essential in Arabidopsis Brassinosteroid Signaling. The Plant Cell **19**: 2749-2762

Samach A, Onouchi H, Gold SE, Ditta GS, Schwarz-Sommer Z, Yanofsky MF, Coupland G. (2000) Distinct roles of CONSTANS target genes in reproductive development of Arabidopsis. Science **288**: 1613-1616

Sawa M, Nusinow DA, Kay SA, Imaizumi T (2007) FKF1 and GIGANTEA complex formation is required for day-length measurement in Arabidopsis. Science **318**: 261-265

Schoeb H, Kunz C, Meins F Jr (1997) Silencing of transgenes introduced into leaves by agroinfiltration: a simple, rapid method for investigating sequence requirements for gene silencing. Mol Gen Genet **256**: 581-585

Shaw PJ, Brown JW (2004) Plant nuclear bodies. Curr Opin Plant Biol **7**: 614-620

Sheerin DJ, Menon C, zur Oven-Krockhaus S, Enderle B, Zhu L, Johnen P, Schleifenbaum F, Stierhof Y-D, Huq E and Hiltbrunner A (2015) Light-Activated Phytochrome A and B Interact with Members of the SPA Family to Promote Photomorphogenesis in Arabidopsis by Reorganizing the COP1/SPA Complex. The Plant Cell **27:** 189-201

Sohn EJ, Rojas-Pierce M, Pan S, Carter C, Serrano-Mislata A, Madueno F, Rojo E, Surpin M, Raikhel NV (2007) The shoot meristem identity gene TFL1 is involved in flower development and trafficking to the protein storage vacuole. Proc Natl Acad Sci USA **104:** 18801-18806

Song YH, Lee I, Lee SY, Imaizumi T, Hong JC (2012a) CONSTANS and ASYMMETRIC LEAVES 1 complex is involved in the induction of *FLOWERING LOCUS T* in photoperiodic flowering in *Arabidopsis*. Plant Journal **69**: 332-342

Song YH, Smith RW, To BJ, Millar AJ, Imaizumi T (2012b) FKF1 conveys timing information for CONSTANS stabilization in photoperiodic flowering. Science **336**: 1045-1049

Sparkes IA, Runions J, Kearns A, Hawes C (2006) Rapid, transient expression of fluorescent fusion proteins in tobacco plants and generation of stably transformed plants. Nat Protoc **1**: 2019-2025

Suárez-López P, Wheatley K, Robson F, Onouchi H, Valverde F, Coupland G (2001) *CONSTANS* mediates between the circadian clock and the control of flowering in *Arabidopsis*. Nature **410**: 1116-1120

Svennelid F, Olsson A, Piotrowski M, Rosenquist M, Ottman C, Larsson C, Oecking C, Sommarin M (1999) Phosphorylation of Thr-948 at the C terminus of the plasma membrane H^+-ATPase creates a binding site for the regulatory 14-3-3 protein. The Plant Cell **11**: 2379-2391

Takashi K, Hayashi K, Kinoshita T (2012) Auxin activates the plasma membrane H^+-ATPase by phosphorylation during hypocotyl elongation in *Arabidopsis*. Plant Phyiol **159**: 632-641

Tamaki S, Matsuo S, Wong HL, Yokoi S, Shimamoto K (2011) Hd3a protein is a mobile flowering signal in rice. Science **316**: 1033-1036

Taoka K, Ohki I, Tsuji H, Furuita K, Hayashi K, Yanase T, Yamaguchi M, Nakashima C, Purwestri YA, Tamaki S *et al.* (2011) 14-3-3 proteins act as intracellular receptors for rice Hd3a florigen. Nature **476:** 332-335

Teo CJ, Takahashi K, Shimizu K, Shimamoto K, Taoka KI (2017) Potato Tuber Induction is Regulated by Interactions Between Components of a Tuberigen Complex. Plant Cell Physiol **58:** 365-374

Tiwari SB, Shen Y, Chang HC, Hou Y, Harris A, Ma SF, McPartland M, Hymus GJ, Adam L, Marion C, *et al.* (2010) The flowering time regulator CONSTANS is recruited to the *FLOWERING LOCUS T* promoter via a unique cis-element. New Phytol **187**: 57-66

Tramier M, Zahid M, Mevel JC, Masse MJ, Coppey-Moisan M (2006) Sensitivity of CFP/YFP and GFP/mCherry pairs to donor photobleaching on FRET determination by fluorescence lifetime imaging microscopy in living cells. Microsc Res Tech **69**: 933-939

Tsuji H, Nakamura H, Taoka K, Shimamoto K (2013) Functional Diversification of FD Transcription Factors in Rice, Components of Florigen Activation Complexes. Plant Cell Physiol **54(3)**: 385-397

van Kleeff PJ, Jaspert N, Li KW, Rauch S, Oecking C, de Boer AH (2014) Higher order Arabidopsis 14-3-3 mutants show 14-3-3 involvement in primary root growth both under control and abiotic stress conditions. J Exp Bot **65(20)**: 5877-5888

Wang H, Yang C, Zhang C, Wang N, Lu D, Wang J, Zhang S, Wang ZX, Ma H, Wang X (2011) Dual role of BKI1 and 14-3-3 s in brassinosteroid signaling to link receptor with transcription factors. Dev Cell **21:** 825-834

Wenkel S, Turck F, Singer K, Gissot L, Gourrierec J, Samach A, Coupland G (2006) CONSTANS and the CCAAT box binding complex share a functionally important domain and interact to regulate flowering of *Arabidopsis*. The Plant Cell **18**: 2971-2984

Wigge PA, Kim MC, Jaeger KE, Busch W, Schmid M, Lohmann JU, Weigel D (2005) Integration of spatial and temporal information during floral induction in Arabidopsis. Science **309:** 1056-1059

Wurtele M, Jelich-Ottmann C, Wittinghofer A, Oecking C (2003) Structural view of a fungal toxin acting on a 14-3-3 regulatory complex. The EMBO J **22**: 987-994

Yaffe MB, Rittinger K, Volinia S, Caron PR, Aitken A, Leffers H, Gamblin SJ, Smerdon SJ, Cantley LC (1997) The structural basis for 14-3-3: phosphopeptide binding specificity. Cell **91**: 961-971

Yoo SC, Chen C, Rojas M, Daimon Y, Ham BK, Araki T, Lucas WJ (2013a) Phloem long-distance delivery of FLOWEIRNG LOCUS T (FT) to the apex. Plant J **75**: 456-468

Yoo SJ, Hong SM, Jung HS, Ahn JH (2013b) The cotyledons produce sufficient FT protein to induce flowering: evidence from cotyledon micrografting in *Arabidopsis.* Plant Cell Physiol **54**: 119-128

Zuo Z, Liu H, Liu B, Liu X, Lin C (2011) Blue light-dependent interaction of CRY2 with SPA1 regulates COP1 activity and floral initiation in *Arabidopsis*. Curr Biol. **21**: 841-847

Zhu Y, Liu L, Shen L, Yu H (2016) NaKR1 regulates long-distance movement of FLOWERING LOCUS T in Arabidopsis. Nat Plants **2:** 16075

6. Supplemental data

6.1 Leaf phenotype of overexpression lines of FDP

Flowering phenotype of *fdp* mutants is disputable. The publication by Jaeger *et al*. (2013) reported that there is a slight flowering phenotype in TILLING lines of *FDP*, which has a point mutation in DNA binding motif. However, the previous publication could not observe any clear flowering phenotype of many *FDP* tilling lines (Hanano and Goto, 2011). To gain insight into the physiological role of FDP, I checked the available the knock-out mutation lines of *fdp* (SALK_200741C). This mutant line was genotyped on genetic and transcript levels, and found to be null mutant (Supplementary Fig. **S1**). Though there was evident delay in flowering formation in *fdp* mutant plant compared to wild-type Columbia-0 (Col-0) plant, no difference was observed in term of rosette leaf number. To check the consequences for the constitutive expression of *FDP* mutations that influence 14-3-3 binding, I created the *35S* promoter driven overexpression lines of GFP fused to FDP or its substitution mutants: FDP^{T231A} and FDP^{T231E} in *fdp* mutant background. In T2 generation, these overexpression plants did not show any difference in flowering in term of rosette leaf number (data not shown). However, some differences in leaves' shape among constitutive expression plant lines as compared to free GFP (empty vector) could be observed. The 3 rosette leaves emanating from at least 2 independent T2 plants of each construct line were photographed (Supplementary Fig. **S2**). The leaves in *35S::GFP-FDP* look comparatively wider than *35S::GFP* and non-phosphorylatable, *35S::GFP-FDP^{T231A}*. But, the phosphomimic mutant *35S::FDP^{T231E}* line has more predominant leaf flattening phenotype among all. Together, these results indicate the possible role of *FDP* in the leaf development. The dwarf plant with smaller leaves has been reported for the constitutive expression lines of *35S::FD* and *35S::FD^{T282S}*, which could complement *fd*-1 mutant (Abe *et al.*, 2005). Different roles of FAC in plant growth and development in addition to flowering has been proposed (Taoka *et al.*, 2013). In this regard, Tsuji *et al.* (2013) published that the function of *OsFD2* in leaf development has diverged from its homolog, *OsFD1*, function in flowering in rice. So, it is possible that FDP might be involved in leaf development other than flowering.
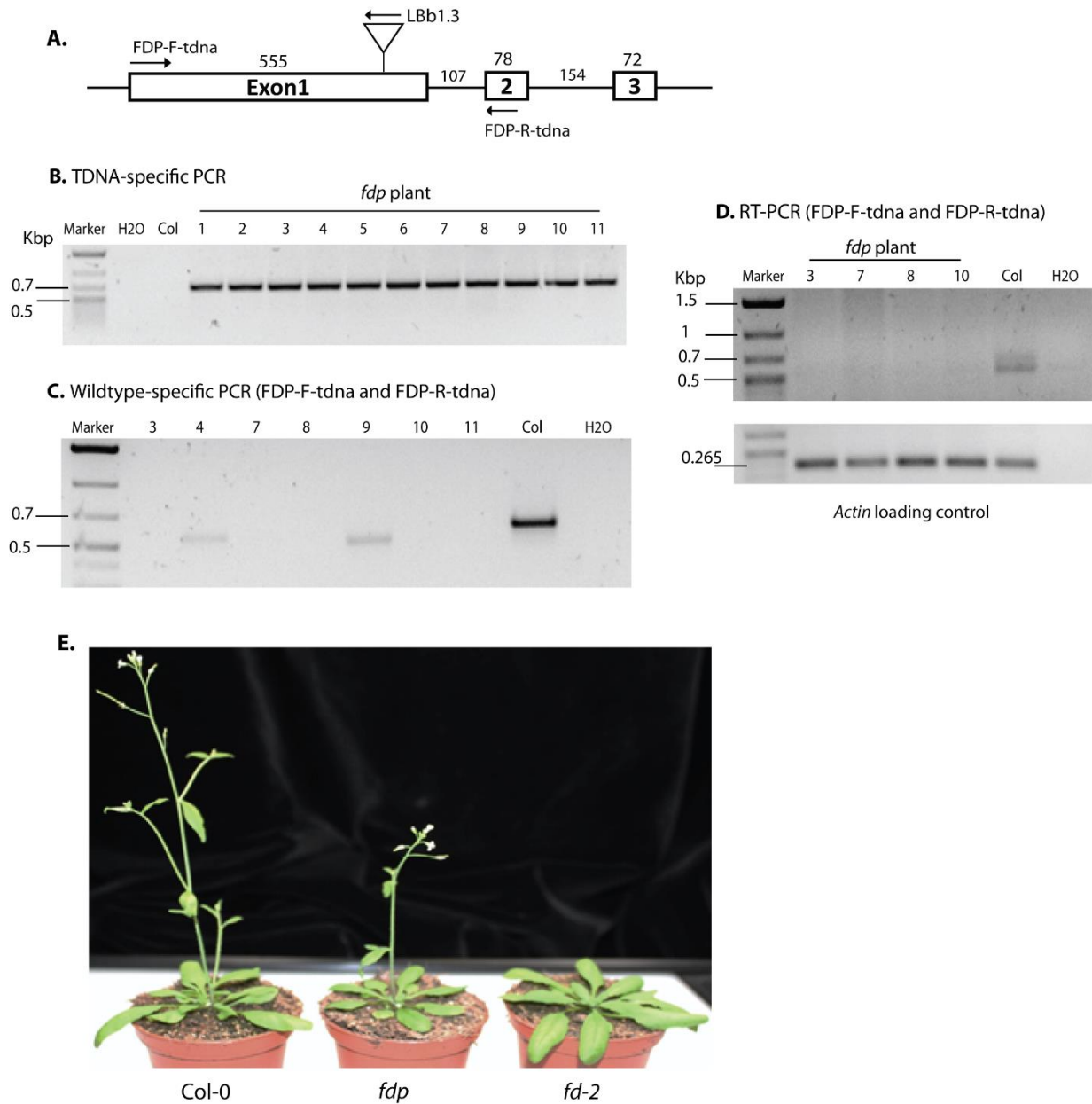
Figure S1: Genotyping and Phenotyping of *fdp* TDNA insertion plant. **A**, schematic representation of *FDP* gene structure. **B**, TDNA-specific PCR on *fdp* mutant plants showing the insertion of TDNA at the end of Exon1 of *FDP* gene. **C**, PCR with insert specific primers on some plant samples from **B**. **D**, Reverse transcription PCR (RT-PCR) on cDNA created from mRNA, which was extracted from shoot apical region. Actin cDNA was used as a loading control. Col- Columbia Col-0, H2O- water control, Marker – DNA ladder. **E**, Flowering Phenotype of Col-0, *fdp* and *fd-2* plants in long-day conditions (16 hr light and 8hr dark; 22°C).

A   Col-0   *35S::GFP/fdp*

35S::GFP-FDP/fdp

35S::GFP-FDP^{T231A}/fdp   *35S::GFP-FDP^{T231E}/fdp*

B

     Col-0   *35S::GFP*   *35S::GFP-FDP*   *35S::GFP-*   *35S::GFP-*
              fdp   *fdp*   *FDP^{T231A}*   *FDP^{T231E}*
                                             fdp   *fdp*
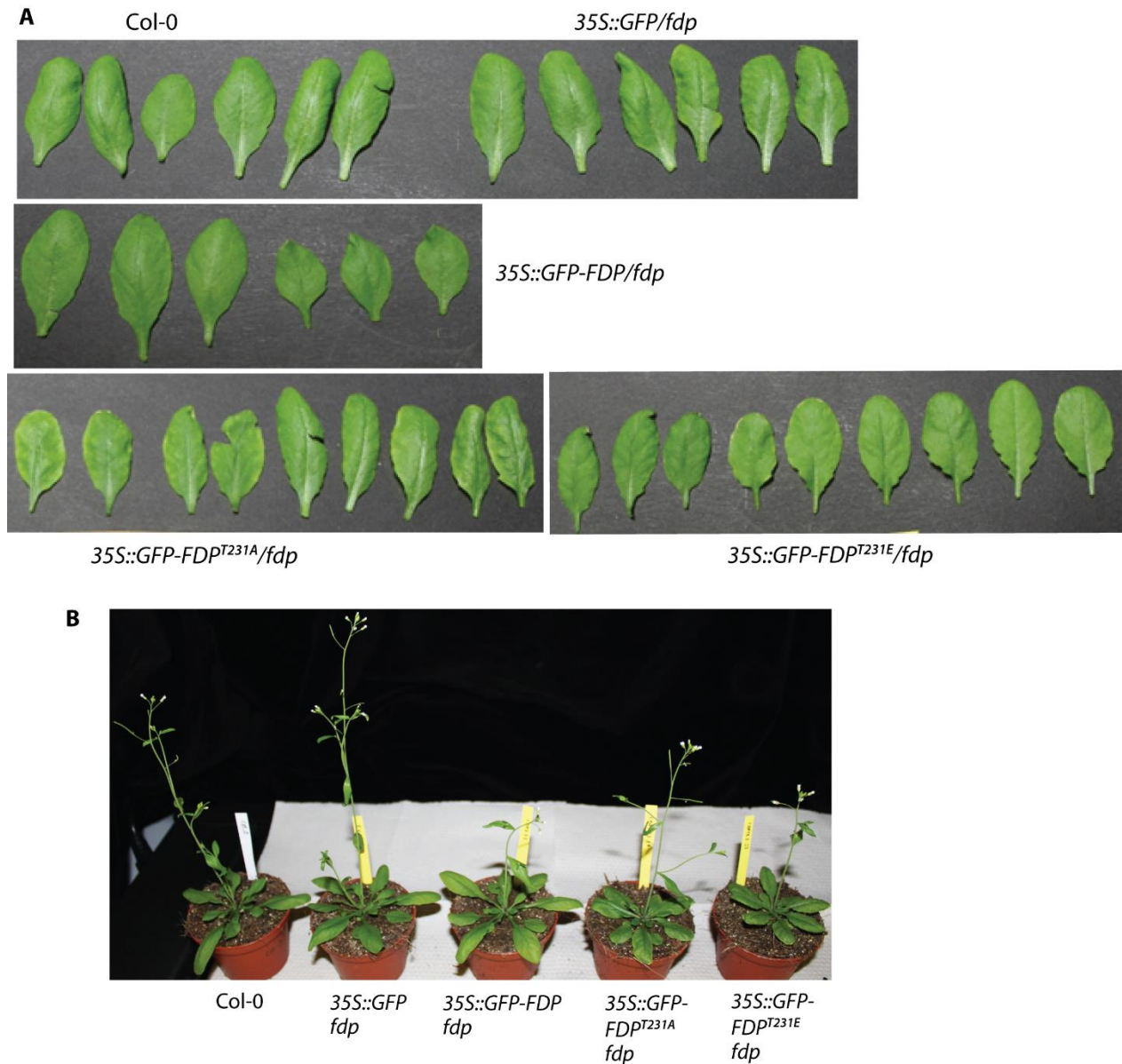
Figure S2: *FDP* overexpression lines show leaf phenotype. **A** and **B**, *fdp* plants transformed with constitutive *35S* promoter driven free GFP, GFP fused to wildtype FDP (GFP-FDP), and its mutant versions - GFP-FDP^{T231A} and GFP-FDP^{T231E}. **A**, Leaves are from segregating T2 generation grown under LDs. Leaves in wildtype, *35S::GFP-FDP*, looks comparatively wider to *35S::GFP* and *35S::GFP-FDP^{T231A}*, while flatter in *35S::GFP-FDP^{T231E}* compare to other lines. Photographs of leaves were taken by Canon D500 camera on black background. **B**, the corresponding overexpression plants grown together with Col-0 at the same LD conditions.
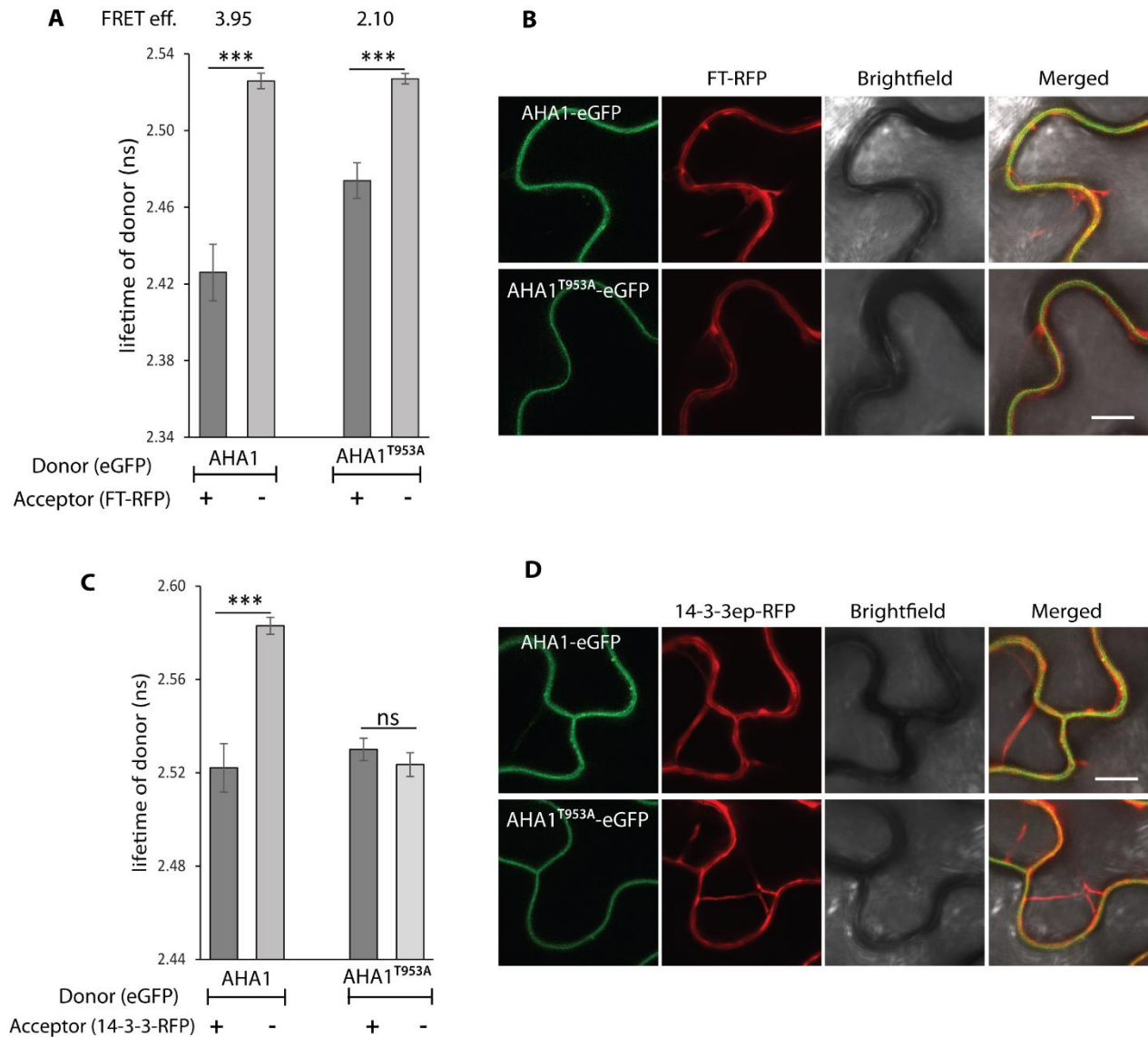
6.2 Supplementary figures

Figure S3: FRET-FLIM analysis illustrating the interaction of AHA1 with FT and 14-3-3 proteins. **A** and **C,** lifetime (ns) of AHA1-eGFP or AHA1^{T953A}-eGFP, when expressed in the absence or presence of FT-RFP and 14-3-3epsilon-RFP, respectively, in the epidermal cells of *N. benthamiana* leaf. Error bar represents the SE from at least 8 number of cells from two independent transformed leaves. *** - significant difference on the basis of paired Student's t-test, ns – not significant. On top of bar graph, FRET efficiency (%) corresponding to AHA1 and AHA1^{T953A} has been calculated. **B** and **D,** exemplary confocal images demonstrating the subcellular localization of AHA1 or AHA1^{T953A} together with FT and 14-3-3epsilon, respectively. Scale bar 10 μm.
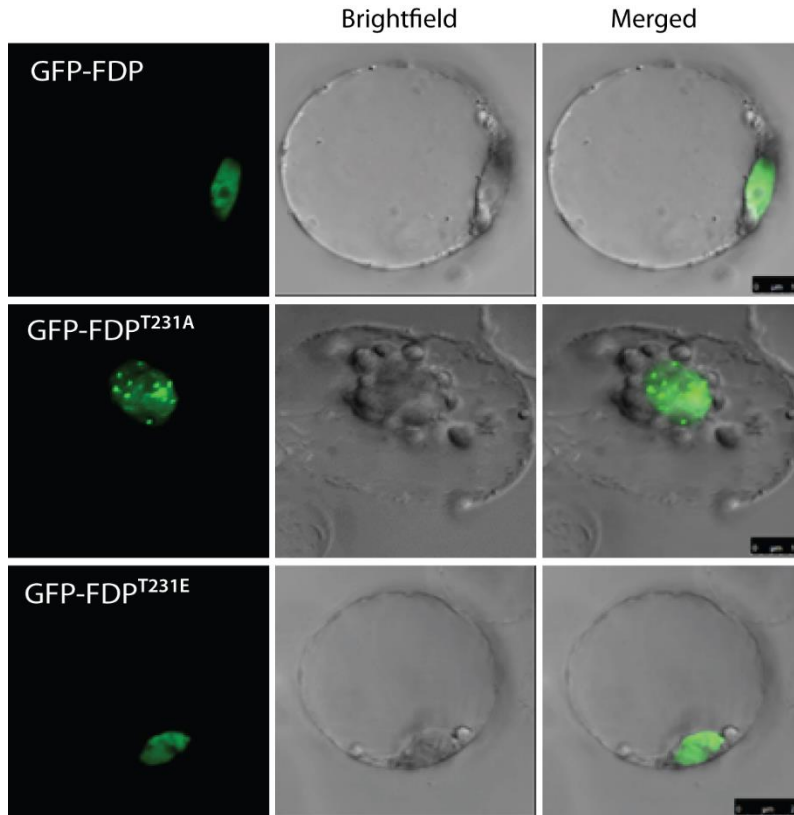
Figure S4: Subcellular localization of FDP and its substitution mutants in the nucleus of *Arabidopsis* protoplast. Confocal images illustrating GFP signal in protoplast transfected with binary vector encoding GFP fusion of FDP, FDP^{T231A} or FDP^{T231E} under the control of 35S promoter. Scale bar 10 μm
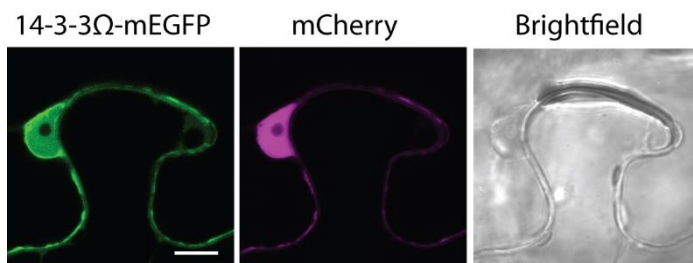

Figure S5: Subcellular localization of 14-3-3Ω. Confocal images demonstrating fluorescence signal from 2in1 vector coexpressing mEGFP fused to 14-3-3Ω, together with free mCherry in epidermal cells of transformed *N. benthamiana* leaf.

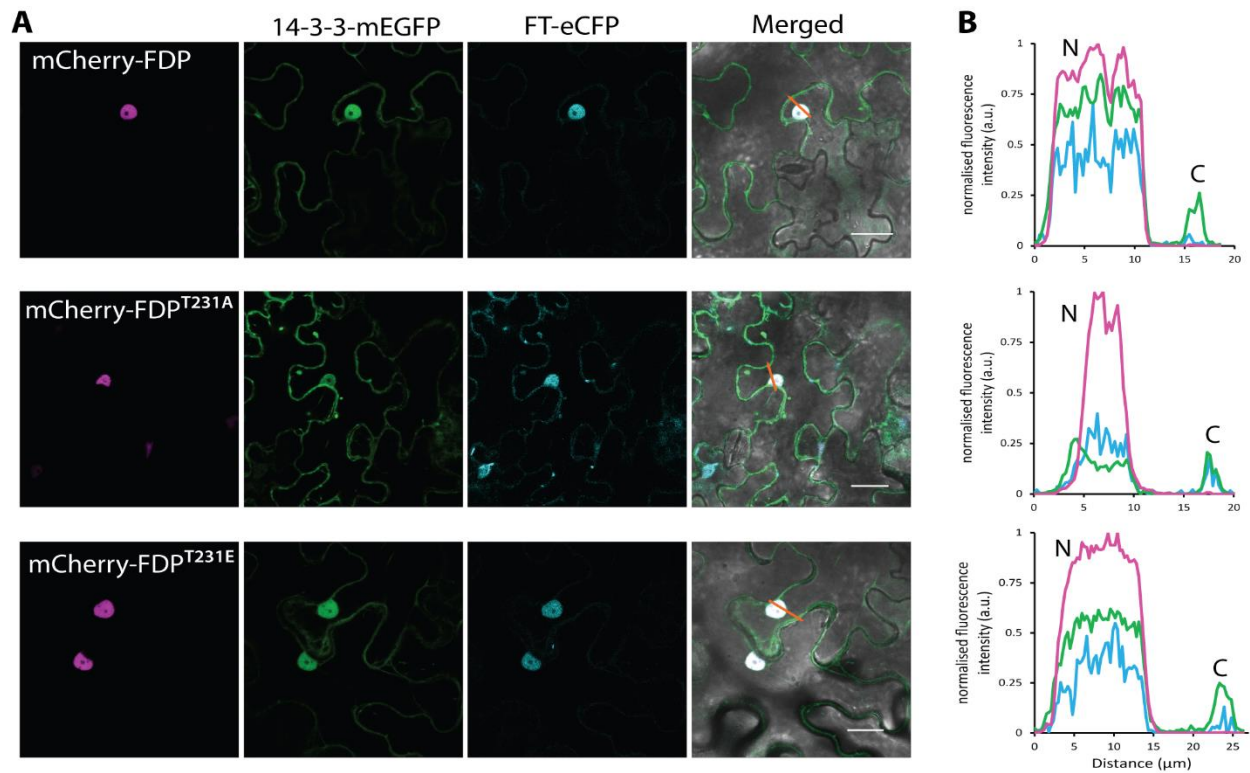**Figure S6**: Phosphorylation of FDP directs the nuclear accumulation of 14-3-3Ω and FT. **A,** confocal images demonstrating three proteins' colocalization by cotransformation in *N. benthamiana* leaves after 2days. 2in1 vectors encoding either mCherry fused to FDP or FDP^T231A or FDP^T231E, and 14-3-3Ω-eGFP, together with FT-eCFP as a third protein, was cotransformed. Scale bar, 25 μm. **B,** normalised intensity graph illustrating the fluorescence intensity of mCherry-FDP, 14-3-3-eGFP and TFL1-eCFP along arrow line drawn on the merged image. N - nucleus, C - cytoplasm
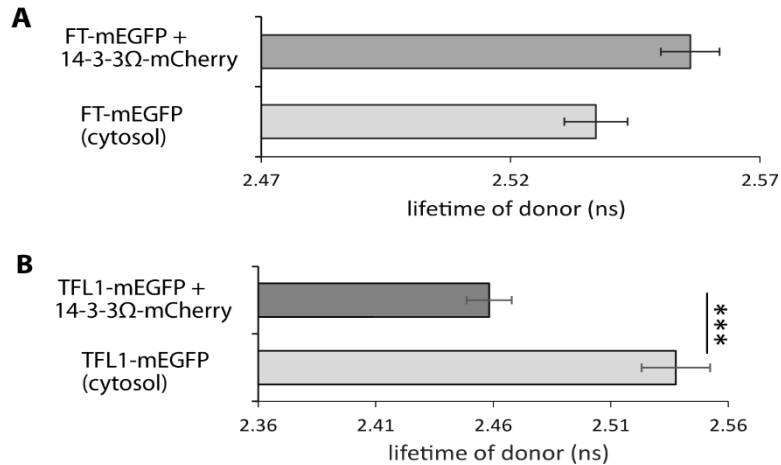
Figure S7: FRET-FLIM interaction study of 14-3-3 with FT and TFL1. 2in1 vector carrying FT-/TFL1-mEGFP with 14-3-3Ω-mCherry or NLS-mCherry was coexpressed in *N. benthamiana* leaf. FRET-FLIM was measured in the cytosol. **A** and **B**, show lifetime of FT-mEGFP and TFL1-mEGFP, respectively, in the presence and absence of 14-3-3Ω-mCherry. *** - indicate significant difference on the basis of paired Student's t-test.
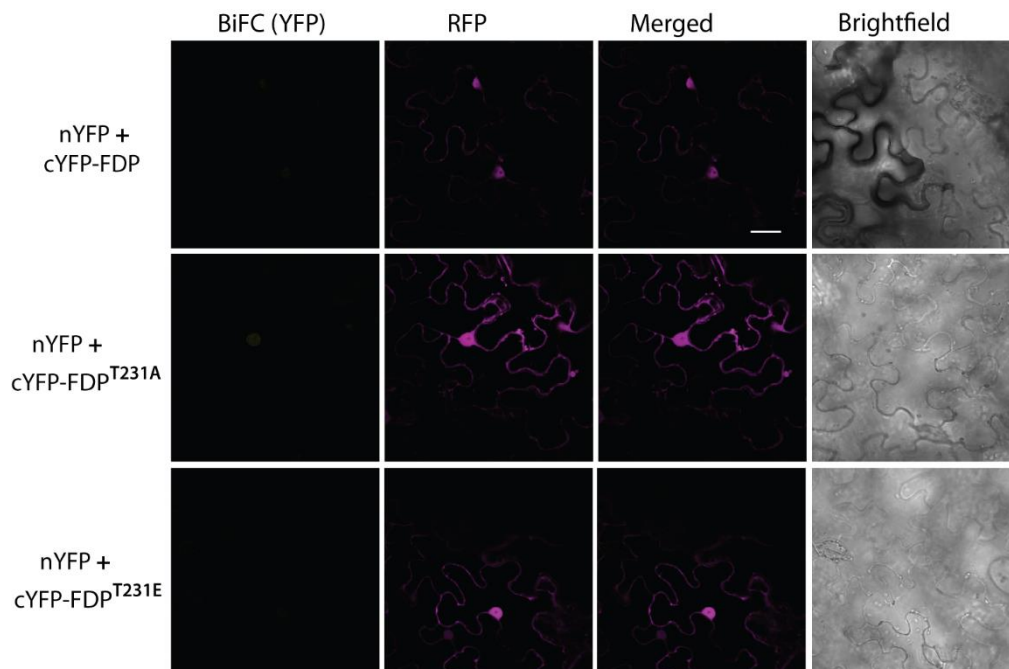

Figure S8: Negative controls of rBiFC studies. Exemplary confocal images showing no or weak BiFC fluorescence signal in leaf epidermal cells of *N. benthamiana* 2 days after *Agrobacterium*-infiltration of cYFP half fused to FDP, FDP^{T231A} or FDP^{T231E}, together with nYFP half. RFP fluorescence was used as expression control and for ratiometric analysis. Scale bar 30 µm

6.3 Supplemental tables

Table 1: Nuclear-cytoplasmic (N/C) ratio for 14-3-3-mCherry and 14-3-3-NLS-mCherry when coexpressed with either FT- or TFL1-mEGFP

	N/C ratio, when FT is coexpressed		N/C ratio, when TFL1 is coexpressed	
	14-3-3Ω	14-3-3Ω-NLS	14-3-3Ω	14-3-3Ω-NLS
Average	0.61	5591.51	0.53	4625.54
SD	0.204	4634.33	0.14	3650.16
n	17	22	19	22

SD – standard deviation, n – number of cells

Table 2: FRET-FLIM result showing competition between FT and TFL1:

Construct	Lifetime (ns)	n
FT-mEGFP + NLS-mCherry	2.49±0.01	12
FT-mEGFP + NLS-mCherry + TFL1-eCFP	2.50±0.04	12
FT-mEGFP + mCherry-FDP^{T231A}	2.48±0.04	10
FT-mEGFP + mCherry-FDP^{T231A} + TFL1-eCFP	2.49±0.04	10
FT-mEGFP + mCherry-FDP^{T231E}	2.31±0.05[a]	12
FT-mEGFP + mCherry-FDP^{T231A} + TFL1-eCFP	2.38±0.07[a,b]	14
TFL1-mEGFP + NLS-mCherry	2.49±0.01	13
TFL1-mEGFP + NLS-mCherry + FT-eCFP	2.48±0.03	9
TFL1-mEGFP + mCherry-FDP^{T231A}	2.49±0.02	12
TFL1-mEGFP + mCherry-FDP^{T231A} + FT-eCFP	2.50±0.03	9
TFL1-mEGFP + mCherry-FDP^{T231E}	2.29±0.06[a]	11
TFL1-mEGFP + mCherry-FDP^{T231A} + FT-eCFP	2.37±0.09[a,b]	14

a - Significantly different from FT-mEGFP + NLS-mCherry and FT-mEGFP + NLS-mCherry+ eCFP-FDP (Pvalue is 0.03), b - Significantly different from FT-mEGFP + 14-3-3NLS-mCherry (Pvalue is 0.03)
n – Number of nuclei taken for measurement

Table 3.1: FRET-FLIM measurement showing the positive effect of on FDP FT-14-3-3 complex formation

Construct	Experiment 1		Experiment 2	
	Lifetime (ns)	n	Lifetime (ns)	n
FT-mEGFP + NLS-mCherry	2.42±0.02	11	2.42±0.02	10
FT-mEGFP + NLS-mCherry + eCFP-FDP	2.40±0.07	11	2.44±0.07	11
FT-mEGFP + 14-3-3ΩNLS-mCherry	2.22±0.04[a]	12	2.24±0.04[a]	11
FT-mEGFP + 14-3-3ΩNLS-mCherry + eCFP-FDP	2.18±0.06[a,b]	13	2.26±0.07[a]	12

a - Significantly different from FT-mEGFP + NLS-mCherry and FT-mEGFP + NLS-mCherry+ eCFP-FDP (Pvalue is 3.28E-13), b - Significantly different from FT-mEGFP + 14-3-3NLS-mCherry (Pvalue is 0.03), n – Number of nuclei taken for measurement

Table 3.2: FRET-FLIM measurement showing the negative effect of FDP on TFL1-14-3-3 complex formation

Construct	Lifetime (ns)	n
TFL1-mEGFP + NLS-mCherry	2.50±0.03	12
TFL1-mEGFP + NLS-mCherry + eCFP-FDP	2.51±0.09	12
TFL1-mEGFP + NLS-mCherry + 3xHA-FDP	2.51±0.05	11
TFL1-mEGFP + 14-3-3ΩNLS-mCherry	2.22±0.05[a]	12
TFL1-mEGFP + 14-3-3ΩNLS-mCherry + eCFP-FDP	2.32±0.06[a,b]	13
TFL1-mEGFP + 14-3-3NLS-mCherry + 3xHA-FDP	2.33±0.05[a,b]	12

a - Significantly different from TFL1-mEGFP + NLS-mCherry, TFL1-mEGFP + NLS-mCherry + eCFP-FDP and TFL1-mEGFP + NLS-mCherry + 3xHA-FDP (Pvalue is < 0.003), b - Significantly different from FT-mEGFP + 14-3-3NLS-mCherry (Pvalue is <1.07E-04). n – Number of nuclei taken for measurement

Table 4: Different combinations of FDP, 14-3-3 and FT or TFL1 proteins used for FRET-FLIM measurement to investigate the formation of a large protein complex

mEGFP (Donor)	mCherry (Acceptor)	3rd Protein	No. of Exp	Result
TFL1	FDP^{T231E} (FDP^{T231A} as control)	14-3-3Ω-HA-NLS	3	Significant Lifetime increase in two experiments, and third one no significant change upon 14-3-3Ω-HA-NLS expression
FT	FDP^{T231E} (FDP^{T231A} as control)	14.3Ω-HA-NLS	3	Significant Lifetime increase in two experiments, and third one no significant change upon 14-3-3Ω-HA-NLS expression
TFL1	FDP (FDP^{T231A} as control)	14.3Ω-HA-NLS	2	1. Significant decrease, 2. neither decrease nor increase in lifetime upon 14-3-3Ω-HA-NLS expression
FT	FDP (1. NLS-mCherry & 2. FDP^{T231A} as control)	14.3Ω-HA-NLS	2	1. Significant decrease, 2. neither decrease nor increase in lifetime upon 14-3-3Ω-HA-NLS expression
14.3Ω-NLS	FDP (FDP^{T231A} as control)	FT-eCFP or TFL1-eCFP	2	1. Significant Lifetime increase dissociation upon both FT-&TFL1-eCFP 2. Significant decrease with FT, no change with TFL1

6.4 List of Primers

Name	Sequence (5'-3')	Length (nt)
For cloning in binary vector pPTKan		
eGFP-Bam-F	tatggatccatggtgagcaagggc	24
FDP-Bam_F	atggatccatgttgtcatcagcaaag	27
FDP-SalI_R	tatgtcgactcaaaatggagctgtggaagaccgttg	36
FDPT231A-SalI_R	tatgtcgactcaaaatggagcttcggaagaccgttg	36
FDPT231E-SalI_R	tatgtcgactcaaaatggagctgcggaagaccgttg	36
At14.3omega_BamHI_F	TATGGATCCatgGCGTCTGGGCGTGAAGA	29
At14.3omega_HA_NLS_STOP_Sal_R	TCAtCCTCCAACCTTTCTCTTCTTCTTAGGCTGCAGcTGCTGTTCCTCGGTCGGT	55
Cloning of codon-optimized FDP for protein expression		
oFDP-Bam-F	tatGGATCCATGCTGAGCAGCGCAA	25
oFDPT231E-SalI-R	tatGTCGACTTAAAACGGTGCTTCGCTGCTACGCTG	36
Cloning in donor vector, pDNOR201		
attB1-FT_F	AAAAAAGCAGGCTTCatgtctataaatataagagac	36
attB2-FT_R	CAAGAAAGCTGGGTTaagtcttcttcctccgcagcc	36
attB1-TFL1_F	AAAAAAGCAGGCTTCatggagaatatgggaactaga	36
attB2-TFL1_R	CAAGAAAGCTGGGTTgcgtttgcgtgcagcggtttc	36
At14.3omega_attB1_F	AAAAAAGCAGGCTTCatgGCGTCTGGGCGTGAAGAG	36
At14.3omega_attB2_-stop codon_R	CAAGAAAGCTGGGTTctgctgttcctcggtcggttt	36
At14.3omega_attB2_NLS_ without stop codon_R	GGGGACCACTTTGTACAAGAAAGCTGGGTTtcctccaaccttctcttctt	51

Genotyping of *fdp* plant		
FDP-F-tdna	taagatcaacaaccatagtgc	22
FDP-R-tdna	gcaatttcaagctcaagttcg	21
LBb1.3	ATTTTGCCGATTTCGGAAC	19
AHA1^{T953A} cloning		
attB1_AHA1T953A	AAAAAAGCAGGCTTCatgTCAGGTCTCGAAGATATC	36
attB2_AHA1T953A	CAAGAAAGCTGGGTTCACagcGTAGTGATGTCCTGC	36

6.5 List of Plasmids

	Construct	Vector
Binary vector	GFP-FDP	pPTKan
	GFP-FDP^{T231A}	
	GFP-FDP^{T231E}	
rBiFC vector	nYFP-FDP and 14.3.3Ω-cYFP	pBiFCt-2in1-CN (V258)
	nYFP-FDP^{T231A} and 14.3.3Ω-cYFP	
	nYFP-FDPTE and 14.3.3Ω-cYFP	
	nYFP-FDP and FT-cYFP	
	nYFP-FDP^{T231A} and FT-cYFP	
	nYFP-FDPTE and FT-cYFP	
	nYFP-FDP^{T231A} and FT-cYFP	
	nYFP-FDPTE and FT-cYFP	
	nYFP-FDP^{T231A} and TFL1-cYFP	
Colocalization vector	mCherry-FDP and 14.3.3Ω-eGFP	pFRETgc-2in1-CN (V322)
	mCherry-FDP^{T231A} and 14.3.3Ω-eGFP	
	mCherry-FDP^{T231E} and 14.3.3Ω-eGFP	
	mCherry-FDP and FT-eGFP	
	mCherry-FDP^{T231A} and FT-eGFP	
	mCherry-FDP^{T231E} and FT-eGFP	

	mCherry-FDP and TFL1-eGFP	
	mCherry-FDP^{T231A} and TFL1-eGFP	
	mCherry-FDP^{T231E} and TFL1-eGFP	
Colocalization and FRET vector (LR reaction)	FT-mEGFP and NLS-mCherry	pFRETgc-2in1-CN (new V322)
	TFL-mEGFP and NLS-mCherry	
	mCherry-FDP and FT-mEGFP	
	mCherry-FDP^{T231A} and FT-mEGFP	
	mCherry-FDP^{T231E} and FT-mEGFP	
	mCherry-FDP and TFL1-mEGFP	
	mCherry-FDP^{T231A} and TFL1-mEGFP	
	mCherry-FDP^{T231E} and TFL1-mEGFP	
	14.3Ω-mCherry and FT-mEGFP	pFRETgc-2in1-CC (new V319)
	14.3Ω-mCherry and TFL1-mEGFP	
	mCherry-FDP and 14.3Ω-mEGFP	pFRETgc-2in1-CN (new V322)
	mCherry-FDP^{T231A} and 14.3Ω-mEGFP	
	mCherry-FDP^{T231E} and 14.3Ω-mEGFP	
	NLS-mCherry and 14.3Ω-mEGFP	
BP reaction	FT	pDonor 201 (attB1B2)
	TFL1	
	FDP	
	At14.3epsilon	
	At14.3omega	
	At14.3Ω_NLS	pDonor 221 p1p4(V006)
	At14.3Ω_NLS	pDONOR 221 p2p3 (V007)
	Free mCherry	pDonr 221 p1p4(V006)
	Free mEGFP	pDONOR 221 p2p3 (V007)
	FDP^{T231A}	pDonor 201 (attB1B2)
conventional cloning	At14.3omega-3xHA-NLS	pPTKan
	TFL1-3xHA	
pGEM-T cloning	14-3-3omega-NLS	pGEM-T

LR reaction	FT-eCFP	pK7CWG2 (eCFP at C-term)
	TFL1-eCFP	
	FDP-eCFP	pK7WGC2 (eCFP at N-term)
	At14.3epsilon-mCherry and FT-mEGFP	pFRETgc-2in1-CC (V319)
	At14.3epsilon-mCherry and TFL1-mEGFP	pFRETgc-2in1-CC (V319)
	At14.3omega	pK7CWG2 (eCFP at C-term)
	FT-mCherry & 14-3omega-mEGFP	pFRETgc-2in1-CC (V319)
	14-3-3-NLS-mCherry and FT	
	14-3-3-NLS-mCherry and TFL1	
	FDP	V342 (3xHA at N-term)
	FDP and At14.3Ω_NLS	pFRETgc-2in1-CN (V322)
	FDP^{T231A} and At14.3Ω_NLS	pFRETgc-2in1-CN (V322)
	V006-mCherry with stop and V007-14.3Ω	pFRETgc-2in1-CC (V319)
	14.3Ω- NLS-mCherry and mEGFP	pFRETgc-2in1-CC (V319)
	FDP^{T231A}	V342 (3xHA at N-term)
	V006-TFL1 and V007-14.3Ω	pFRETgc-2in1-CC (V319)
	AHA1^{T953A}	pH7FWG2 (eGFP at C-term)
Protein Expression	FDPopti	pET28a-His-MBP
	FDP^{T231E}opti	
	FDP^{T231A}opti	

Acknowledgement

Curriculum vitae

Personal Information

Name   Om Narayan

Date of birth   27.06.1987

Nationality   Nepal

Marital status   Married

Email   om.narayan@zmbp.uni-tueibngen.de; onarayan@gmail.com

Education

04/2014 – Present   PhD in Plant Molecular Biology, University of Tuebingen, Germany

10/2010 – 12/2012   MS Agrobiotechnology, University of Giessen, Germany

08/2004 – 06/2008   BTech Biotechnology, Kathmandu University, Nepal

Research Experience

07/2012 – 09/2012   Internship, Max Planck for Terrestrial Microbiology, Marburg

09/2009 - 02/2010   Internship, Biotechnology unit of Nepal Agricultural Research
                         Council